CELLULOSE NANOCRYSTALS DERIVED FROM WASTE TEXTILE FOR THE CONSTRUCTION OF ANTIBACTERIAL PACKAGING MATERIALS

Shuting Huang

Department of Food Science and Agricultural Chemistry

McGill University, Montreal

October 2022

A thesis submitted to McGill University in partial fulfillment of the requirements of the degree of Doctor in Philosophy

Table of Contents

Abstract

Increasing concerns about textile waste have required the development of promising approaches to recycling them into valuable products. One of the most consumed fibers in textile industry is cotton, which contains more than 90% of cellulose and could act as useful biomass feedstock for cellulose nanocrystals (CNCs). CNCs are the most abundant crystalline polysaccharide nanomaterials on Earth and are the promising building blocks for active packaging materials due to their high crystallinity, biocompatibility, nontoxicity, and abundant active sites for further modification. The primary aim of this project was to extract CNCs from waste textile to develop antibacterial packaging materials. The study in chapter 3 aimed to explore the possibility of directly extracting CNCs from textile waste using sulfuric acid hydrolysis and three-step oxidization, respectively. The obtained CNCs had a rod-like shape and cellulose I_β crystalline structure with ~89% crystallinity index. The aspect ratio of CNCs extracted from acid hydrolysis and oxidization were 10.00 ± 3.39 and 17.10 ± 12.85, respectively. Moreover, we investigated the reinforcing effect of CNCs on soybean protein isolate films, and the results confirmed that the addition of CNCs could improve the films' mechanical performance and water vapor barrier property. Chapter 4 developed an approach to producing CNC-based nanofillers with multifunction. In light of the findings in Chapter 3, we modified CNCs with methacrylamide to explore their potential as antibacterial nanofillers in commercial plastic films. The modified CNCs could eliminate 99.999% of *Staphylococcus aureus* and *Escherichia coli*, and the incorporation of modified CNCs into polymer matrices could effectively inactivate both bacteria at a concentration of 10^6 CFU/mL after 1-hour contact.

The antibacterial activity could be fully recharged by chlorination without impacting their mechanical properties. Chapter 5 compared different antibacterial modifications of CNCs and investigated the effects of modified CNCs on the performance of polylactic acid (PLA) packaging films. Particularly, CNCs were modified with methacrylamide, cetyltrimethyl-ammonium bromide, and zinc oxide, respectively, and applied on the surface of PLA films by spray-coating. All the modified CNCs showed high antibacterial efficacy against *Staphylococcus aureus* and *Escherichia coli* (>99.999%). The coating of modified CNCs endowed PLA films with excellent antibacterial activity and improved performance, including mechanical strength, gas barrier properties, and compost disintegration rate. The obtained PLA/CNC composite films also exhibited the capacity to extend meat shelf life from 3 days to more than 10 days. Chapter 6 developed a mechano-bactericidal surface by depositing CNCs on the surface of regenerated cellulose (RC) films with the assistance of vacuum filtration. Two types of CNCs were compared, including shorter HCNCs from textile waste (aspect ratio of 10) and longer t-CNCs from tunicate cellulose (aspect ratio of 55). The obtained structure could eliminate over 80% of four bacteria strains upon 3-minute contact, namely *Staphylococcus aureus*, *Escherichia coli*, *Listeria monocytogenes*, and *Salmonella enterica*, and the antibacterial efficiency was related to the characteristics of bacteria and the surface topography. Compared to RC/HCNC films, RC/t-CNC films showed better bactericidal activity. A remarkable reduction ($p < 0.05$) of the antibacterial activity was observed for RC/CNC films after pressing at 50,000 lbs for 15 minutes. Overall, this research revealed that textile waste is a potential feedstock for extracting CNCs, and the obtained CNCs are a promising candidate

for fabricating antibacterial packaging materials.

Résumé

Les préoccupations croissantes concernant les déchets textiles ont conduit au développement d'approches prometteuses pour les recycler en produits de à valeur ajoutée. L'une des fibres les plus consommées dans l'industrie textile est le coton, qui contient plus de 90% de cellulose et pourrait servir de nouvelle biomasse pour les nanocristaux de cellulose (CNC). Les CNC sont les nanomatériaux polysaccharidiques cristallins les plus abondants sur Terre et des éléments constitutifs prometteurs pour les matériaux d'emballage actifs en raison de leur haute cristallinité, de leur biocompatibilité, de leur non-toxicité et de l'abondance de sites actifs pour des modifications ultérieures. L'objectif principal de ce projet était d'extraire les CNC des déchets textiles pour construire des matériaux d'emballage antibactériens. L'étude présentée au chapitre 3 visait à explorer la possibilité d'extraire directement les CNC des déchets textiles en utilisant l'hydrolyse à l'acide sulfurique et l'oxydation en trois étapes, respectivement. Les CNCs obtenus avaient une forme de tige et une structure cristalline de cellulose I_β avec un indice de cristallinité de ~89%. Les rapports d'aspect des CNCs extraites de l'hydrolyse acide et de l'oxydation étaient de 10,00 ± 3,39 et 17,10 ± 12,85, respectivement. Par ailleurs, les résultats ont confirmé que l'ajout de CNC pouvait améliorer les performances mécaniques des films et la propriété de barrière à la vapeur d'eau. Le chapitre 4 a développé une approche pour produire des nanocharges multifonctionnelles à base de CNC. Nous avons modifié les CNCs avec du méthacrylamide pour explorer le potentiel en tant que nanocharges antibactériennes dans les films plastiques commerciaux. Les CNC modifiés ont pu éliminer 99,999 % de *Staphylococcus aureus* et d'*Escherichia coli*, et l'incorporation des CNC modifiés dans des

matrices polymères a pu inactiver efficacement les deux bactéries à une concentration de 10^6 UFC/mL après 1 heure de contact. L'activité antibactérienne a pu être entièrement rechargée par chloration sans impact sur leurs propriétés mécaniques. Le chapitre 5 a comparé différentes modifications antibactériennes des CNC et a étudié les effets des CNC modifiés sur la performance des films d'emballage en acide polylactique (PLA). Les CNC ont été modifiés avec du méthacrylamide, du bromure de cétyltriméthylammonium et de l'oxyde de zinc, respectivement, et appliqués sur la surface des films PLA par pulvérisation. Tous les CNC modifiés ont montré une grande efficacité antibactérienne contre *Staphylococcus aureus* et *Escherichia coli* (>99,999%). L'enrobage de CNC modifiés a conféré aux films PLA une excellente activité antibactérienne et une meilleure performance. Les films composites PLA/CNC obtenus ont également montré leur capacité à prolonger la durée de conservation de la viande de 3 jours à plus de 10 jours. Le chapitre 6 a développé une surface mécano-bactéricide en déposant des CNCs sur la surface de films de cellulose régénérée (RC) à l'aide d'une filtration sous vide. Deux types de CNC ont été comparés, notamment des HCNC plus courtes provenant de déchets textiles et des t-CNC plus long provenant de cellulose tuniquée. La structure obtenue a pu éliminer plus de 80 % de quatre souches de bactéries après un contact de 3 minutes, à savoir *Staphylococcus aureus*, *Escherichia coli*, *Listeria monocytogenes* et *Salmonella enterica*, et l'efficacité antibactérienne était liée aux caractéristiques des bactéries et à la topographie de la surface. Comparés aux films RC/HCNC, les films RC/t-CNC ont montré une meilleure activité bactéricide. Une réduction remarquable de l'activité antibactérienne a été observée pour les films RC/CNC après un pressage à 50 000 livres

pendant 15 minutes. Cette recherche a révélé que les déchets textiles sont une matière première potentielle pour la production de CNC, et que les CNC obtenus sont un candidat prometteur pour la fabrication de matériaux d'emballage antibactériens.

Acknowledgments

First and foremost, I would like to express my sincere gratitude and admiration to my supervisor Dr. Yixiang Wang for serving as my advocate when necessary and giving constructive feedback on my work. His energy and enthusiasm for research and life have encouraged me all the time. I am always grateful for his patience and support, giving me the chance to make my own decision and discover where it gets me.

Also, I would like to thank all professors and staff in the Department of Food Science and Agricultural Chemistry for their support, especially my committee members, Dr. Saji George and Dr. Stéphane Bayen, for their insightful comments and suggestions. Great thanks to Dr. Xiaonan Lu for his invaluable advice and allowing me to use their laboratory equipment. Warm thanks to Dr. Benjamin K. Simpson for his encouragement.

I would like to thank all the lab mates. Their kind help and support made my research time a wonderful memory. I can never forget all your laughing out loud and the beer after the failed experiments. My heartfelt thanks also go to my friends for their continuous support to my work and life, with a special mention to my Sainte-Anne "family" for the cherished time we spent together in Canada. I cannot even begin to explain how much you guys meant to me.

Finally, I would like to thank my family for their endless love and always having my back. Thanks, Dad and Mom, for making a great example to never give up and always keep the passion for work and life.

Contribution of Authors

The following authors contributed to the publication of work undertaken as part of this thesis:

Shuting Huang[a], Yixiang Wang[a], Xinghai Liu[b], Chunyu Chang[c], Ran Tao[a], Ashraf Ismail[a], Shenmiao Li[a], Xiaonan Lu[a], Sheng Zou[a], Kaidi Wang[a]

Authors affiliation

[a] Department of Food Science and Agricultural Chemistry, McGill University

[b] School of Printing and Packaging, Wuhan University

[c] College of Chemistry and Molecular Sciences, Wuhan University

Contribution of work by co-authors for each paper:

PAPER 1: Huang, S., Liu, X., Chang, C., & Wang, Y. (2020). Recent developments and prospective food-related applications of cellulose nanocrystals: A review. *Cellulose*, *27*(6), 2991-3011. (Chapter 2)

Author contributions: Conceptualization, visualization, and writing: S.H.; writing-review and editing: X.L. and C.C.; writing-reviewing and editing, and supervision: Y.W.

PAPER 2: Huang, S., Tao, R., Ismail, A., & Wang, Y. (2020). Cellulose nanocrystals derived from textile waste through acid hydrolysis and oxidation as reinforcing agent of soy protein film. *Polymers*, *12*(4), 958. (Chapter 3)

Author contributions: Conceptualization: S.H. and Y.W.; investigation: S.H. and R.T.; writing-original draft preparation: S.H.; writing-review and editing: A.I. and Y.W.; and supervision: Y.W.

PAPER 3: Huang, S., Li, S., Lu, X., & Wang, Y. (2022). Modification of cellulose nanocrystals as antibacterial nanofillers to fabricate rechargeable nanocomposite films for active packaging. *ACS Sustainable Chemistry & Engineering*, *10*(28), 9265-9274. (Chapter 4)

Author contributions: Conceptualization, investigation, and writing: S.H.; methodology and writing: S.L.; writing-review and editing: X.L.; and writing-review and editing and supervision: Y.W.

PAPER 4: Huang, S., Zou, S., & Wang, Y. (2022). Coatings of modified cellulose nanocrystals endow PLA packaging with antibacterial property and improved performance. *Carbohydrate Polymers* (Under review). (Chapter 5)

Author contributions: Conceptualization, investigation, and writing: S.H.; data collection: S.Z.; and writing-review & editing and supervision: Y.W.

PAPER 5: Huang, S., Wang, K., Lu, X., & Wang, Y. (2022). Mechano-bactericidal surface developed from cellulose nanocrystals and regenerated cellulose films as sustainable active packaging. To be submitted. (Chapter 6)

Author contributions: Conceptualization, investigation, and writing: S.H.; methodology and writing: K.W.; writing-review and editing: X.L.; and writing-review & editing and supervision: Y.W.

List of Figures

Figure 5.6. (a) Stress-stain curves, (b) tensile strength, (c) elongation at break, and (d) Young's modulus of neat and coated PLA films. Means with different letters on the column top were significantly different ($p < 0.05$).

Figure 5.7. (a) WVP, (b) OTR, and (c) water contact angle of neat and coated PLA films. Means with different letters on the top of the columns were significantly different ($p < 0.05$).

Figure 5.8. (a) Photos and (b) weight loss of neat and coated PLA films after incubating under composting conditions.

Figure 5.9. Total viable counts of pork samples during storage at 4 °C.

Figure 6.1. Representative TEM images (a, b), FTIR spectra (c), XRD patterns (d), and ^{13}C solid-state NMR spectra of t-CNCs and HCNCs.

Figure 6.2. Representative SEM images of RC/t-CNCs (a) and RC/HCNCs (b).

Figure 6.3. Antibacterial efficiency of RC, RC/t-CNCs, and RC/HCNCs against *S. aureus*, *L. monocytogenes*, *E. coli*, and *S. enterica.* Statistical significance ($p < 0.05$) among different bacterial strains is indicated by letters, and significant difference ($p < 0.05$) among the RC films is indicated by symbol*.

Figure 6.4. Antibacterial efficiency of RC/t-CNCs and RC/HCNCs against *E. coli* before and after pressing under the forces of 1,000 lbs and 50,000 lbs. Statistical significance ($p < 0.05$) between different pressing forces is indicated by letters.

Figure 6.5. 3D AFM images of RC/t-CNCs (a-c) and RC/HCNCs (d-f) before and after pressing under the forces of 1,000 lbs and 50,000 lbs.

Figure 6.6. Representative SEM images of *S. aureus* (a-c), *L. monocytogenes* (d-e), *E. coli* (g-i), and *S. enterica* (j-l) without treatment (left), and after treatments on the surfaces of RC/t-CNCs (middle) and RC/HCNCs (right) for 3 minutes.

Figure 6.7. Average Raman spectra of *S. aureus* (a), *L. monocytogenes* (b), and *E. coli* (c) without and with treatments on the surfaces of RC/t-CNCs and RC/HCNCs for 3 minutes.

List of Tables

List of Abbreviations

$[BMIm]HSO_4$	1-butyl-3-methylimidazolium hydrogen sulfate
AFM	Atomic force microscope
ANOVA	Analysis of variance
ATR	Attenuated total reflectance
CA	Cellulose acetate
CDCF	5(and 6)-carboxy-2',7'-dichlorofluorescein
CMC	Carboxymethyl cellulose
CNCs	Cellulose nanocrystals
CNFs	Cellulose nanofibers
CrI	Crystallinity index
CTAB	Cetyltrimethylammonium bromide
DMAc	Simethylacetamide
E. coli	*Escherichia coli*
FDA	Food and drug administration
FT-IR	Fourier-transform infrared spectroscopy
GRAS	Generally regarded as safe
HDTMA	Hexadecyltrimethylammonium
IL	Ionic liquid
L. monocytogenes	*Listeria monocytogenes*
LAE	Ethyl lauroyl arginate

LB	Luria–Bertani
LLDPE	Linear low-density poly(ethylene)
MAM	Methacrylamide
NMR	Nuclear magnetic resonance
OTR	Oxygen transmission rate
PAA	Poly(acrylic acid)
PBS	Phosphate-buffered saline
PET	Poly(ethylene terephthalate)
PLA	Polylactic acid
PVA	Polyvinyl alcohol
PVC	Poly(vinyl chloride)
RC	Regenerated cellulose
RH	Relative humidity
S. aureus	*Staphylococcus aureus*
S. enterica	*Salmonella enterica*
SD	Standard deviation
SEM	Scanning electron microscopy
SPI	Soybean protein isolate
TEM	Transmission electron microscopy
TEMPO	(2,2,6,6-tetramethylpiperidine-1-yl)oxyl
THF	Tetrahydrofuran

TSA	Tryptic soy agar
TSB	Tryptic soy broth
TVC	Total viable counting
WVP	Water vapor permeability
WVTR	Water vapor transmission rate
XRD	X-ray diffraction

Chapter 1. General Introduction

1.1. Introduction

Cellulose is the most abundant natural polymer on Earth. It is expected to be used in the fabrication of high-tech sustainable materials, contributing to addressing global climate change and plastic pollution (Li et al., 2021). Generally, cellulose is a long chain linear polysaccharide consisting of hundreds of anhydro-D-glucose units linked by β-1,4-glycosidic bonds with a chemical formula $(C_6H_{10}O_5)_n$ (Figure 1.1) (Zainal et al., 2021). Cellulose is readily available and renewable in plants and animals, and exists as a structural component in biofilms secreted by bacteria such as *Acetobacter xylinum* (Niu et al., 2021).

With the advancement in nanotechnology, cellulose nanocrystals (CNCs) have attracted worldwide attention because of their high crystallinity, lightweight, high stiffness, biocompatibility, large specific surface area, and exceptional reactivity (Ferreira, Rezende, & Cranston, 2021; Kumar & Chauhan, 2022). CNCs have a diameter <100 nm and length in semi-micro/nanoscale, which can be derived from a wide range of sources (e.g., cotton linter (do Nascimento, Nunes, Feitosa, Dufresne, & Rosa, 2022), tree wastes (Schiavi, Francesconi, Taddei, Fortunati, & Balestra, 2022), and tunicate cellulose (Wu et al., 2022)). On account of their great properties, CNCs provide an economically viable and sustainable solution for various applications, such as wastewater treatment (Badawy, Ghanem, Yassin, Youssef, & Rehim, 2021), drug delivery systems (Seabra, Bernardes, Fávaro, Paula, & Durán, 2018), and packaging materials (H. Li, Shi, He, Fei, & Peng, 2020). Notably, the potential applications in food packaging have been frequently reported, where the incorporation of CNCs was found to improve the mechanical strength and gas barrier properties of packaging materials (Rojas-

Lema et al., 2021). With the changes in consumer behavior and increasing awareness of food safety, there is a growing need for antibacterial packaging from sustainable materials.

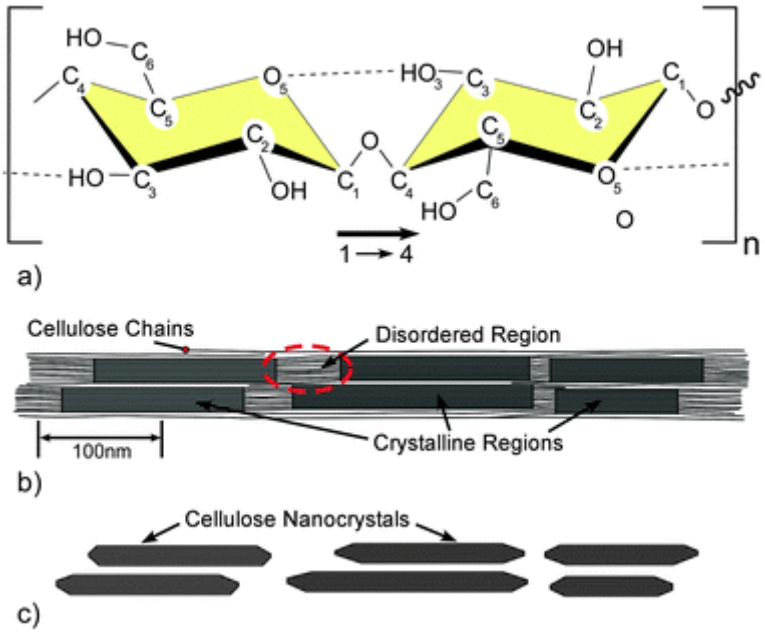

Figure 1.1. Schematics of (a) single cellulose chain repeat unit, showing the directionality of the 1→4 linkage and intrachain hydrogen bonding (dotted line), (b) idealized cellulose microfibril showing one of the suggested configurations of the crystalline and amorphous regions, and (c) cellulose nanocrystals after acid hydrolysis dissolved the disordered regions. Reproduced from (Moon, Martini, Nairn, Simonsen, & Youngblood, 2011) with permission from the Royal Society of Chemistry.

Antimicrobial packaging is an effective approach to controlling the foodborne disease by reducing or hindering microbial growth. Antimicrobials could protect packaged food from microbial hazards during storage and transportation, improving food safety and quality (Ahmed et al., 2022). Generally, antimicrobial packaging works by the employment of antimicrobial substances (e.g., essential oil (Eghbalian, Shavisi, Shahbazi, & Dabirian, 2021), silver (Sun et al., 2021), titanium dioxide (Ezati, Riahi, & Rhim, 2022), etc.) in packaging materials. Many

efforts have been made to develop natural antibacterial nanomaterials to address safety and environmental concerns. In this perspective, we explored the emerging potential of CNCs and their derivatives as a sustainable and practical alternative to construct antibacterial packaging materials.

1.2. Rationale and Objectives of the Proposed Research

The hypotheses of this project are that (1) textile waste will be capable of serving as feedstock of cellulose nanocrystals, and (2) cellulose nanocrystals with high reactivity and high stiffness will be promising candidates to construct antibacterial packaging materials.

The overall objective of this study is to extract CNCs from textile waste and construct antibacterial packaging materials enabled by CNCs. Waste biomass such as textile waste has been selected as the model feedstock of CNCs, and various strategies have been investigated to develop antibacterial packaging materials, including CNC-based antibacterial nanofillers, antibacterial coatings, and mechano-bactericidal surfaces.

The specific objectives of this research are:

1. To explore the possibility to directly extract CNCs from cotton textile waste by sulfuric acid hydrolysis and three-step oxidation (Chapter 3).

2. To develop an approach for producing functional CNCs that can be easily incorporated into commercial plastic films as antibacterial nanofillers (Chapter 4).

3. To investigate the effects of different antibacterial modifications of CNCs on the performance of compostable packaging materials (Chapter 5).

4. To study the mechano-bactericidal efficiency of different CNC coatings and surface

topography (Chapter 6).

1.3. Organization of the Thesis

This dissertation consists of seven chapters: Chapter 1, general introduction, provides the research background and states the rationale and objectives of the research; Chapter 2, literature review, provides a comprehensive review of the literature on the subject matters involved in this research; Chapters 3-6 each represents a full manuscript including the methodology and research findings in their entirety; Connecting text between the manuscripts shows the bridge in the logical progression from one chapter to the next; Chapter 7, conclusion and summary, states how the objectives of the research are met, the implications of findings, and recommendations for future research.

Chapter 2. Recent Developments and Prospective Food-related Applications of Cellulose Nanocrystals: A Review

2.1. Abstract

Cellulose nanocrystals (CNCs) with prominent mechanical properties are well known as the natural reinforcing elements in composites and have received considerable interest over the past decades. Numerous original resources and extraction methods were applied to obtaining CNCs, and the surface properties of CNCs were modified to improve the compatibility with polymeric matrices. Despite these different raw materials and treatments, various novel applications of CNCs have been developed in recent years. Among them, the food-related applications of CNCs have attracted more and more attention because of their renewability, outstanding mechanical properties, unique nanoscale structure, biocompatibility, and easy surface modifications. This review summarized the recent work on the extraction, modification, and food-related applications of CNCs. Traditional raw materials, such as cotton, wood, and tunicate, were still widely used, while there is a new trend to obtain CNCs from waste biomass. Different pretreatments, extraction processes, and surface modifications were compared and discussed. Moreover, the potential applications of CNCs in food packaging, food thickener, emulsion stabilization, quality sensor, and active compound immobilization were presented. Finally, concerns about safety and sustainability have been addressed.

2.2. Introduction

Cellulose is the most abundant natural polymer on Earth. Cellulose nanomaterials, such as cellulose nanocrystals (CNCs) and cellulose nanofibers (CNFs), have received considerable interest over the past decades due to their unique mechanical properties.

CNCs display a high crystallinity, biocompatibility, nontoxicity, and a large specific surface

area. Besides, CNCs contain abundant hydroxyl groups (-OH), which have the potential for further modifications, and the modified CNCs can be applied to various practical utilizations (Bai et al. 2019a). On account of these great properties, CNCs have been employed in widespread applications in environmental, medical, and manufacturing fields. For example, they can commonly serve as a stabilizing agent in Pickering emulsions (Bai et al. 2019c; Capron et al. 2017; Hu et al. 2015; Kalashnikova et al. 2011). The resultant products displayed satisfying stability and other enhanced properties, such as stronger gel-like behavior (Chen et al. 2018). CNCs can also be used in the environmental field for metal ion detection (Zhang et al. 2018a). Furthermore, CNCs have potential in medical applications, which have attracted enormous interest recently. It was found that CNCs can be used as promising materials for wound dressing (Dong and Li 2018; Tavakolian et al. 2018). Zhang et al. (Zhang et al. 2018b) investigated the CNC-based film with superior antibacterial properties and high mechanical strength. The film showed improved antibacterial properties against *Staphylococcus aureus* and *Escherichia coli*. At the same time, scientists are curious if these CNCs, mainly derived from plants and animals, can be used in food or food-related applications.

On the other hand, new raw materials, extraction methods, and surface modifications of CNCs have also attracted much attention. Some plants (walnut shells (Hemmati et al. 2018), *ampelodesmos mauritanicus* (Luzi et al. 2019), shaddock peel (Tang et al. 2017), and corn cob (Souza et al. 2016)) and marine animal (Halocynthia roretzi Drasche (Cheng et al. 2017)) have been used as new sources of CNCs. Also, CNCs can be extracted from synthetic biofilm generated by bacteria (Wu et al. 2018a) and from waste such as waste paper (Lei et al. 2018).

Regardless of the raw materials used, there are several general steps to follow to extract CNCs, as shown in Figure 2.1. The pretreatments are performed to remove impurities of the feedstock. According to the different impurities, specific treatments are needed. Afterward, extraction of the crystal region of cellulose is performed to obtain CNCs, followed by some post-treatments to purify the product.

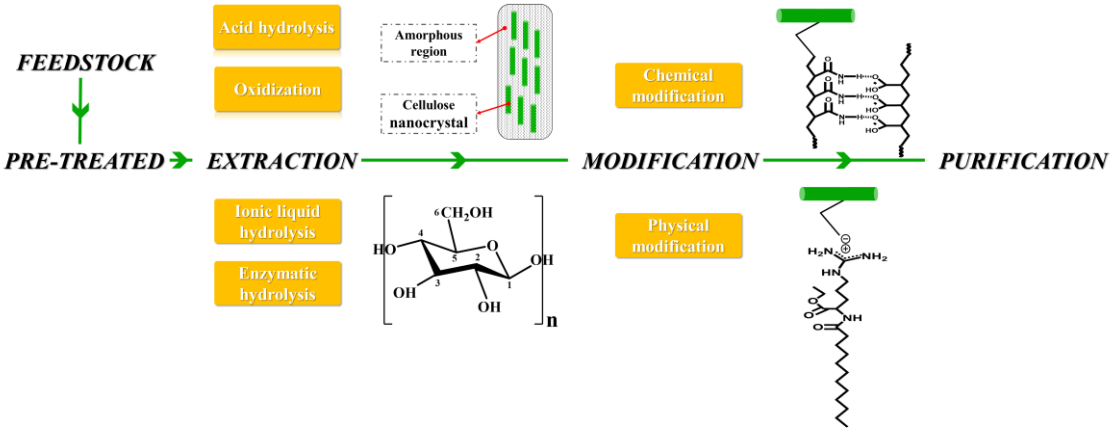

Figure 2.1. Scheme of production of CNCs.

Sulfuric acid (H_2SO_4) hydrolysis is known as a traditional extraction method, obtaining CNCs with sulfate half-ester group (-O-SO_3H) on the surface (Kumar et al. 2018). In the past 5 years, many studies focused on optimizing the experimental conditions to improve CNC performance. However, the sulfate half-ester groups might restrict the application of CNCs in thermoplastic nanocomposites due to the considerable decrease in degradation temperatures (Jiang et al. 2010; Roman and Winter 2004). Even so, H_2SO_4 hydrolysis has still been the most widely used method to extract CNCs. The reason is that this method provides a thorough experimental scheme with convenient operation and low cost compared to the other extraction methods (Malucelli et al. 2017). The synthesized functional groups are negatively charged from approximately pH 3 and up, which offers CNCs a broad range of colloidal stability (Lu et al.

2017). Meanwhile, another traditional method, hydrochloric acid (HCl) hydrolysis, has also been presented to prepare CNCs (Zulnazri et al. 2017).

Generally, modifications of CNCs after extraction are performed to meet the requirements for different applications. For example, Kalantari et al. (Kalantari et al. 2018) successfully modified CNCs for avoiding the aggregation in *N,N*-dimethylformamide, which might affect the electrospinning process. Kim et al. (Kim et al. 2018) applied the silylation method to obtaining CNCs with improved thermal durability, and the products could be used as flame retardant with satisfying performance. These modification methods can be briefly divided into physical modifications and chemical modifications. As for physical modification, it is usually carried out through electrostatic interaction. Liu et al. (Liu et al. 2018a) used cationic bovine serum albumin to physically modify negatively charged CNCs. The composite efficiently improved the stability of Pickering emulsions, leading to a long shelf-life of more than 30 days. On the other hand, chemical modification is implemented by reacting with the functional groups on the CNC surface. Song et al. (Song et al. 2018a) prepared polyvinyl alcohol (PVA)/CNC composite by chemical cross-linking to promote the mechanical properties and thermal stability. Shang et al. (Shang et al. 2018) used thiol-containing castor oil to chemically modify CNCs to increase the hydrophobicity.

2.3. Sources, extraction, and modification

2.3.1. Original sources

CNCs can be derived from a wide range of sources. Among them, cotton stands out as the most common raw material (Ling et al. 2018). Decades ago, Favier et al. successfully extracted CNCs from tunicate and applied them to reinforcing composite polymers (Favier et al. 1995a; Favier et al. 1995b). Also, some bacteria could produce biofilm containing cellulose, which has been considered as a new source of CNCs (Salari et al. 2018).Today, making the best use of recycling materials has become the research focus in many fields. Thus, many researchers have made efforts to use waste biomass as an alternative source of CNCs, which is eco-friendly. For example, waste paper products contain a certain amount of cellulose. The production of CNCs involves the pretreatment of waste paper to regain pulp, followed by the extraction of CNCs. Lei et al. (Lei et al. 2018) prepared CNCs from office waste paper and used them as coating materials. Rahman et al. (Rahman et al. 2017) successfully extracted CNCs from tea leaf fibers, and Ogundare et al. (Ogundare et al. 2017) yielded CNCs from discarded cigarette filters. Additionally, bagasse, rice straw, and wheat straw have also reported being the conventional sources because of their high contents of cellulose and low cost (El Miri et al. 2018; Oun and Rhim 2016; Oun and Rhim 2018).

The dimension, crystallinity, and yield of CNCs, which are recently prepared from various raw materials using H_2SO_4 hydrolysis extraction, are summarized in Table 2.1. All the synthesized CNCs have similar rod-like morphology with different aspect ratios. The lengths of CNCs extracted from waste biomass are around 200 nm. However, the CNCs extracted from animal

sources presented longer lengths in the submicron scale, leading to high aspect ratios. It was reported that the higher aspect ratio of CNCs contributes to the better reinforcing properties. The crystallinity index of obtained CNCs ranges from 70% to 95%. The yield of CNCs from various raw materials was rarely on regular because the calculation methods were not consistent among different articles.

2.3.2. Pretreatment

The various raw materials not only determine the dimensions of CNCs but also require the selection of adequate pretreatment methods. In general, a series of steps are carried out involving cutting the raw materials into small pieces, removing the non-cellulose components, and sometimes followed by the bleaching and washing processes. The recently reported methods to pretreat novel raw materials of CNCs are summarized in Table 2.2. These methods were determined by the non-cellulose compositions in the feedstock. For instance, Coelho et al. (Coelho et al. 2018) prepared CNCs from grape pomace, which contained several non-cellulose polysaccharides and polyphenolics. The pretreatment with dilute H_2SO_4 was used to remove the acid-soluble components, and the alkali treatment was to eliminate the others (such as hemicellulose and lignin) before extracting CNCs. The pretreatments of pineapple crown, including water immersion, mercerization, and bleaching, were recently investigated (Prado and Spinace 2018). Those methods were selected on account of the existence of soluble sugars, hemicellulose (19%), and lignin (5-15%) in pineapple crown. Nagarajan et al. (K. J et al. 2018) used toluene-ethanol solution to remove wax from Saharan aloe vera cactus leave fibers, followed by a sodium chlorite treatment to eliminate lignin. The similar dewaxing and

delignifying procedures were also employed to pretreat Agave fibers (Reddy et al. 2014) and lettuce leaves (Ko et al. 2018). The same pretreatment can be repeated multiple times to completely remove the non-cellulose compositions (Coelho et al. 2018). Extra steps are usually needed to clean up the chemical residues after pretreatments. For example, it was necessary to remove toluene/ethanol residue by vacuum drying. Specific devices, like capacity acid digestion bomb, could facilitate the pretreatment process, but the cost also increased (Dunlop et al. 2018).

Table 2.1. Dimension, crystallinity and yield of CNCs recently prepared from various raw materials.

Category	Raw materials	Diameter (nm)	Length (nm)	Aspect ratio	Crystallinity index	Yield	Reference
Plant	cotton linter	19 ± 8	229 ± 97	12	82%	59–72%	(Hemmati et al. 2019)
	Lettuce leaves	33 ± 12	237 ± 26	N/A	95.70%	N/A	(Ko et al. 2018)
	Grape pomace	7.00	323.00	46	74.89%	20.96%	(Coelho et al. 2018)
Animal	Vase tunicate	17.4 ± 10.7	1374 ± 600	80 ± 60	73 ± 6%	44 ± 8% after pretreatment	(Dunlop et al. 2018)
	Club tunicate	18.3 ± 10.1	1567 ± 638	90 ± 57	89 ± 7%	32 ± 7% after pretreatment	
Microorganism	G. xylinus (bacteria)	22	600	27	95.6%	N/A	(Ambrosio-Martin et al. 2015)
Waste	Office waste paper	33 ± 5	238 ± 72	N/A	84%	9%	(Orue et al. 2017)
	Kelp	20-45	100-500	5-20	69.4%	52.3% after pretreatment	(Liu et al. 2017)
	Newspapers	5.78 ± 2.14	121.42 ± 32.51	N/A	90.15%	54.6% after pretreatment	(Mohamed et al. 2015)
	Posidonia oceanica	4.9 ± 1.3	180 ± 28	36.73	N/A	14%	(Fortunati et al. 2015)

Table 2.2. Pretreatments involved in recent CNCs preparation from novel raw materials.

Raw materials	Non-cellulose compositions	Pretreatment method	Time (h)	Reference
Leaves	Wax, pigments and phenolics	Soxhlet extraction using toluene/ethanol (2:1 v/v)	24	(Ko et al. 2018)
	Hemicellulose	4% NaOH	2	
	Coloring materials	Bleaching 2% $NaClO_2$-CH_3COOH	3	
Grape pomace	Phenolics, pigments and oils	0.067 UGP/mL Ethanol	1	(Coelho et al. 2018)
	Acid-soluble polysaccharides and polyphenolics, hemicellulose, lignin	2% H_2SO_4	5	
	Hemicellulose, lignin, alkali-soluble polysaccharides	5% NaOH	5	
	Lignin and phenolics residual	5% H_2O_2	8	
Nut shell	Wax	Benzene/methanol (4:1)	6	(Hemmati et al. 2018)
	Hemicellulose, lignin	1M NaOH	4	
Waste paper	Inks and fillers	7.5 wt% NaOH	1.5	(Orue et al. 2017)
Posidonia oceanica	Sand and other soil contaminants	Water	24	(Fortunati et al. 2015)
	Wax	Toluene/ethanol (2:1 v/v)	6	
	Coloring materials	Bleaching with 0.7% w/v $NaClO_2$ 5% w/v $NaHSO_4$ 17.5% w/v NaOH	4	

2.3.3. Extraction

After pretreatments, the major component in raw materials is cellulose, which is composed of amorphous and crystalline regions. The extraction process is to selectively destroy the disordered amorphous region, leaving the nanocrystals intact (Lorenz et al. 2017). For example, the pretreated raw materials were hydrolyzed in H_2SO_4 solution (ca. 65 wt%) at 45 ℃ - 55 ℃ to extract CNCs from the soluble hydrolysates (Chieng et al. 2017; Demetrescu et al. 2016; Ko et al. 2018). Chen et al. (Chen et al. 2016) used formic acid (HCOOH) and HCl mixed solution to prepare CNCs with formate groups. The phosphoric acid hydrolysis was also successfully employed to extract CNCs (Ding et al. 2017). Acid hydrolysis was compared with mechanical extraction (pulp refining), and it was found that mechanical treatment cannot serve as an effective method to extract CNCs (Liu et al. 2016). The other extraction methods are enzyme hydrolysis and oxidization.

2.3.3.1. Acid catalytic hydrolysis

In general, it is easier to attack the connections in the disordered amorphous region by chemicals, and the acid hydrolysis is an incomplete process under controlled reaction time and temperature. The hydronium ions (H_3O^+) in an acid solution protonate the oxygen atom of the glucoside bond in cellulose molecular chain, weakening the bond energy and then breaking the bond. Meanwhile, the hydrogen bonds among cellulose molecules in amorphous regions are broken by H_3O^+, accompanied by some secondary reactions (Chen et al. 2017). The research work mainly focuses on two aspects: optimizing the hydrolysis conditions and exploring the new acid solution to prepare CNCs with better properties. Usually, a hydrolysis reaction could

be affected by acid concentration, temperature, and hydrolysis time. Excessive hydrolysis can damage the crystallization region, or even thoroughly break cellulose into small molecules. The optimized hydrolysis time can be calculated through the leveling off of the degree of polymerization (Lorenz et al. 2017).

Over the past years, significant efforts have been made towards exploring new acid systems for the hydrolysis of cellulose. Espinosa et al. (Camarero Espinosa et al. 2013) attempted to add phosphate groups on CNCs by phosphoric acid hydrolysis to improve their thermal stability and dispersibility in water. The results showed that the slightly phosphorylated CNCs formed stable dispersions in polar solvents. Monika et al. (Monika et al. 2017) compared the effects of four mineral acids (H_2SO_4, H_3PO_4, HCl, and HNO_3) and found that CNCs obtained by HNO_3 hydrolysis had the highest thermal stability. Yu et al. (Yu et al. 2017) used mixed acids of HCOOH and HCl to yield rod-like CNCs with formate groups. However, these acid hydrolysis processes required harsh experimental conditions, such as high reaction temperatures and extended hydrolysis time. It is worth noting that using liquid acids may lead to severe equipment corrosion and high purification cost. Therefore, the use of solid acids has been proposed as an alternative with the advantages of feedstock cycling used, less corrosion, and less hazard operations. For instance, Liu et al. (Liu et al. 2014) successfully obtained rod-like CNCs by using phosphotungstic acid-catalyzed hydrolysis. The primary advantages of this method are easy acid recycle after hydrolysis and moderate reaction conditions.

Overall, the acid hydrolysis method is simple, and several acids or their mixtures can be selected. However, some issues, such as the vast usage of acid and corrosion of equipment,

should be addressed.

2.3.3.2. Oxidization

The oxidization method is useful in introducing anionic groups to cellulose molecules. The experimental procedure can be briefly divided into oxidization of cellulose and separation of oxidized CNCs. In the first step, the oxidization of -OH groups and the removal of the amorphous region proceed simultaneously. The resultant products possess negatively charged carboxyl groups (-COOH), which could not only facilitate the dispersion of CNCs in aqueous solutions but also be used for further modifications, such as coupling amine-containing molecules.

Oxidization, using (2,2,6,6-tetramethylpiperidine-1-yl)oxyl (TEMPO) as a radical, is a widely used method. TEMPO is a stable radical that selectively mediates the oxidation of primary alcohols into carboxylic acids through an aldehyde intermediate. Usually, TEMPO oxidization is cooperative with mechanical disintegration, and the fine, middle and coarse fractions of extracted CNCs could be separated by a simple centrifugation method (Peyre et al. 2015). Zhang et al. (Zhang et al. 2016) applied TEMPO oxidation to preparing CNCs from sugarcane with the further assistance of ultrasound. It was found that the yield of CNCs could reach 70%, and the carboxylate content was about 1.5 mmol/g.

Recently, a three-step oxidation method has been developed to prepare CNCs. Firstly, the cellulose feedstock was oxidized by $NaIO_4$/NaCl solution, forming partial 2,3-dialdehyde units on the cellulose chain. Then, the oxidized cellulose was treated with a mixed solution of hydrogen peroxide (H_2O_2)/$NaClO_2$/NaCl to converse dialdehyde groups into dicarboxylic

groups. The third step was TEMPO oxidation, and the C-6 hydroxyl groups were oxidized into carboxyl groups (Zhang et al. 2017). Due to the negatively charged carboxyl groups, the resultant CNCs could be easily dispersed in water and had high stability.

H_2O_2 is an alternative oxidant that can emerge radicals of hydroxyl and hydroperoxyl groups, cause the breakage of glycoside bonds, and simultaneously convert hydroxyl groups into carboxyl groups (Dias et al. 2011). Koshani et al. (Koshani et al. 2018) applied H_2O_2 to preparing CNCs with -COOH groups, using $CuSO_4$ as the catalyst. Also, Huang et al. (Huang et al. 2017) successfully prepared CNCs by H_2O_2 treatment under alkaline conditions. Another one-step oxidation method to prepare CNCs has been reported using ammonium persulfate as a strong oxidant. Ammonium persulfate is an oxidant with several advantages, such as low cost and high-water solubility. It can be used to prepare CNCs along with removing the other non-cellulose components without any pretreatment (Ye et al. 2018b). Therefore, this method has been considered as a 'green' and low-cost approach. Zhou et al. (Zhou et al. 2018) further decreased the dosage of potassium permanganate and prepared the carboxylate CNCs with 1.58 mmol/g of carboxylate content. Recently, Ye et al. (Ye et al. 2018a) compared CNCs obtained from ammonium persulfate oxidization and H_2SO_4 hydrolysis and found that the oxidized CNCs showed stronger promotion of crystallization ability when incorporated into poly(butylene adipate) matrix.

2.3.3.3. Ionic liquid hydrolysis

Ionic liquid (IL) hydrolysis has received numerous attention as a low-energy-consuming and sustainable process because it allows the recycling of reagents and limited use of corrosive

chemicals. This hydrolysis involves two main steps. Firstly, the pretreated cellulose is immersed in IL for a period to allow swelling. Secondly, water is added to initiate the hydrolysis stage. During the reaction, taking 1-butyl-3-methylimidazolium hydrogen sulfate ([BMIm]HSO_4) as an example, the hydrogen and oxygen atoms of amorphous cellulose are easily accessible by the dissociated $[BMIm]^+$ and $[HSO_4]^-$ to form the electron donor-electron acceptor. Then, the hydroxyl groups break, resulting in the selective removal of the amorphous area. Mao et al. (Mao et al. 2015) successfully used IL hydrolysis to prepare CNCs with high product quality and reaction yields (57%) under mild conditions (Mao et al. 2016). It was of significance to find that the hydrolysis kinetics (under 120 ℃) in weak links and the amorphous area followed the heterogeneous first order, which provided a theory guide for future research. Similar results, along with a higher crystallinity index of CNCs, were obtained by using several types of ILs (Tan et al. 2015). Lazko et al. (Lazko et al. 2016) used [BMIm]Cl to swell and [BMIm]HSO_4 to hydrolyze the raw material. Besides, tetrabutylammonium acetate and dimethylacetamide combined with acetic anhydride were used to yield rod-shape CNCs with acetylation on the surface (Miao et al. 2016). However, although ILs are recyclable, the additional processes, such as distillation, filtration, and centrifugation, require extra cost and time.

2.3.3.4. Enzymatic hydrolysis

The extraction methods, as mentioned above, are based on chemical treatments. In contrast, enzymatic hydrolysis is a bio-based ‘green’ method to prepare CNCs. The enzymes with specific functionalities can selectively depolymerize the amorphous region of cellulose to

prepare CNCs with high crystallinity. Additionally, the enzymatic method can potentially recycle lignocellulose biomass during the hydrolysis (Du et al. 2017; Li et al. 2016). Cellulase is the generic term for a group of enzymes, including endo-1,4-β-glucanases, exoglucanases or cellobiohydrolases, and β-glucosidases. (Siqueira et al. 2019). Among them, endo-1,4-β-glucanases can degrade the amorphous regions of cellulose, while cellobiohydrolases are for attacking the low crystalline part. Cellulase hydrolysis can generate CNCs through a simple process and equipment. The traditional procedure is to disperse cellulose in buffer solution, followed by adding enzymes and washing the products after hydrolysis. Zhao et al. (Zhao et al. 2015) compared three methods, enzymatic hydrolysis, TEMPO-mediated oxidation, and sulfuric acid hydrolysis, to prepare CNCs using tunicate as feedstock. They found that the morphology and crystallinity were similar despite different methods. However, the enzymatically hydrolytic products showed little charge on the surface. A similar result was observed in the coproduction of CNCs and glucose using cellulase enzymatic hydrolysis (Rovera et al. 2018). The capacity of different enzymes has been investigated. Yarbrough et al. (Yarbrough et al. 2017) prepared CNCs by a fungal enzyme (Cel7A, Trichoderma *reesei*) and a bacterial enzyme (CelA, Caldicellulosiruptor bescii). The fungal enzyme system expressed the processive hydrolysis, while the bacterial enzyme system presented the localized hydrolysis. The different hydrolysis mechanism of two enzymes led to inconsistent yields and properties. It was demonstrated that CelA performed better in production rate and product uniformity. Besides, the enzymatic hydrolysis has also been combined with other treatments to prepare CNCs. For example, the combination of enzymatic treatment and H_2SO_4 hydrolysis has

recently been investigated (Fortunati et al. 2016; Pang et al. 2018). They discovered that the yield exceedingly increased while shorter reaction time and lower acid cost were required (Beltramino et al. 2018; Beyene et al. 2017). The use of enzymatic treatment, together with IL hydrolysis, has also been reported (Zhao et al. 2017) as an acid-free process.

Generally, the advantages of enzymatic hydrolysis include the use of convenient technique, moderate reaction conditions, and low energy cost. It also provides an approach to coproduce CNCs and biofuels. However, it is not widely adopted because of the high cost of enzymes and prolonged reaction time.

2.3.4. Modification

The modification of CNCs is guided by the final targeted performance, responding to the made-to-order application requests. Although the above-extracted CNCs have outstanding mechanical and physicochemical properties, they aggregate in most organic solvents and cannot be well dispersed in hydrophobic polymer matrices, limiting their applications. Thus, modifications are usually carried out to increase the hydrophobicity of CNCs, and various chemical groups have been grafted on the surface of CNCs by either covalent bonding or electrostatic interaction (as shown in Figure 2.2).

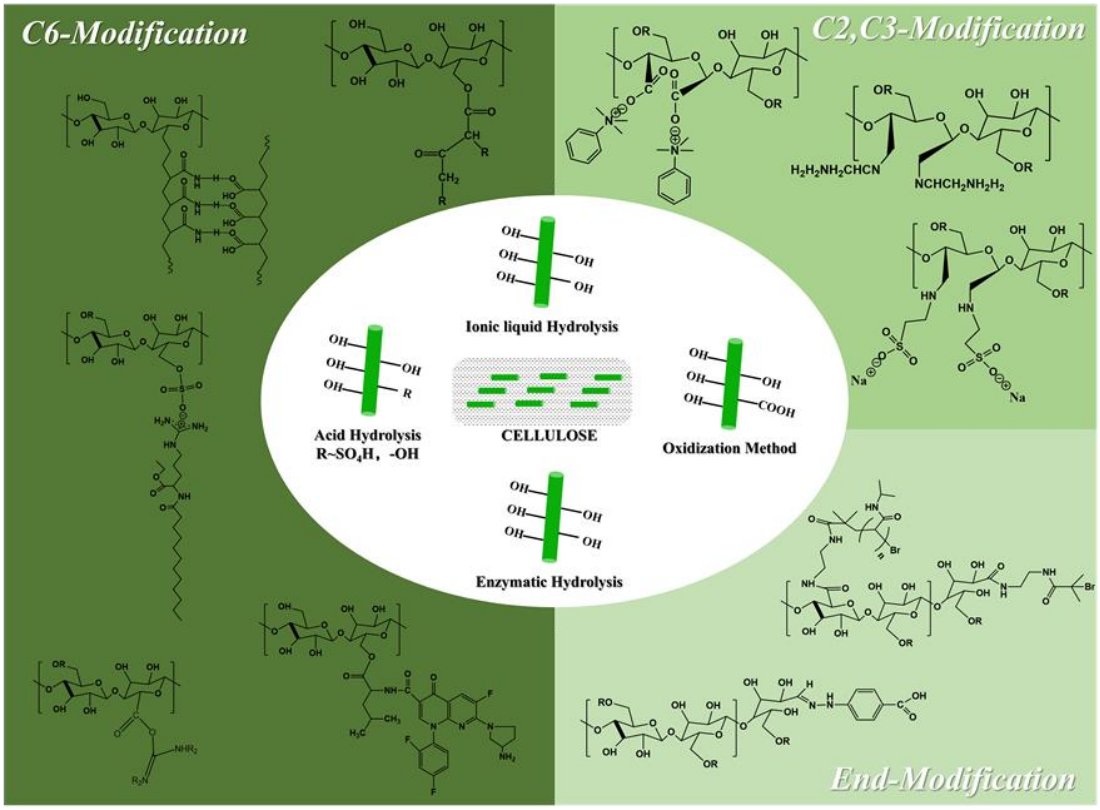

Figure 2.2. Chemical structures of unmodified and modified CNCs.

2.3.4.1. Chemical modification

Chemical modification is the frequently used method and can permanently change the functional groups and bonding mode of CNCs. There are abundant -OH groups on CNCs and a certain amount of aldehyde or carboxyl groups on the oxidized CNCs, which are the active sites to perform chemical modifications. Tang et al. have made a series of efforts to chemically modify CNCs. They put forward an organic solvent-free method to prepare CNCs with maleic anhydride modification. The process of CNC extraction and chemical grafting coincided under ultrasonication (Tang et al. 2013). Then, they yielded a pH-sensitive fluorescent CNCs through multiple steps. Firstly, amino groups were introduced to CNCs by esterification between the -OH groups of CNCs and -COOH groups of L-leucine amino acid. Secondly, the fluorescein derivative, 5(and 6)-carboxy-2',7'-dichlorofluorescein (CDCF), was joint through amidation

reaction between the amino groups and -COOH groups of CDCF (Tang et al. 2016). Based on these studies, they linked the tosufloxacin tosilate drug to the L-leucine amino acid modified CNCs and applied them to the colon-targeted drug delivery (Tang et al. 2018b).

Meanwhile, many other chemical modifications have been reported. Poaty et al. (Poaty et al. 2014) selected several alkyl quaternary ammonium bromides to modify CNCs to establish the ionic coupling between CNCs and polymer matrix and increase their interactions. Kaboorani and Riedl (Kaboorani and Riedl 2015) used hexadecyltrimethylammonium (HDTMA) to modify CNCs without causing any damage to the crystalline structure. They found that the concentration of HDTMA could affect the hydrophobicity of the products. Similar results have been reported by Auclair et al. (Auclair et al. 2018). Yuan and Wen (Yuan and Wen 2018) introduced alkyl ketene dimer to CNCs through esterification reaction, obtaining modified CNCs with a contact angle of larger than 90°. Li et al. (Li et al. 2018a) synthesized polyacrylamide grafted CNCs with crosslinked poly(acrylic acid) (PAA) networks. The modified products showed self-healing property and advanced mechanical strength. Additionally, Ngwabebhoh et al. (Ngwabebhoh et al. 2018) used H_2SO_4 hydrolysis to prepare CNCs with the -O-SO_3H group. The amidation modification was then performed after desulfation and epoxidation treatments to enhance the reactivity of CNCs.

Chemical modifications can occur at the C-6, C-2, and C-3 positions of cellulose. For example, the oxidized CNCs with dialdehyde groups are a reactive intermediate for further derivatization (Li et al. 2009; Lu et al. 2014). Sirvio et al. (Sirvio et al. 2014) successfully prepared the dialdehyde CNCs using periodate oxidation, followed by bisulfite addition. The modified

CNCs were applied to the self-standing nanocellulose film that presented high tensile strength (162.9 MPa) and low oxygen permeability (0.12 cm^3 μm/(m^2 d kPa) at 50% relative humidity). Jin et al. (Jin et al. 2015) grafted ethylenediamine to dialdehyde CNCs through a reductive amination reaction. The amine groups reacted with the aldehyde groups to build the imine bonds, which were then reduced to C-N bonds. The modified CNCs showed an amphoteric property with the change of pH and a high adsorption capability towards acid red (555.6 mg g^{-1}) and thus can be applied to the adsorption of anionic dyes.

Besides the above-mentioned binding sites for chemical modifications, it was also proven that there are active semi-acetal groups on the end of cellulose molecular chains. Arcot et al. (Arcot et al. 2014) investigated a mild asymmetric thiolation procedure to chemically modify CNCs at their reducing aldehyde ends by grafting thiol groups. The modified CNCs chemisorbed on gold in the up-right orientation. Li et al. (Li et al. 2018b) used triazole to modify CNCs at the end position, and the modified CNCs were applied to fabricating a compatible composite with natural rubber, which showed an increase of 160% in tensile strength compared to the neat natural rubber material.

2.3.4.2. Physical modification

Aside from the chemical modification, the physical modification of CNCs is a promising alternative because the process is usually convenient, fast, and solvent-free. However, in recent years, physical modifications have been rarely reported. Gong et al. (Gong et al. 2017) improved the interfacial properties of the oxidized CNCs by physically combining phenyltrimethylammonium chloride with carboxyl groups. Bai et al. (Bai et al. 2018c) used a

cationic surfactant (ethyl lauroyl arginate) to modify CNCs physically. It was proved that the complex could keep the emulsion stable for one month. Miri et al. (El Miri et al. 2016) put forward a new approach to combine CNCs with graphene oxide via hydrogen bonding. The composite could overcome the agglomeration and enhancing the interaction with the PVA matrix. However, the physical modifications sometimes are not efficient. A similar attempt has been carried out to modify the oxidized CNCs with lysozyme via electrostatic interaction, but the resultant products showed a weaker activity as a bio-nanostructure compared to the chemically modified products (Abouhmad et al. 2017). Toncheva et al. (Toncheva et al. 2018) assembled Ag nanoparticles with CNCs. Compared to the chemical bonding, the physically linked nanoparticles tended to aggregate with limited property improvement.

2.4. Current food-related applications

Due to the abundant raw materials, various extraction methods, outstanding mechanical properties, unique nanoscale structure, biocompatibility, biodegradability, and easy surface modifications, CNCs have various application in many fields, such as healthcare, environmental protection, chemical engineering, and manufacture. In the past five years, the use of CNCs as a reinforcing agent was still the most common application. CNCs with/without surface modifications were mixed with various polymers to improve the tensile strength and thermal properties (El Miri et al. 2015; Ferreira et al. 2018; Fumagalli et al. 2018; Yin et al. 2018). CNCs were also served as the template for synthesizing nanomaterials. Dhar et al. (Dhar et al. 2018) used CNCs to prepare graphene with tunable dimensions. Shaheen and Fouda (Shaheen and Fouda 2018) investigated the positively-charged Ag nanoparticles to be absorbed

on the CNC surface, obtained Ag nanorods with remarkable antibacterial activity and stable structure. Moreover, CNCs have been applied to biomedical materials. For example, the addition of CNCs in chitosan-g-d, l-lactic acid tissue engineering material facilitated cell growth and viability (Ko et al. 2018). CNCs were also used to improve the biocompatibility and mechanical properties of chitin based surgical sutures, which could promote wound healing (Wu et al. 2018a). Besides these promising applications, CNC-based materials have also been applied to monitoring or improving the quality of food products.

2.4.1. Pickering emulsion stabilizer

An emulsion is a mixture of two immiscible liquids in which the stabilizer, normally a surfactant, is required. Conventional surfactants are usually small molecules containing both hydrophilic and hydrophobic groups. Apart from them, CNCs are also able to stabilize the liquid droplets on account of shape anisotropy, electrostatic stabilization, interfacial adsorption, and interfacial network, and form the Pickering emulsions (Bai et al. 2019b). The recent work reported that CNCs produced from different origins showed great emulsifying capacity (Figure 2.3), and the resultant emulsions were envisioned for food application. Hedjazi and Razavi (Hedjazi and Razavi 2018) used the unmodified CNCs, prepared from H_2SO_4 hydrolyzed cotton linter, to stabilize canthaxanthin/coconut oil/water Pickering emulsion. They found that the emulsions with cotton linter CNCs were more stable than the emulsions with bacterial CNCs, and the prepared CNCs were potential for food industries, pharmacology, and cosmetics. Liu et al. (Liu et al. 2018b) also demonstrated that the unmodified CNCs were able to stabilize corn oil-in-water Pickering emulsion. Furthermore, they investigated the effect of salt on the

stability of emulsion and found that CNCs with little amount of salt could stabilize the emulsions with low viscosity and density. The relationship between the droplet size and stability of Pickering emulsions has also been studied. Gestranius et al. (Gestranius et al. 2017) applied unmodified CNCs prepared from filter paper to the stable Pickering emulsions with the droplet size of 10-40 μm, and Bai et al. (Bai et al. 2018b) suggested that the submicron droplet size could increase the stability of emulsion with low oil fraction. The latter employed CNCs obtained from ashless cotton fiber filter paper to stabilize the sunflower oil-in-water emulsion, and the visual appearance indicated that the CNC-stabilized Pickering emulsion could remain stable for over a week. It was worth noting that the relatively high hydrophilicity of CNCs limits the stability of emulsions. To overcome this challenge, Tang et al. (Tang et al. 2018a) introduced the hydrophobic chains (polystyrene) to CNCs to emulsify toluene and hexadecane (over four months of storage).

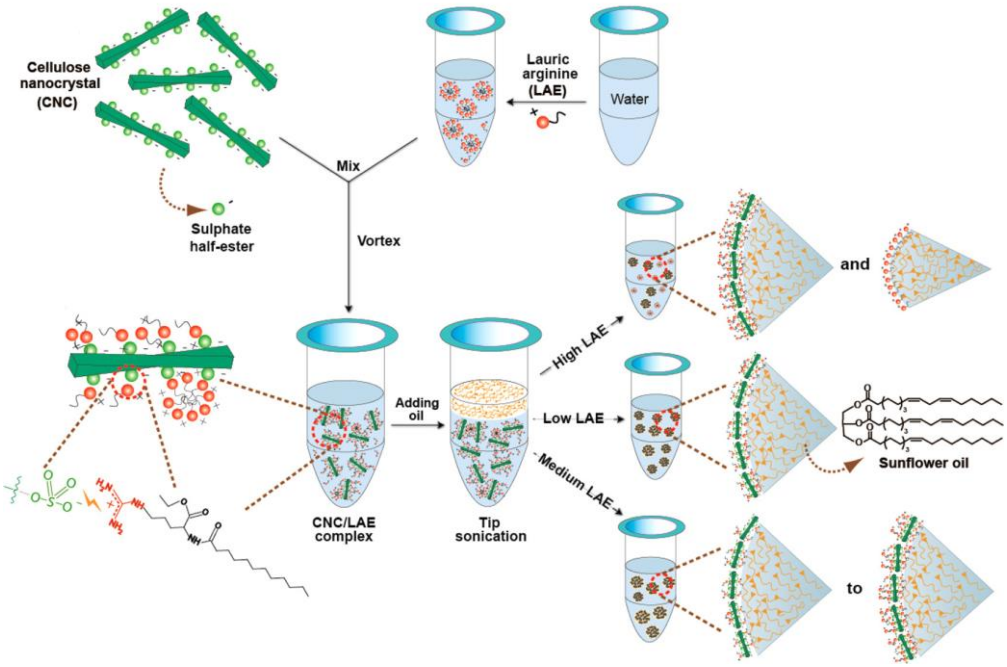

Figure 2.3. Schematic illustration of the formulation, preparation, and oil droplet stabilization via electrostatic interactions involving CNC and Ethyl lauroyl arginate (LAE). The proposed Pickering emulsion stabilization mechanism at different LAE loading levels is introduced (reproduced from (Bai et al. 2018c) with permission of the American Chemical Society).

2.4.2. Food packaging

Numerous studies focused on using CNCs to reinforce food packaging materials, and the significant improvement in mechanical properties are attributed to the interactions between CNCs and polymer matrix. Various polymers have been employed as the matrixes. Anzlovar et al. (Anzlovar et al. 2018) reported that the acetic anhydride-modified CNCs could serve as a reinforcing agent for linear low-density poly(ethylene) (LLDPE) nanocomposite. The modification enhanced the compatibility between CNCs and matrix, increasing the nanocomposite breaking strain by 90%. However, the addition of CNCs affected the crystallinity of LLDPE, and thus limited the reinforcing effect. In general, the adhesion

between the reinforcing agent and the matrix in the interface region is usually due to wettability and adsorption, interdiffusion, electrostatic attraction, chemical bonding, and mechanical adhesion. César et al. (Cesar et al. 2018) approached a novel method to improve the mechanical properties of nanocomposite combined by covalent linkages between OH groups of modified CNCs and cellulose acetate. CNCs were extracted from Typha domingensis followed by modification with 3,3',4,4'-benzophenone tetracarboxylic dianhydride, contributing to restrict the hydrogen-bonding between CNCs. The tensile strength at break of modified CNC-filled nanocomposites increased by 66%. Perumal et al. (Perumal et al. 2018) prepared CNCs from rice straw through acid hydrolysis and used them to reinforce PVA/chitosan nanocomposite film. According to the FTIR results, strong electrostatic interactions and hydrogen bonds existed among CNCs and PVA/chitosan, contributing to an increase of 130% in tensile strength. Other than the improved mechanical properties, the nanocomposites containing CNCs also showed higher barrier properties. Plappert et al. (Plappert et al. 2018) reported the preparation of 2,3-dialdehyde CNCs through sodium periodate oxidation of microcrystalline cellulose and applied them to film fabrication with unmodified CNCs. The resultant film was transparent and had low permeability (< 0.009 mL μm m^{-2} day^{-1} KPa^{-1}) even at a relative humidity of 80%. According to the report of Lei et al. (Lei et al. 2018), the water vapor barrier property of PET/CNC film had been improved. The original PET film possessed the water vapor transmission rate of 37 g m^{-2} day^{-1}, which is treble as quick as the PET/CNC film (~ 10 g m^{-2} day^{-1}).

The methods of fabricating film have also attracted great interest. For example, casting is a

commonly used method to fabricate the film containing CNCs. Firstly, the casting solution was prepared by dissolving the matrix material and dispersing CNCs in a universal solvent. Then, the solution was cast on a flat plate followed by drying for a specified period (Grzabka-Zasadzinska et al. 2018; Yu et al. 2016; Yu et al. 2018). The obtained film possessed a thickness ranging from 0.1 mm to 1 mm. Besides, the melt blending process has been used to make a film with a smaller thickness of 10-30 μm (Arrieta et al. 2015). Also, there were laboratory methods created to prepare film. Li et al. (Li et al. 2016) developed a sandwich method to achieve a thin film (20-30 μm), where filter membranes were used.

Although the research has gone through an extended period, there are still many studies on developing CNCs with multiple functions. For example, CNCs have been used as coating materials, showing enhanced gas barrier (oxygen and carbon dioxide) and satisfying thermal stability (Rampazzo et al. 2017). El Achaby et al. (El Achaby et al. 2017) developed the nanocomposite film with CNCs, PVA, and carboxymethyl cellulose (CMC) via solvent casting and found that the film could take advantage of the combination (Figure 2.4). The tensile strength of the optimized product increased by 82%, accompanied by an 81% decrease in its water vapor permeability. At the same time, the optical transparency maintained at around 90%. However, these preparation methods are incapable of mass production, limiting the promising application for food packaging. Besides, limited research has focused on applying the prepared film to practical food packaging and studying the effects on food preservation.

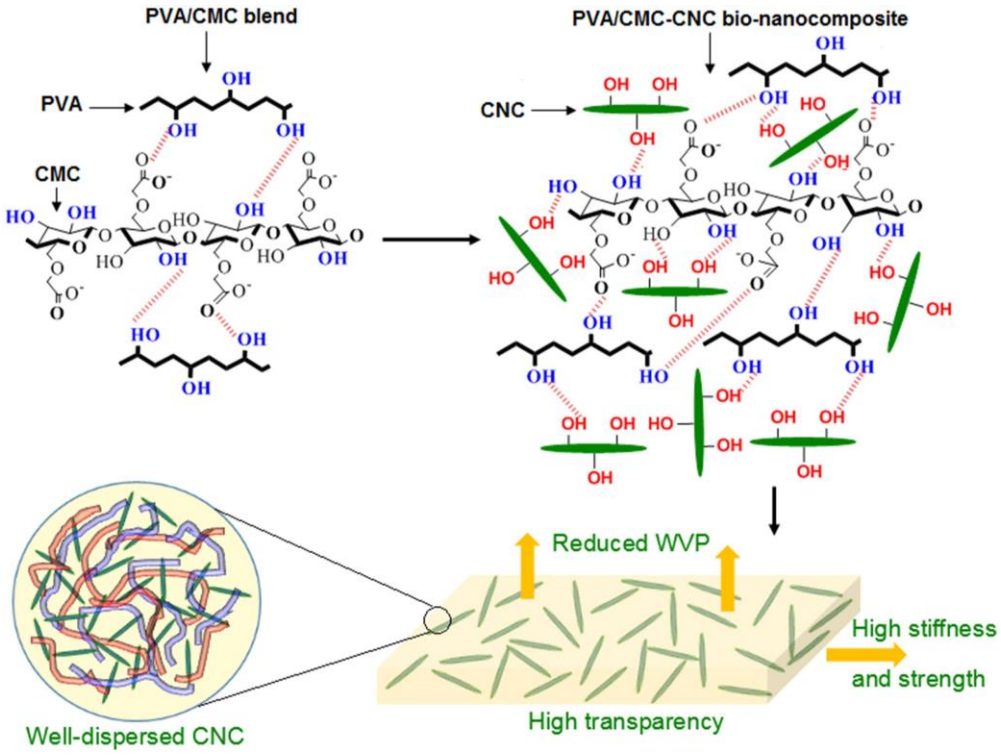

Figure 2.4. Schematic representation of intermolecular hydrogen bonds that occurred in PVA/CMC blend and PVA/CMC-CNC bio-nanocomposites and the structure of the resulting bio-nanocomposite film with well-dispersed CNC (reproduced from (El Achaby et al. 2017) with permission of Elsevier).

2.4.3. Food thickener

CNCs possess the potential to serve as a food thickener, which could be inferred from their rheological properties. In general, the thickening effect occurred when CNC concentration reached the overlap concentration, where CNCs started to contact each other and form the entangled network, contributing to a higher viscosity (Saha and Bhattacharya 2010). Qiao et al. (Qiao et al. 2016) studied the rheological properties of CNC suspensions (isolated from cotton). They found that there was a positive correlation between CNC concentrations and their apparent viscosity, and the CNC suspensions presented the shear-thinning behavior. Tang et al.

(Tang et al. 2018c) reported that CNCs were the effective thickening agent in chitosan/guar gum nanocomposite suspension. With the addition of 3% CNC, the viscosity of suspension increased by 27%. This improvement was attributed to the hydrogen bonds among the hydroxyl groups of chitosan, guar gum, and CNCs. Peng et al. (Peng et al. 2018) demonstrated that rod-like CNCs with a higher aspect ratio were more efficient in increasing the viscosity, and the thickening effect related to the charge of polymer matrices (cationic>anionic>nonionic). However, the research on the potential usage of CNCs as food thickener has been seldom reported, which may be due to their uncertain safety level.

2.4.4. Carrier system

CNCs have been considered as a promising material for carrier systems on account of their biocompatibility, biodegradability, and low toxicity. Furthermore, the relative ease of surface modification allows CNCs to conjugate with small molecules or particles.

Presently, most CNC-based carriers were designed for future biomedical applications. Abo-Elseoud et al. (Abo-Elseoud et al. 2018) suggested that the increase of the carboxylic groups on the CNC surface could retard the release of the loaded drug. They attempted to use chitosan/CNC nanoparticles as the carrier system of repaglinide, which is an anti-hyperglycemic drug. The results showed that the release kinetics followed the Higuchi model, indicating that the drug diffused and released through the nanoparticle matrix. Moreover, CNCs extracted from bacteria with methacrylamide modification has shown the potential as the carrier of nucleic acid (Singhsa et al. 2018). Although the modified CNCs fully complexed with nucleic acid, further investigation was demanded to evaluate the transfection efficacy.

Also, Bai et al. (Bai et al. 2018a) aimed to use PVA/CNC hydrogel as the carrier of methylene blue dye. The results showed that the adsorption capacity of pure PVA hydrogels to remove dye is 46%, while the addition of CNCs increased the adsorption capacity to 65%. It is due to the porous wall of PVA/CNC hydrogel has become thicker, and the binding sites for dye adsorption have increased.

According to current studies, the surface properties of CNCs could be easily modified through physical or chemical methods to enhance the interactions with the targeted molecules or improve the stability at the water/oil interface. Then, they could be used to build carrier systems for various purposes. In terms of previous research reviews, it was predicted that the carrier systems based on CNCs could be applied to functional foods. However, some challenges remained to be dealt with in the future, such as the stability of carrier systems in different food matrices and the safety issues as the food additives.

2.4.5. Sensor

CNCs and their derivatives can serve as the matrix of the intelligent sensors. Sadasivuni et al. (Sadasivuni et al. 2016) fabricated a nitrogen dioxide gas sensor based on CNCs and iron oxide, where iron oxide grew on the acid-form CNCs to prepare a flexible and transparent hybrid film for sensing. According to quantitative analysis, the sensor exhibited a detection limit of 2 ppm with excellent response and good reversibility at room temperature. This sensing system also has the potential for other gas detection with further application in intelligent packaging. Esmaeili et al. (Esmaeili et al. 2015) investigated the CNC-based sensors for detecting glucose. They prepared an electrochemical glucose sensor by pyrrole polymerization on the CNC

surface. The sensor had the limit of detection of 50 ± 10 μm and the period of validity of 17 days. Another sensor made from poly(diallyldimethylammonium chloride) modified CNCs has been reported by Dong et al. (Dong et al. 2016). The limit of glucose detection had been reduced to 2.4 μm. Ma and Wang (Ma and Wang 2016) prepared a colorimetric pH-sensing film, using tara gum and CNCs as the matrix and extracts from grape skins as the pH-responsive components. The resultant film responded to pH changes with the evident change in coloration (from bright to dark green), which could be applied to intelligent food packaging for providing information.

Intelligent sensors could also be fabricated through grafting the responsive components onto CNCs. Yuan et al. (Yuan et al. 2018) applied 2-bromoisobutyryl groups modified CNCs to fabricating a fluorescent sensor, in which CNCs served as backbones, and AzoC6MA and DMAEMA monomers were employed as UV light-, temperature- and pH-responsive components (Figure 2.5). The results indicated that the monomers were successfully grafted onto CNCs with slight morphology change. The sensor exhibited repeatable and reversible transformation in the fluorescence intensity between 40-50 ℃ and pH 6-8, and under the irradiation of UV light, which was promising for monitoring several parameters during food storage.

Song et al. (Song et al. 2018b) developed a colorimetric sensor by chemically modifying CNCs with amine groups. It could change color when it was exposed to aldehyde gases, such as formaldehyde. Principal component analysis indicated that the prepared sensor could distinguish different types of aldehydes and differentiate between aldehyde and non-aldehyde

gases. Other fluorescent CNCs have shown to be responsive to solvent polarity and ionic strength (Wu et al. 2018b). The smart sensor was based on the modified CNCs through covalent conjugation of a 1, 8-naphthalimide dye onto TEMPO-oxidized CNCs. It showed magnified fluorescence response, where its fluorescence emission was inversely proportional to the reducing solvent permittivity or increasing ionic strength, because of the effect of aggregation-enhanced emission.

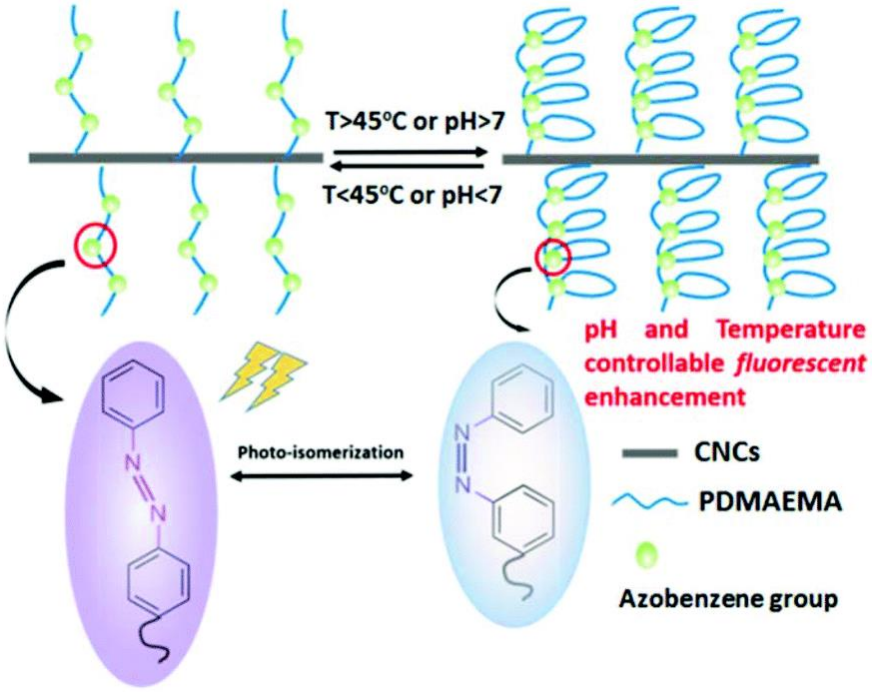

Figure 2.5. Schematic temperature- and pH-responsive properties and the photo-isomerization and fluorescence performance of CNC-g-P(AzoC6MA-co-DMAEMA) nanosensors (reproduced from (Yuan et al. 2018) with permission from the Royal Society of Chemistry).

2.4.6. Water purification

CNCs have also been applied to other applications, such as wastewater purification, which is a significant solution to the shortage of water resources. There are many types of pollutants in wastewater, such as high concentrations of metals and some organic substances. Yousefi et al.

(Yousefi et al. 2018) proposed a solution to use graphene/CNC composite to adsorb a cationic dye, methylene blue, in contaminated water. The adsorption capacity of graphene/CNC composite was 2-fold higher than that of traditional activated carbon, due to the presence of hydroxyl and carboxyl groups. The composite was also able to adsorb the metal ions with a capacity of 76 mg g^{-1} for Cd^{2+} and 63.8 mg g^{-1} for Cu^{2+}. Moreover, it was reported that the aerogels based on acrylic acid grafting modified CNCs could effectively adsorb methylene blue in wastewater due to their high swelling ratio (Liu et al. 2018c). On the other hand, the modified CNCs have potential in environmental ion detection. Zhang et al. (Zhang et al. 2018a) successfully prepared the modified CNCs through controlled esterification, where ethylenediaminetetraacetic dianhydride was applied to oxidizing CNCs followed by the conjugation of fluorescent 7-amino-4-methylcoumarin. The products were used to quantitively detect Cu^{2+} by the change of fluorescence signals. These attempts have shown the potential of CNCs and their derivatives in various applications, but the economic viability and performance during practice remain the challenges.

2.4.7. Safety issues

Cellulose has been designated as "generally regarded as safe" (GRAS) substance by the FDA (Food and Drug Administration). However, CNC is not on the list because it has different chemical characteristics, such as size, shape, crystal structures, and surface charge (FDA 2019). Generally, biocompatibility refers to the ability of a material to perform with an appropriate host response in a specific application (Williams 1999), and toxicity is the degree to which a substance can damage a whole organism or a substructure of the organism. Some recent

investigations have attempted to clarify these safety issues of CNCs. For example, Coelho et al. (Coelho et al. 2018) evaluated the cytotoxicity of CNCs extracted from grape pomace. After incubation with CNCs (0.2 mg/mL) for 48 h, the viability of colon epithelial cells (Caco-2) was as high as the control. A similar result was reported by Xiao et al. (Xiao et al. 2019). There was no significant effect on Caco-2 cell viability after exposure to CNCs extracted from wheat bran at a concentration of 1000 μg/ml.

Besides the above-mentioned *in vitro* experiment, more studies focused on the health concerns of CNCs for the human body. Roberts et al. (Roberts et al. 2019) pointed out that it was crucial to monitor the CNC concentration in the air because CNCs might enter the body through inhalation. Koshani and Madadlou (Koshani and Madadlou 2018) suggested that the study of the CNC orogastrointestinal process was significant toward understanding the associated safety issues. They expounded that CNCs were indigestible, and there might be some interactions between the gut microbiome and CNCs in the distal ileum and colon. These interactions would affect the metabolism of the microbiome, but it was uncertain whether this effect was good or bad. DeLoid et al. (DeLoid et al. 2019) reported the *in vitro* and *in vivo* toxicity of ingested CNCs and CNFs. They found that CNCs and CNFs (0.75% w/w) showed minimal or no cytotoxicity in a cellular model of the intestinal epithelium and no significant growth in reactive oxygen species production. When the dose of CNCs increased to 1.5% w/w, the growth of reactive oxygen species production (<1.1 fold) and cytotoxicity (~12%) were observed. However, the *in vivo* results of hematology, serum markers, and histology exhibited no significant differences between the rats with or without given CNF suspensions. The results

about the *in vivo* effects of CNCs were not provided.

2.5. Conclusion and outlook

In the past five years, numerous studies focused on the extraction and modification of CNCs. Besides the traditional raw materials such as cotton, wood, and tunicate, waste biomass became the new feedstock of CNCs. Several novel extraction methods have been developed, while sulfuric acid hydrolysis was still widely used. Various chemical and physical modifications have been reported, and most of them aimed to increase the hydrophobicity of CNCs to improve their compatibility with nonpolar polymeric matrices. The food-related applications of CNCs have attracted increasing interest. Notably, the potential applications in food packaging and Pickering emulsion have been frequently reported. Due to the unique morphology and high rigidity, the incorporation of CNCs could improve the mechanical and gas barrier properties of packaging materials, and the amphiphilic feature of CNCs allows them to act as a 'green' stabilizer to prepare Pickering emulsions.

It is believed that CNCs are promising building blocks of nanomaterials for various practical applications, and commercial CNC products are available on the market. However, future research in the following areas is required to promote their food applications:

1. Proper applications of CNCs are the key to future development. CNC extraction has become a proven technique. However, there is still a lack of suitable applications for the produced CNCs. The attempt to add CNCs into food packaging is promising because the materials with light weight, high strength, and low gas permeability are usually required. It will also help reduce the usage of non-degradable plastics. Moreover, it will be interesting to combine CNC

based nano-sensors with packaging materials to fabricate new active and intelligent food packaging, which will be beneficial to food quality and safety.

2. 'Green' and cost-effective modifications of CNCs are expected in future studies. Till now, many methods have been reported to improve the hydrophobicity of CNCs. However, most of these modifications increased the cost of products, and sometimes even affected the biocompatibility of CNCs. Therefore, it is necessary to assess the efficiency, feasibility, and cost of different modification methods, and develop the eco-friendly routes to produce modified CNCs.

3. Safety issues of CNCs need to be investigated for their potential food applications. Current research work on the *in vitro* and *in vivo* toxicity of CNCs is limited. CNCs originated from different raw materials have various aspect ratios, and their surface functional groups and charges are determined by the extraction and modification methods. These features, as well as the dosage, may affect the biocompatibility and toxicity of CNCs, so the case-by-case safety studies are required. Moreover, the occupational exposure, *in vivo* digestion and accumulation, and migration from packaging materials also need to be taken into consideration.

2.6. References

Abo-Elseoud WS, Hassan ML, Sabaa MW, Basha M, Hassan EA, Fadel SM (2018) Chitosan nanoparticles/cellulose nanocrystals nanocomposites as a carrier system for the controlled release of repaglinide. Int J Biol Macromol 111:604–613

Abouhmad A, Dishisha T, Amin MA, Hatti-Kaul R (2017) Immobilization to positively charged cellulose nanocrystals enhances the antibacterial activity and stability of hen egg

white and T4 Lysozyme. Biomacromol 18:1600–1608. https://doi.org/10.1021/acs.biomac.7b00219

Ambrosio-Martin J, Fabra MJ, Lopez-Rubio A, Lagaron JM (2015) Melt polycondensation to improve the dispersion of bacterial cellulose into polylactide via melt compounding: enhanced barrier and mechanical properties. Cellulose 22:1201–1226. https://doi.org/10.1007/s10570-014-0523-9

Anzlovar A, Kunaver M, Zagar E, Krajnc A (2018) Nanocomposites of LLDPE and surface-modified cellulose nanocrystals prepared by melt processing. Molecules 23:1782. https://doi.org/10.3390/molecules23071782

Arcot LR, Lundahl M, Rojas OJ, Laine JJC (2014) Asymmetric cellulose nanocrystals: thiolation of reducing end groups via NHS–EDC coupling. Cellulose 21:4209–4218. https:// doi.org/10.1007/s10570-014-0426-9

Arrieta MP, Fortunati E, Dominici F, Lopez J, Kenny JM (2015) Bionanocomposite films based on plasticized PLAPHB/cellulose nanocrystal blends. Carbohyd Polym 121:265–275

Auclair N, Kaboorani A, Riedl B, Landry V, Hosseinaei O, Wang S (2018) Influence of modified cellulose nanocrystals (CNC) on performance of bionanocomposite coatings. Prog Org Coat 123:27–34

Bai HY, Li ZK, Zhang SW, Wang W, Dong WF (2018a) Interpenetrating polymer networks in polyvinyl alcohol/cellulose nanocrystals hydrogels to develop absorbent materials. Carbohyd Polym 200:468–476. https://doi.org/ 10.1016/j.carbpol.2018.08.041

Bai L, Huan S, Xiang W, Rojas OJ (2018b) Pickering emulsions by combining cellulose

nanofibrils and nanocrystals: phase behavior and depletion stabilization. Green Chem 20:1571–1582. https://doi.org/10.1039/C8GC00134K

Bai L, Xiang W, Huan S, Rojas OJ (2018c) Formulation and stabilization of concentrated edible oil-in-water emulsions based on electrostatic complexes of a food-grade cationic surfactant (ethyl lauroyl arginate) and cellulose nanocrystals. Biomacromol 19:1674–1685. https://doi.org/10.1021/acs.biomac.8b00233

Bai L et al (2019a) Adsorption and assembly of cellulosic and lignin colloids at oil/water interfaces. Langmuir 35:571–588. https://doi.org/10.1021/acs.langmuir.8b01288

Bai L, Lv SS, Xiang WC, Huan SQ, McClements DJ, Rojas OJ (2019b) Oil-in-water pickering emulsions via microfluidization with cellulose nanocrystals: 2 In vitro lipid digestion. Food Hydrocolloids 96:709–716. https://doi.org/10.1016/j.foodhyd.2019.04.039

Bai L, Lv SS, Xiang WC, Huan SQ, McClements DJL, Rojas OJ (2019c) Oil-in-water Pickering emulsions via microfluidization with cellulose nanocrystals: 1. For Stab Food Hydrocoll 96:699–708. https://doi.org/10.1016/j.foodhyd.2019.04.038

Beltramino F, Roncero MB, Vidal T, Valls C (2018) A novel enzymatic approach to nanocrystalline cellulose preparation. Carbohyd Polym 189:39–47

Beyene D, Chae M, Dai J, Danumah C, Tosto F, Demesa AG, Bressler DC (2017) Enzymatically-mediated co-production of cellulose nanocrystals and fermentable sugars. Catalysts 7:322. https://doi.org/10.3390/catal7110322

Camarero Espinosa S, Kuhnt T, Foster EJ, Weder C (2013) Isolation of thermally stable cellulose nanocrystals by phosphoric acid hydrolysis. Biomacromol 14:1223–1230.

https://doi.org/10.1021/bm400219u

Capron I, Rojas OJ, Bordes R (2017) Behavior of nanocelluloses at interfaces. Curr Opin Colloid Interface Sci 29:83–95

Cesar NR, de Menezes AJ, Botaro VR (2018) Nanocomposite of cellulose acetate reinforced with nanocrystals modified chemically: modification with bifunctional reagent. Polym Compos 40:E321–E332. https://doi.org/10.1002/pc.24660

Chen GY, Yu HY, Zhang CH, Zhou Y, Yao JM (2016) A universal route for the simultaneous extraction and functionalization of cellulose nanocrystals from industrial and agricultural celluloses. J Nanopart Res 18:48

Chen YW, Tan TH, Lee HV, Abd Hamid SB (2017) Easy fabrication of highly thermal-stable cellulose nanocrystals using Cr(NO3)(3) catalytic hydrolysis system: a feasibility study from macro- to nano-dimensions. Materials 10:42. https://doi.org/10.3390/ma10010042

Chen Q-H, Zheng J, Xu Y-T, Yin S-W, Liu F, Tang C-H (2018) Surface modification improves fabrication of pickering high internal phase emulsions stabilized by cellulose nanocrystals. Food Hydrocolloids 75:125–130

Cheng Q, Ye D, Chang C, Zhang L (2017) Facile fabrication of superhydrophilic membranes consisted of fibrous tunicate cellulose nanocrystals for highly efficient oil/water separation. J Membr Sci 525:1–8

Chieng B, Lee S, Ibrahim N, Then Y, Loo Y (2017) Isolation and characterization of cellulose nanocrystals from oil palm mesocarp fiber. Polymers. https://doi.org/10.3390/polym9080355

Coelho CCS et al (2018) Cellulose nanocrystals from grape pomace: production, properties and cytotoxicity assessment. Carbohydr Polym 192:327–336. https://doi.org/10.1016/j.carbpol.2018.03.023

DeLoid GM et al (2019) Toxicological effects of ingested nanocellulose in in vitro intestinal epithelium and in vivo rat models Environ Sci. NANO 6:2105–2115. https://doi.org/10.1039/c9en00184k

Demetrescu I et al (2016) Isolation of nanocrystalline cellulose from oil palm empty fruit bunch—a response surface methodology study. Paper presented at the MATEC Web of Conferences, 2016/06/08

Dhar P, Gaur SS, Kumar A, Katiyar V (2018) Cellulose nanocrystal templated graphene nanoscrolls for high performance supercapacitors and hydrogen storage: an experimental and molecular simulation study. Sci Rep 8:1–15. https://doi.org/10.1038/s41598-018-22123-0

Dias ARG, Zavareze ED, Helbig E, de Moura FA, Vargas CG, Ciacco CF (2011) Oxidation of fermented cassava starch using hydrogen peroxide. Carbohyd Polym 86:185–191

Ding MC, Li CW, Chen FS (2017) Isolation and characterization of cellulose nanocrystals from cloth hairs and evaluation of their compatibility with PLLA. Cellulose 24:4785–4792. https://doi.org/10.1007/s10570-017-1461-0

Dong F, Li S (2018) Wound dressings based on chitosan-dialdehyde cellulose nanocrystals-silver nanoparticles: mechanical strength, antibacterial activity and cytotoxicity. Polymers (Basel, Switz) 10:673. https://doi.org/10.3390/polym10060673

Dong L, Zhang X, Ren S, Lei T, Sun X, Qi Y, Wu Q (2016) Poly(diallyldimethylammonium chloride)-cellulose nanocrystals supported Au nanoparticles for nonenzymatic glucose sensing. RSC Adv 6:6436–6442. https://doi.org/10.1039/c5ra23935d

Du LX, Wang JW, Zhang Y, Qi CS, Wolcott MP, Yu ZM (2017) A co-production of sugars, lignosulfonates, cellulose, and cellulose nanocrystals from ball-milled woods. Bioresour Technol 238:254–262

Dunlop MJ, Acharya B, Bissessur R (2018) Isolation of nanocrystalline cellulose from tunicates. J Environ Chem Eng 6:4408–4412

El Achaby M, El Miri N, Aboulkas A, Zahouily M, Bilal E, Barakat A, Solhy A (2017) Processing and properties of eco-friendly bio-nanocomposite films filled with cellulose nanocrystals from sugarcane bagasse. Int J Biol Macromol 96:340–352. https://doi. org/10.1016/j.ijbiomac.2016.12.040

El Miri N, Abdelouandi K, Barakat A, Zahouily M, Fihri A, Solhy A, El Achaby M (2015) Bio-nanocomposite films reinforced with cellulose nanocrystals: rheology of filmforming solutions, transparency, water vapor barrier and tensile properties of films. Carbohyd Polym 129:156–167

El Miri N et al (2016) Synergistic effect of cellulose nanocrystals/graphene oxide nanosheets as functional hybrid nanofiller for enhancing properties of PVA nanocomposites. Carbohyd Polym 137:239–248

El Miri N, Aziz F, Aboulkas A, El Bouchti M, Ben Youcef H, El Achaby M (2018) Effect of plasticizers on physicochemical properties of cellulose nanocrystals filled alginate

bionanocomposite films. Adv Polym Technol. https://doi.org/10.1002/adv.22087

Esmaeili C, Abdi MM, Mathew AP, Jonoobi M, Oksman K, Rezayi M (2015) Synergy effect of nanocrystalline cellulose for the biosensing detection of glucose. Sensors 15:24681–24697. https://doi.org/10.3390/s151024681

Favier V, Canova GR, Cavaille JY, Chanzy H, Dufresne A, Gauthier C (1995a) Nanocomposite materials from latex and cellulose whiskers. Polym Adv Technol 6:351–355. https://doi.org/10.1002/pat.1995.220060514

Favier V, Chanzy H, Cavaille JY (1995b) Polymer nanocomposites reinforced by cellulose whiskers. Macromolecules 28:6365–6367. https://doi.org/10.1021/ma00122a053

FDA US (2019) SCOGS (Select Committee on GRAS Substances). U.S. Food and Drug Administration. https://www. accessdata.fda.gov/scripts/fdcc/?set=SCOGS. Accessed 10/24 2019

Ferreira FV, Pinheiro IF, Gouveia RF, Thim GP, Lona LMF (2018) Functionalized cellulose nanocrystals as reinforcement in biodegradable polymer nanocomposites. Polym Compos 39:E9–E29

Fortunati E, Luzi F, Puglia D, Petrucci R, Kenny JM, Torre L (2015) Processing of PLA nanocomposites with cellulose nanocrystals extracted from Posidonia oceanica waste: innovative reuse of coastal plant. Ind Crops Prod 67:439–447

Fortunati E et al (2016) Revalorization of barley straw and husk as precursors for cellulose nanocrystals extraction and their effect on PVA_CH nanocomposites. Ind Crops Prod 92:201–217

Fumagalli M, Berriot J, de Gaudemaris B, Veyland A, Putaux J-L, Molina-Boisseau S, Heux L (2018) Rubber materials from elastomers and nanocellulose powders: filler dispersion and mechanical reinforcement. Soft Matter 14:2638–2648

Gestranius M, Stenius P, Kontturi E, Sjoblom J, Tammelin T (2017) Phase behaviour and droplet size of oil-in-water pickering emulsions stabilised with plant-derived nanocellulosic materials. Colloids Surf A 519:60–70. https://doi.org/10.1016/j.colsurfa.2016.04.025

Gong X, Wang Y, Chen L (2017) Enhanced emulsifying properties of wood-based cellulose nanocrystals as Pickering emulsion stabilizer. Carbohydr Polym 169:295–303. https://doi.org/10.1016/j.carbpol.2017.04.024

Grzabka-Zasadzinska A, Smulek W, Kaczorek E, Borysiak S (2018) Chitosan biocomposites with enzymatically produced nanocrystalline cellulose. Polym Compos 39:E448– E456

Hedjazi S, Razavi SH (2018) A comparison of Canthaxanthine Pickering emulsions, stabilized with cellulose nanocrystals of different origins. Int J Biol Macromol 106:489–497. https://doi.org/10.1016/j.ijbiomac.2017.08.030

Hemmati F, Jafari SM, Kashaninejad M, Barani Motlagh M (2018) Synthesis and characterization of cellulose nanocrystals derived from walnut shell agricultural residues. Int J Biol Macromol 120:1216–1224. https://doi.org/10.1016/j.ijbiomac.2018.09.012

Hemmati F, Jafari SM, Taheri RA (2019) Optimization of homogenization-sonication technique for the production of cellulose nanocrystals from cotton linter. Int J Biol Macromol 137:374–381

Hu Z, Patten T, Pelton R, Cranston ED (2015) Synergistic stabilization of emulsions and emulsion gels with water-soluble polymers and cellulose nanocrystals. ACS Sustain Chem Eng 3:1023–1031. https://doi.org/10.1021/acssuschemeng.5b00194

Huang X et al (2017) Dilute alkali and hydrogen peroxide treatment of microwave liquefied rape straw residue for the extraction of cellulose nanocrystals. J Nanomater 2017:4049061/4049061–4049061/4049069. https://doi.org/10.1155/2017/4049061

Jiang F, Esker AR, Roman M (2010) Acid-catalyzed and solvolytic desulfation of H2SO4-hydrolyzed cellulose nanocrystals. Langmuir 26:17919–17925. https://doi.org/10.1021/la1028405

Jin LQ, Li WG, Xu QH, Sun QC (2015) Amino-functionalized nanocrystalline cellulose as an adsorbent for anionic dyes. Cellulose 22:2443–2456

Kaboorani A, Riedl B (2015) Surface modification of cellulose nanocrystals (CNC) by a cationic surfactant. Ind Crops Prod 65:45–55

Kalantari M, Du R, Ayranci C, Boluk Y (2018) Effects of interfacial interactions and interpenetrating brushes on the electrospinning of cellulose nanocrystals-polystyrene fibers. J Colloid Interface Sci 528:419–430

Kalashnikova I, Bizot H, Cathala B, Capron I (2011) New pickering emulsions stabilized by bacterial cellulose nanocrystals. Langmuir 27:7471–7479

Kim H, Youn JR, Song YS (2018) Eco-friendly flame retardant nanocrystalline cellulose prepared via silylation. Nanotechnology 29:455702

Ko SW, Soriano JPE, Lee JY, Unnithan AR, Park CH, Kim CS (2018) Nature derived scaffolds

for tissue engineering applications: design and fabrication of a composite scaffold incorporating chitosan-g-d, l-lactic acid and cellulose nanocrystals from Lactuca sativa L. cv green leaf. Int J Biol Macromol 110:504–513

Koshani R, Madadlou A (2018) A viewpoint on the gastrointestinal fate of cellulose nanocrystals. Trends Food Sci Technol 71:268–273

Koshani R, van de Ven TGM, Madadlou A (2018) Characterization of carboxylated cellulose nanocrytals isolated through catalyst-assisted H2O2 oxidation in a one-step procedure. J Agric Food Chem 66:7692–7700. https://doi.org/10.1021/acs.jafc.8b00080

Kumar A, Rao KM, Han SS (2018) Mechanically viscoelastic nanoreinforced hybrid hydrogels composed of polyacrylamide, sodium carboxymethylcellulose, graphene oxide, and cellulose nanocrystals. Carbohyd Polym 193:228–238

Lazko J et al (2016) Acid-free extraction of cellulose type I nanocrystals using Bronsted acid-type ionic liquids. Nanocomposites 2:65–75. https://doi.org/10.1080/20550324.2016.1199410

Lei WQ et al (2018) Cellulose nanocrystals obtained from office waste paper and their potential application in PET packing materials. Carbohyd Polym 181:376–385

Li J, Wan Y, Li L, Liang H, Wang J (2009) Preparation and characterization of 2,3-dialdehyde bacterial cellulose for potential biodegradable tissue engineering scaffolds. Mater Sci Eng, C 29:1635–1642. https://doi.org/10.1016/j.msec.2009.01.006

Li Y, Liu Y, Chen W, Wang Q, Liu Y, Li J, Yu H (2016) Facile extraction of cellulose nanocrystals from wood using ethanol and peroxide solvothermal pretreatment followed by

ultrasonic nanofibrillation. Green Chem 18:1010–1018. https://doi.org/10.1039/C5GC02576A

Li B, Zhang Y, Wu C, Guo B, Luo Z (2018a) Fabrication of mechanically tough and self-recoverable nanocomposite hydrogels from polyacrylamide grafted cellulose nanocrystal and poly(acrylic acid). Carbohyd Polym 198:1–8

Li L, Tao H, Wu B, Zhu G, Li K, Lin N (2018b) Triazole endgrafting on cellulose nanocrystals for water-redispersion improvement and reactive enhancement to nanocomposites. ACS Sustain Chem Eng 6:14888–14900. https://doi.org/10.1021/acssuschemeng.8b03407

Ling Z et al (2018) Structural variations of cotton cellulose nanocrystals from deep eutectic solvent treatment: micro and nano scale. Cellulose 26:861–876. https://doi.org/10.1007/s10570-018-2092-9

Liu YF, Wang HS, Yu G, Yu QX, Li B, Mu XD (2014) A novel approach for the preparation of nanocrystalline cellulose by using phosphotungstic acid. Carbohyd Polym 110:415–422

Liu C et al (2016) Properties of nanocellulose isolated from corncob residue using sulfuric acid, formic acid, oxidative and mechanical methods. Carbohydr Polym 151:716–724. https://doi.org/10.1016/j.carbpol.2016.06.025

Liu Z, Li X, Xie W, Deng H (2017) Extraction, isolation and characterization of nanocrystalline cellulose from industrial kelp (Laminaria japonica) waste. Carbohyd Polym 173:353–359

Liu F, Zheng J, Huang C-H, Tang C-H, Ou S-Y (2018a) Pickering high internal phase emulsions stabilized by proteincovered cellulose nanocrystals. Food Hydrocolloids 82:96–105

Liu L, Hu Z, Sui X, Guo J, Cranston ED, Mao Z (2018b) Effect of counterion choice on the

stability of cellulose nanocrystal pickering emulsions. Ind Eng Chem Res 57:7169–7180. https://doi.org/10.1021/acs.iecr.8b01001

Liu X et al (2018c) Hydrothermal synthesis of cellulose nanocrystal-grafted-acrylic acid aerogels with superabsorbent properties. Polymers 10:1168. https://doi.org/10.3390/polym 10101168

Lorenz M, Sattler S, Reza M, Bismarck A, Kontturi E (2017) Cellulose nanocrystals by acid vapor: towards more effortless isolation of cellulose nanocrystals. Faraday Discuss 202:315–330. https://doi.org/10.1039/C7FD00053G

Lu TH, Li Q, Chen WS, Yu HP (2014) Composite aerogels based on dialdehyde nanocellulose and collagen for potential applications as wound dressing and tissue engineering scaffold. Compos Sci Technol 94:132–138

Lu T et al (2017) Cellulose nanocrystals/polyacrylamide composites of high sensitivity and cycling performance to gauge humidity. ACS Appl Mater Interfaces 9:18231–18237. https://doi.org/10.1021/acsami.7b04590

Luzi F et al (2019) Valorization and extraction of cellulose nanocrystals from North African grass: ampelodesmos mauritanicus (Diss). Carbohyd Polym 209:328–337

Ma Q, Wang L (2016) Preparation of a visual pH-sensing film based on tara gum incorporating cellulose and extracts from grape skins. Sens Actuators, B 235:401–407. https://doi. org/10.1016/j.snb.2016.05.107

Malucelli LC, Lacerda LG, Dziedzic M, Carvalho MAD (2017) Preparation, properties and future perspectives of nanocrystals from agro-industrial residues: a review of recent

research. Rev Environ Sci Biol 16:131–145. https://doi.org/10.1007/s11157-017-9423-4

Mao J, Heck B, Reiter G, Laborie M-P (2015) Cellulose nanocrystals' production in near theoretical yields by 1-butyl-3-methylimidazolium hydrogen sulfate ([Bmim]HSO4)—mediated hydrolysis. Carbohydr Polym 117:443–451. https://doi.org/10.1016/j.carbpol. 2014.10. 001

Mao J, Abushammala H, Pereira LB, Laborie M-P (2016) Swelling and hydrolysis kinetics of Kraft pulp fibers in aqueous 1-butyl-3-methylimidazolium hydrogen sulfate solutions. Carbohydr Polym 153:284–291. https://doi.org/10.1016/j.carbpol.2016.07.092

Miao J, Yu Y, Jiang Z, Zhang L (2016) One-pot preparation of hydrophobic cellulose nanocrystals in an ionic liquid. Cellulose 23:1209–1219. https://doi.org/10.1007/s10570-016-0864-7

Mohamed MA, Salleh WNW, Jaafar J, Asri SEAM, Ismail AF (2015) Physicochemical properties of "green" nanocrystalline cellulose isolated from recycled newspaper. RSC Adv 5:29842–29849. https://doi.org/10.1039/c4ra17020b

Monika Dhar P, Katiyar V (2017) Thermal degradation kinetics of polylactic acid/acid fabricated cellulose nanocrystal based bionanocomposites. Int J Biol Macromol 104:827–836. https://doi.org/10.1016/j.ijbiomac.2017.06.039

Nagarajan KJ, Balaji AN, Ramanujam NR (2018) Isolation and characterization of cellulose nanocrystals from Saharan aloe vera cactus fibers. Int J Polym Anal Charact. https://doi. org/10.1080/1023666x.2018.1478366

Ngwabebhoh FA, Erdem A, Yildiz U (2018) A design optimization study on synthesized

nanocrystalline cellulose, evaluation and surface modification as a potential biomaterial for prospective biomedical applications. Int J Biol Macromol 114:536–546

Ogundare SA, Moodley V, van Zyl WE (2017) Nanocrystalline cellulose isolated from discarded cigarette filters. Carbohyd Polym 175:273–281

Orue A, Santamaria-Echart A, Eceiza A, Pen˜a-Rodriguez C, Arbelaiz A (2017) Office waste paper as cellulose nanocrystal source. J Appl Polym Sci. https://doi.org/10. 1002/app.45257

Oun AA, Rhim JW (2016) Isolation of cellulose nanocrystals from grain straws and their use for the preparation of carboxymethyl cellulose-based nanocomposite films. Carbohyd Polym 150:187–200

Oun AA, Rhim JW (2018) Isolation of oxidized nanocellulose from rice straw using the ammonium persulfate method. Cellulose 25:2143–2149

Pang Z, Wang P, Dong C (2018) Ultrasonic pretreatment of cellulose in ionic liquid for efficient preparation of cellulose nanocrystals. Cellulose 25:7053–7064. https://doi.org/10.1007/s10570-018-2070-2

Peng B, Tang J, Wang P, Luo J, Xiao P, Lin Y, Tam KC (2018) Rheological properties of cellulose nanocrystal-polymeric systems. Cellulose 25:3229–3240. https://doi.org/10.1007/s10570-018-1775-6

Perumal AB, Sellamuthu PS, Nambiar RB, Sadiku ER (2018) Development of polyvinyl alcohol/chitosan bio-nanocomposite films reinforced with cellulose nanocrystals isolated from rice straw. Appl Surf Sci 449:591–602. https://doi.org/10.1016/j.apsusc.2018.01.022

Peyre J, Paakkonen T, Reza M, Kontturi E (2015) Simultaneous preparation of cellulose

nanocrystals and micron-sized porous colloidal particles of cellulose by TEMPO-mediated oxidation. Green Chem 17:808–811. https://doi.org/10.1039/C4GC02001D

Plappert SF et al (2018) Transparent, flexible, and strong 2,3- dialdehyde cellulose films with high oxygen barrier properties. Biomacromol 19:2969–2978. https://doi.org/10.1021/acs.biomac.8b00536

Poaty B, Vardanyan V, Wilczak L, Chauve G, Riedl B (2014) Modification of cellulose nanocrystals as reinforcement derivatives for wood coatings. Prog Org Coat 77:813–820

Prado KS, Spinace MAS (2018) Isolation and characterization of cellulose nanocrystals from pineapple crown waste and their potential uses. Int J Biol Macromol 122:410–416. https://doi.org/10.1016/j.ijbiomac.2018.10.187

Qiao C, Chen G, Zhang J, Yao J (2016) Structure and rheological properties of cellulose nanocrystals suspension. Food Hydrocolloids 55:19–25. https://doi.org/10.1016/j.foodhyd.2015.11.005

Rahman NHA, Chieng BW, Ibrahim NA, Rahman NA (2017) Extraction and characterization of cellulose nanocrystals from tea leaf waste fibers. Polymers-Basel 9:588. https://doi.org/10.3390/polym9110588

Rampazzo R, Alkan D, Gazzotti S, Ortenzi MA, Piva G, Piergiovanni L (2017) Cellulose nanocrystals from lignocellulosic raw materials, for oxygen barrier coatings on food packaging films. Packag Technol Sci 30:645–661. https://doi.org/10.1002/pts.2308

Reddy KO, Zhang JM, Zhang J, Rajulu AV (2014) Preparation and properties of self-reinforced cellulose composite films from Agave microfibrils using an ionic liquid. Carbohyd Polym

114:537–545

Roberts R, Gettz K, Stebounova LV, Shatkin JA, Peters T, Foster EJ (2019) Collection of airborne ultrafine cellulose nanocrystals by impinger with an efficiency mimicking deposition in the human respiratory system. J Occup Environ Hyg 16:141–150. https://doi.org/10.1080/15459624.2018.1540876

Roman M, Winter WT (2004) Effect of sulfate groups from sulfuric acid hydrolysis on the thermal degradation behavior of bacterial cellulose. Biomacromol 5:1671–1677. https://doi.org/10.1021/bm034519+

Rovera C, Ghaani M, Santo N, Trabattoni S, Olsson RT, Romano D, Farris S (2018) Enzymatic hydrolysis in the green production of bacterial cellulose nanocrystals. ACS Sustain Chem Eng 6:7725–7734. https://doi.org/10.1021/acssuschemeng.8b00600

Sadasivuni KK, Ponnamma D, Ko H-U, Kim HC, Zhai L, Kim J (2016) Flexible NO2 sensors from renewable cellulose nanocrystals/iron oxide composites. Sens Actuators, B 233:633–638. https://doi.org/10.1016/j.snb.2016.04.134

Saha D, Bhattacharya S (2010) Hydrocolloids as thickening and gelling agents in food: a critical review. J Food Sci Technol 47:587–597. https://doi.org/10.1007/s13197-010-0162-6

Salari M, Sowti Khiabani M, Rezaei Mokarram R, Ghanbarzadeh B, Samadi Kafil H (2018) Preparation and characterization of cellulose nanocrystals from bacterial cellulose produced in sugar beet molasses and cheese whey media. Int J Biol Macromol 122:280–288. https://doi.org/ 10.1016/j.ijbiomac.2018.10.136

Shaheen TI, Fouda A (2018) Green approach for one-pot synthesis of silver nanorod using cellulose nanocrystal and their cytotoxicity and antibacterial assessment. Int J Biol Macromol 106:784–792

Shang Q, Liu C, Hu Y, Jia P, Hu L, Zhou Y (2018) Bio-inspired hydrophobic modification of cellulose nanocrystals with castor oil. Carbohyd Polym 191:168–175

Singhsa P, Narain R, Manuspiya H (2018) Bacterial cellulose nanocrystals (BCNC) preparation and characterization from three bacterial cellulose sources and development of functionalized BCNCs as nucleic acid delivery systems. ACS Applied Nano Mater 1:209–221

Siqueira GA, Dias IKR, Arantes V (2019) Exploring the action of endoglucanases on bleached eucalyptus kraft pulp as potential catalyst for isolation of cellulose nanocrystals. Int J Biol Macromol 133:1249–1259

Sirvio JA, Kolehmainen A, Visanko M, Liimatainen H, Niinimaki J, Hormi OEO (2014) Strong, self-standing oxygen barrier films from nanocelluloses modified with regioselective oxidative treatments. ACS Appl Mater Interfaces 6:14384–14390

Song M, Yu H, Gu J, Ye S, Zhou Y (2018a) Chemical crosslinked polyvinyl alcohol/cellulose nanocrystal composite films with high structural stability by spraying Fenton reagent as initiator. Int J Biol Macromol 113:171–178

Song W, Lee J-K, Gong MS, Heo K, Chung W-J, Lee BY (2018b) Cellulose nanocrystal-based colored thin films for colorimetric detection of aldehyde gases. ACS Appl Mater Interfaces 10:10353–10361. https://doi.org/10.1021/acsami.7b19738

Souza VC, Niehues E, Quadri MGN (2016) Development and characterization of chitosan bionanocomposites containing oxidized cellulose nanocrystals. J Appl Polym Sci. https://doi.org/10.1002/app.43033

Tan XY, Abd Hamid SB, Lai CW (2015) Preparation of high crystallinity cellulose nanocrystals (CNCs) by ionic liquid solvolysis. Biomass Bioenergy 81:584–591. https://doi.org/10.1016/j.biombioe.2015.08.016

Tang LR, Huang B, Yang NT, Li T, Lu QL, Lin WY, Chen XR (2013) Organic solvent-free and efficient manufacture of functionalized cellulose nanocrystals via one-pot tandem reactions. Green Chem 15:2369–2373

Tang LR, Li T, Zhuang SY, Lu QL, Li PF, Huang B (2016) Synthesis of pH-sensitive fluorescein grafted cellulose nanocrystals with an amino acid spacer. ACS Sustain Chem Eng 4:4842–4849. https://doi.org/10.1021/acssuschemeng.6b01124

Tang Q, Pan D, Sun Y, Cao J, Guo Y (2017) Preparation, characterization and antimicrobial activity of sodium alginate nanobiocomposite films incorporated with epolylysine and cellulose nanocrystals. J Food Process Preserv 41:e13120

Tang CX, Spinney S, Shi ZQ, Tang JT, Peng BL, Luo JH, Tam KC (2018a) Amphiphilic cellulose nanocrystals for enhanced pickering emulsion stabilization. Langmuir 34:12897–12905

Tang LR, Lin FC, Li T, Cai ZH, Hong BY, Huang B (2018b) Design and synthesis of functionalized cellulose nanocrystals-based drug conjugates for colon-targeted drug delivery. Cellulose 25:4525–4536

Tang Y, Zhang X, Zhao R, Guo D, Zhang J (2018c) Preparation and properties of chitosan/guar gum/nanocrystalline cellulose nanocomposite films. Carbohydr Polym 197:128–136

Tavakolian M, Okshevsky M, van de Ven TGM, Tufenkji N (2018) Developing antibacterial nanocrystalline cellulose using natural antibacterial agents. ACS Appl Mater Interfaces 10:33827–33838. https://doi.org/10.1021/acsami.8b08770

Toncheva A, Khelifa F, Paint Y, Voue M, Lambert P, Dubois P, Raquez J-M (2018) Fast IR-actuated shape-memory polymers using in situ silver nanoparticle-grafted cellulose nanocrystals. ACS Appl Mater Interfaces 10:29933–29942

Williams DF (1999) The Williams dictionary of biomaterials. Liverpool University Press, Liverpool

Wu H et al (2018a) Regenerated chitin fibers reinforced with bacterial cellulose nanocrystals as suture biomaterials. Carbohydr Polym 180:304–313. https://doi.org/10.1016/j.carbpol.2017.10.022

Wu W, Song R, Xu Z, Jing Y, Dai H, Fang G (2018b) Fluorescent cellulose nanocrystals with responsiveness to solvent polarity and ionic strength. Sens Actuators, B 275:490–498. https://doi.org/10.1016/j.snb.2018.07.085

Xiao Y, Liu Y, Wang X, Li M, Lei H, Xu H (2019) Cellulose nanocrystals prepared from wheat bran: characterization and cytotoxicity assessment. Int J Biol Macromol 140:225–233. https://doi.org/10.1016/j.ijbiomac.2019.08.160

Yarbrough JM et al (2017) Multifunctional cellulolytic enzymes outperform processive fungal cellulases for coproduction of nanocellulose and biofuels. ACS Nano 11:3101–3109

Ye HM, Wang CS, Zhang ZZ, Yao SF (2018a) Effect of cellulose nanocrystals on the crystallization behavior and enzymatic degradation of poly(butylene adipate). Carbohyd Polym 189:99–106

Ye SN, Yu HY, Wang DC, Zhu JY, Gu JP (2018b) Green acidfree one-step hydrothermal ammonium persulfate oxidation of viscose fiber wastes to obtain carboxylated spherical cellulose nanocrystals for oil/water Pickering emulsion. Cellulose 25:5139–5155

Yin Y, Ma J, Tian X, Jiang X, Wang H, Gao W (2018) Cellulose nanocrystals functionalized with amino-silane and epoxypoly(ethylene glycol) for reinforcement and flexibilization of poly(lactic acid): material preparation and compatibility mechanism. Cellulose 25:6447–6463. https://doi.org/10.1007/s10570-018-2033-7

Yousefi N, Wong KKW, Hosseinidoust Z, Soerensen HO, Bruns S, Zheng Y, Tufenkji N (2018) Hierarchically porous, ultra-strong reduced graphene oxide-cellulose nanocrystal sponges for exceptional adsorption of water contaminants. Nanoscale 10:7171–7184

Yu H-Y, Yang X-Y, Lu F-F, Chen G-Y, Yao J-M (2016) Fabrication of multifunctional cellulose nanocrystals/ poly(lactic acid) nanocomposites with silver nanoparticles by spraying method. Carbohyd Polym 140:209–219

Yu HY, Zhang H, Song ML, Zhou Y, Yao JM, Ni QQ (2017) From cellulose nanospheres, nanorods to nanofibers: various aspect ratio induced nucleation/reinforcing effects on polylactic acid for robust-barrier food packaging. ACS Appl Mater Interfaces 9:43920–43938

Yu Z, Sun L, Wang W, Zeng W, Mustapha A, Lin M (2018) Soy protein-based films

incorporated with cellulose nanocrystals and pine needle extract for active packaging. Ind Crops Prod 112:412–419. https://doi.org/10.1016/j.indcrop.2017.12.031

Yuan Z, Wen Y (2018) Enhancement of hydrophobicity of nanofibrillated cellulose through grafting of alkyl ketene dimer. Cellulose (Dordrecht, Netherlands):Ahead of Print

Yuan W, Wang C, Lei S, Chen J, Lei S, Li Z (2018) Ultraviolet light-, temperature- and pH-responsive fluorescent sensors based on cellulose nanocrystals. Polym Chem 9:3098–3107. https://doi.org/10.1039/c8py00613j

Zhang K, Sun P, Liu H, Shang S, Song J, Wang D (2016) Extraction and comparison of carboxylated cellulose nanocrystals from bleached sugarcane bagasse pulp using two different oxidation methods. Carbohydr Polym 138:237–243. https://doi.org/10.1016/j.carbpol.2015.11.038

Zhang Y, Karimkhani V, Makowski B, Samaranayake G, Rowan S (2017) Nanoemulsions and nanolatexes stabilized by hydrophobically functionalized cellulose nanocrystals. Macromolecules 16:6032–6042. https://doi.org/10.1021/acs.macromol.7b00982

Zhang Y-J, Ma X-Z, Gan L, Xia T, Shen J, Huang J (2018a) Fabrication of fluorescent cellulose nanocrystal via controllable chemical modification towards selective and quantitative detection of Cu(II) ion. Cellulose 25:5831–5842. https://doi.org/10.1007/s10570-018-1995-9

Zhang Y, Liu Y, Li R, Ren X, Huang T-S (2018b) Preparation and characterization of antimicrobial films based on nanocrystalline cellulose. J Appl Polym Sci. https://doi.org/10.1002/app.47101

Zhao YD, Zhang YJ, Lindstrom ME, Li JB (2015) Tunicate cellulose nanocrystals: preparation, neat films and nanocomposite films with glucomannans. Carbohyd Polym 117:286–296

Zhao G, Wang F, Lang X, He B, Li J, Li X (2017) Facile one-pot fabrication of cellulose nanocrystals and enzymatic synthesis of its esterified derivative in mixed ionic liquids. RSC Adv 7:27017–27023. https://doi.org/10.1039/C7RA02570J

Zhou L et al (2018) One-pot preparation of carboxylated cellulose nanocrystals and their liquid crystalline behaviors. ACS Sustain Chem Eng 6:12403–12410. https://doi.org/10.1021/acssuschemeng.8b02926

Zulnazri Z, Anjana F, Roesyadi A (2017) Temperature effect of crystalinity in cellulose nanocrystal from oil palm empty fruit bunch (OPEFB) using sonication-hydrothermal methods. J Pure Appl Chem Res 6:14–21. https://doi.org/10.21776/ub.jpacr.2017.006.01.296

Connecting Text

Chapter 2 summarized the recent work on the extraction and modification of CNCs from various feedstocks and the food-related applications of CNCs. A new trend to use waste biomass as an alternative source of CNCs was pointed out. In chapter 3, the possibility to directly extract CNCs from textile waste was explored, and the reinforcing effect of CNCs on soy protein isolate (SPI) films was investigated. Firstly, two different methods, namely sulfuric acid hydrolysis and three-step oxidization, were used to extract CNCs. Secondly, the morphology and structure of CNCs from different extraction methods were characterized and compared by transmission electron microscopy, Fourier-transform infrared spectroscopy, and X-ray diffraction. Thirdly, the effects of CNCs on the performance of SPI films were studied.

Chapter 3. Cellulose Nanocrystals Derived from Textile Waste through Acid Hydrolysis and Oxidation as Reinforcing Agent of Soy Protein Film

3.1. Abstract

More than 10 million tons of textile waste are disposed through landfill every year in North America. The disposal of textile waste via landfill or incineration causes environmental problems and represents a waste of useful resources. In this work, we explored the possibility to directly extract cellulose nanocrystals (CNCs) from untreated textile waste through two methods, namely sulfuric acid hydrolysis and three-step oxidization. CNCs with cellulose I_β crystalline structure and rod-like shape were successfully obtained. The aspect ratios of CNCs prepared from acid hydrolysis and oxidization were 10.00 ± 3.39 and 17.10 ± 12.85, respectively. Their application as reinforcing agent of soybean protein isolate (SPI) film was evaluated. With the addition of 20% CNCs, the composite film maintained the high transparency, while their water vapor barrier property, tensile strength, and Young's modulus were significantly improved. This research demonstrates a promising approach to recycle textile waste, and more value-added applications based on the derived CNCs could be expected.

3.2. Introduction

Today, there is a concern about the rapid increase in textile waste, which leads to numerous disposal problems and governance issues [1]. According to the statement of Waste Reduction Week in Canada [2], textile waste has shown a dramatic increase in the past two decades, and about 10 million tons of clothing are disposed of through landfill every year. It was reported that only 20% of post-consumer clothes were recycled, but without appropriate processing [3]. Therefore, in one aspect, some efforts, such as implementing circular economy principles, are needed to reduce textile waste and achieve sustainable development; on the other hand, it is

necessary to find a promising approach to recycle textile waste into valuable products. For instance, Çay et al. converted textile waste into biochar by low-temperature carbonization, and applied the derived biochar to cotton fabrics, which possessed the odor masking function and high thermo-physiological comfort [4]. Besides, Xu et al. derived char-based adsorbents from textile waste by a one-step low-temperature pyrolysis approach with iron salts, and the prepared adsorbents owned adequate adsorption capacity of Cr(VI) removal [5]. However, more efforts are required to promote the recycling of textile waste.

One of the most consumed fibers in the textile industry is cotton, which contains more than 90% of cellulose. Therefore, it was supposed that waste cotton fibers could act as the new source of cellulose nanocrystals (CNCs). CNCs have received considerable interest over the past decades owing to their unique mechanical properties. They possess high crystallinity and large specific surface area [6]. Additionally, CNCs contain abundant hydroxyl groups, contributing to the high potential for modifications and applications. CNCs could be extracted from three types of raw materials: plant, animal, and microorganism, where sulfuric acid (H_2SO_4) hydrolysis is the most frequently used method [7]. For instance, Favier et al. successfully used acid hydrolysis to extract CNCs from tunicate and applied them to reinforce polymer nanocomposites [8]. Darpentigny et al. also obtained CNCs with a high aspect ratio of 63 from tunicate by H_2SO_4 hydrolysis, and the prepared tunicate CNC-based cryogels presented high mechanical resistance and stiffness (Young's modulus of 138 KPa) [9]. Wood was another common raw material of CNCs. The rod-shaped CNCs with 11.4 nm diameter and 153.2 nm length were obtained from wood via acid hydrolysis [10]. Furthermore, Ambrosio-Martin et al. obtained

CNCs, with a length of around 600 nm and diameter of around 22 nm, from bacteria through H_2SO_4 hydrolysis, which were used to improve the barrier and mechanical properties of polylactide (PLA) [11]. Recently, a new trend has been found to prepare CNCs from waste materials. For example, Jiang et al. successfully extracted CNCs from wastepaper fibers by acid hydrolysis. The obtained CNCs had a rod-like structure with the crystallinity of 77.56% [12]. Similar rod-like CNCs were extracted from the disposed paper cup through citric acid hydrolysis and were applied to reinforce composite films [13].

In addition to acid hydrolysis, oxidation methods have been developed recently, which could introduce anionic groups to CNCs for better performance [14–16]. Leung et al. developed an approach to prepare carboxylic CNCs using ammonium persulfate as oxidant. The results indicated that the presence of carboxylic acid groups on CNC surface provided active sites for further modification, such as protein/enzyme immobilization. Additionally, carboxylic CNC offered an opportunity for tuning hydrophobicity by conjugation of the carboxyl groups with pertinent molecules [17]. TEMPO, (2,2,6,6-Tetramethylpiperidin-1-yl)oxyl, is another widely used radical for oxidizing CNCs, which could selectively oxidize the primary alcohol groups of CNCs into carboxyl groups. For example, Liu et al. used TEMPO-mediated oxidation to prepare CNCs with a rod-like morphology (diameter of 2–4 nm and length of 20-50 nm), higher surface charge, and better redispersibility [18]. Recently, a three-step oxidation method has been developed to introduce more anionic groups for better dispersability and further modifications. The first step was performed by periodate oxidation, resulting in partial 2.3-dialdehyde CNCs. The dialdehyde CNCs were then treated with chlorite oxidation to converse

dialdehyde groups into dicarboxylic groups. The third step was TEMPO oxidation, and the C-6 hydroxyl groups were oxidized into carboxyl groups [19].

It was noticed that Wang et al. reported the extraction of CNCs from waste cotton cloth by a series of pre-treatments and a mixed acid solution [20]. However, the application of the obtained CNCs has not been evaluated. Therefore, the current work aims to explore the possibility to directly extract CNCs from untreated textile waste through two different methods, namely sulfuric acid hydrolysis and three-step oxidization. The morphology and structure of CNCs were characterized by transmission electron microscopy (TEM), Fourier-transform infrared spectroscopy (FT-IR), and X-ray diffraction (XRD). Moreover, soy protein isolate (SPI) was selected as the model of biodegradable materials. SPI is the major component of soybean, and various applications such as adhesives, plastics, and binders have been suggested in recent years. However, SPI-based materials suffer from their poor water resistance and low strength [21]. Therefore, the effects of CNCs derived from textile waste on the optical, water vapor barrier, and mechanical properties of SPI films were studied.

3.3. Materials and Methods

3.3.1. Materials

Waste cotton clothes were kindly provided by Renaissance (Montreal, QC Canada), and soybean protein isolate (SPI) was provided by Cargill (Minneapolis, MN, USA). Hydrogen peroxide (H_2O_2), sodium dihydrogen phosphate (NaH_2PO_4), and disodium hydrogen phosphate (Na_2HPO_4) were purchased from Fisher Scientific (Ottawa, ON, Canada) and used as received. Reagent alcohol (95%) was obtained from the RICCA Chemical company (Arlington, VA,

USA). Sulfuric acid (H_2SO_4), and sodium periodate ($NaIO_4$), sodium chloride (NaCl), ethylene glycol, sodium chlorite ($NaClO_2$), sodium hypochlorite (NaClO), sodium hydroxide (NaOH), glycerol, and (2,2,6,6-Tetramethylpiperidin-1-yl)oxyl (TEMPO) were purchased from Sigma-Aldrich (Oakville, ON, Canada) and used without further treatment.

3.3.2. Extraction of CNCs

Sulfuric acid hydrolysis. No chemical pretreatment was performed before extraction, and CNCs were separated by sulfuric acid hydrolysis as described by Ko et al. [22]. In brief, cotton clothes (5.00 g) were mixed with 60 wt % H_2SO_4 solution (100.00 g) and stirred for 1 h at 25 °C. Then, the suspension was diluted with 1 L cold water to stop the hydrolysis. CNCs were washed three times with distilled water followed by freeze-drying and coded as HCNCs.

Three-step oxidization. Oxidized CNCs were prepared via a modified method of Yang et al. [23]. Firstly, cotton clothes (3.00 g) were added to the solution of 3.33 g $NaIO_4$, 19.50 g NaCl, and 300 mL distilled water. The mixture was stirred at 25 °C for 36 h under the prevention of light. After that, the reaction was ended by adding ethylene glycol to quench the residual periodate, and the oxidized fibers were washed thoroughly with distilled water by filtration. Secondly, the oxidized fibers were mixed with 3.56 g $NaClO_2$, 14.60 g NaCl, 3.30 g H_2O_2, and 250 mL distilled water, and the mixture was stirred at 25 °C for 24 h. Then, the suspension was washed thoroughly with a water–ethanol solution and freeze-dried. Thirdly, 1.00 g of chlorite oxidized sample, 0.0016 g of TEMPO, 1.13 g of $NaClO_2$, and 90 mL of phosphate buffer (pH 6.8) were mixed and stirred in the heated water bath. After the temperature reached 50 °C, 250 μL NaClO (diluted with 10mL phosphate buffer) was added to the mixture. The translucent

suspension was obtained after 48 h, followed by washing with a water-ethanol solution and freeze-drying. The resultant sample was coded as TCNCs. The yield (%) of CNCs was calculated using a gravimetric method in terms of Equation (1):

$$\text{Yield} = \frac{w_2}{w_1} \quad (1)$$

where w_2 is the weight of freeze-dried CNCs, and w_1 is the weight of cotton clothes [24].

3.3.3. Preparation of CNC/SPI Films

Soy protein isolate (SPI) films containing HCNCs and TCNCs were prepared by the solvent casting method [25], as illustrated in Figure 3.1. Briefly, 0.50 g of SPI was dissolved in 15 mL distilled water under magnetic stirring at 25 °C. Then, 0.30 g of glycerol (as the plasticizer) and 3 mL of NaOH solution (1 wt %) were added to the SPI solution, and the mixture was stirred for 15 min at 50 °C. After that, the desired amounts of CNCs (10% and 20% of SPI dry weight) were added and stirred overnight. The homogeneous solutions were cast on the plastic plate and dried at 25 °C for 24 h. SPI film without the addition of CNCs was prepared as control. All the samples were stored in the desiccator (~40% relative humidity (RH)) before further measurement [26].

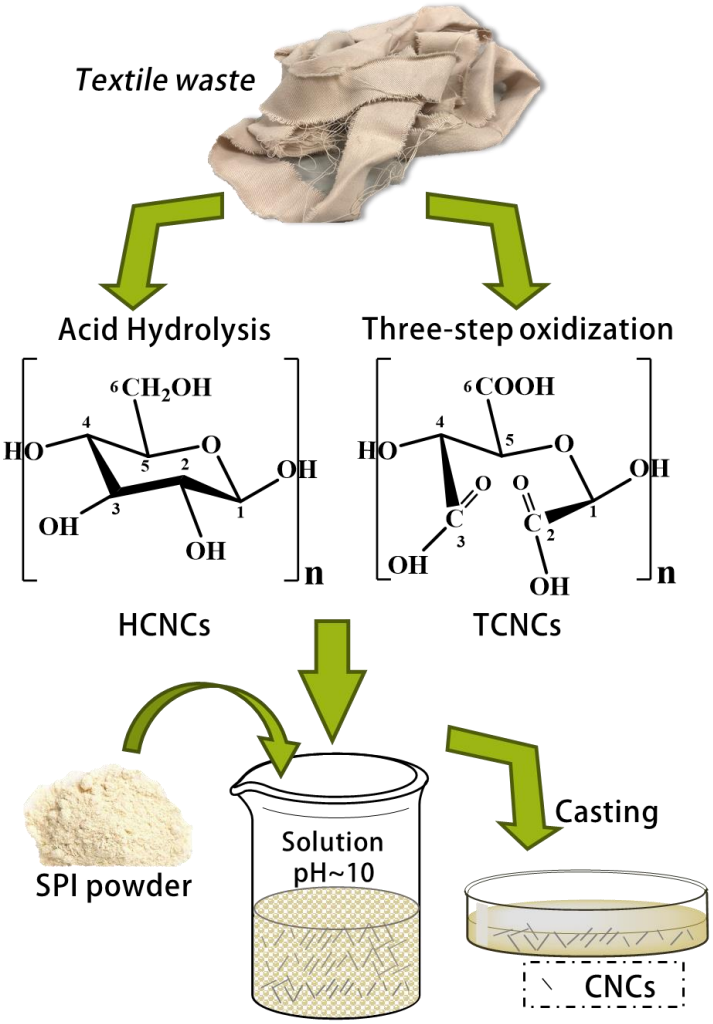

Figure 3.1. Schematic illustration of soy protein isolate (SPI)/cellulose nanocrystal (CNC) composite film preparation.

3.3.4. Characterization

3.3.4.1. Transmission Electron Microscopy (TEM)

The morphology of HCNCs and TCNCs was observed on a transmission electron microscope (TEM, Morgagni 268, Philips-FEI, Hillsboro, OR, USA) at ×110,000 magnification. A small droplet of diluted CNC aqueous suspension was deposited on a polycarbon film supported on a copper grid, and a thin layer was suspended over the holes of the grid. The specimen was dried in air at ambient pressure, and was then imaged on TEM at an accelerating voltage of 80

kV. The dimensions of HCNCs and TCNCs were measured using the ImageJ image analysis software, which is developed by the National Institute of Health (version 1.52a, NIH, Bethesda, MD, USA).

3.3.4.2. X-Ray Diffraction (XRD)

XRD patterns of HCNCs and TCNCs were collected using a Bruker D8 Discover diffractometer (Bruker, Billerica, MA, USA) operating at 40 kV and 40 mA, with a VANTEC detector and Cu-source. The crystallinity index (CrI) was determined by the peak height method [27] in terms of Equation (2):

$$\mathrm{CrI} = \frac{I_{(200)} - I_{am}}{I_{(200)}} \quad (2)$$

where $I_{(200)}$ is the maximum diffraction intensity associated with surface areas of crystalline cellulose, and I_{am} is the diffraction intensity of an amorphous cellulose fraction.

3.3.4.3. Fourier-Transform Infrared Spectroscopy (FT-IR)

FT-IR spectra of HCNCs, TCNCs, and SPI/CNC films were obtained using the Varian Excalibur 3100 FT-IR spectrometer (Varian, Melbourne, VIC, Australia) equipped with an attenuated total reflectance (ATR) accessory (Specac, Orpington, UK). The spectra were collected as the average of 64 scans with a resolution of 4 cm^{-1} and 25 °C, using the empty accessory as blank. The measurements were carried out at 400–4000 cm^{-1} [28].

3.3.4.4. Optical Transmittance Spectra

The optical transmittance of SPI/CNC films (the thickness was about 0.08 mm) was measured via a DU 800 UV/vis spectrophotometer (Beckman Coulter, Brea, CA, USA). The spectra were recoded with air as background.

3.3.4.5. Water Vapor Permeability (WVP)

A gravimetric method was used to determine the WVP of SPI/CNC films [29]. In brief, anhydrous calcium chloride (15 g) was placed at the bottom of a glass jar. After sealing with film sample, the jar was placed in a desiccator filled with saturated sodium chloride solution (75% RH). The weight of the jar was measured periodically at 25 °C. Then, the WVP of SPI/CNC film was determined using Equation (3):

$$\mathrm{WVP} = \frac{\Delta m \times n}{A \times t \times \Delta p} \quad (3)$$

where Δm is the change in jar weight (g), n is the film thickness (m), A is the exposed area of the film (m^2), t is the time (s), and Δp is the partial pressure difference existing between the two sides of film sample (Pa).

3.3.4.6. Mechanical Properties

The tensile strength, elongation at break, and Young's modulus of SPI/CNC films were tested on an eXpert 8612 biaxial testing machine (ADMET, Norwood, MA, USA) at 25 °C according to standard ASTM D882. The dimension of film specimen was 60 mm × 10 mm. The initial grip separation distance was set as 20 mm, and the separation speed was 20 mm/min.

3.3.4.7. Statistical Analysis

The experimental data were presented as the mean of three batches ± SD (standard deviation) [30–32]. Analysis of variance (ANOVA) was applied for the statistical analysis followed by multiple comparison tests via Duncan's multiple-range test, and differences within samples were identified at $p < 0.05$. All analyses were carried out using SPSS statistical software (version 24.0, IBM, New York, NY, USA).

3.4. Results and Discussion

The yields of HCNCs and TCNCs were 90.40% and 60.41%, respectively, which were comparable to those reported values [23,33–36]. Their morphology was observed by transmission electron microscopy (TEM). As shown in Figure 3.2, both of them had a typical rod-like shape, indicating the successful preparation of CNCs without any chemical pre-treatments. Particularly, the length and diameter of HCNCs were around 111.76 ± 38.73 nm and 11.18 ± 2.33 nm, and their aspect ratio was 10.00 ± 3.39. The TCNC samples presented a slightly shorter and thinner rod-like structure (diameter of 5.69 ± 2.08 and length of 97.25 ± 25.18, $p > 0.05$), which might be caused by the harsher reaction conditions during the three-step oxidation [37]. However, the aspect ratio of TCNCs was relatively higher (17.10 ± 12.85, $p > 0.05$). It was known that the higher aspect ratio of CNCs is conducive to a better reinforcing effect, as it increases the interface area and allows a higher load to be transferred within the crystal percolating network [38]. The aspect ratio of TCNCs was also higher than that of the CNC samples extracted from lettuce leaf [22] and comparable to those from cotton linters [39]. Therefore, it was demonstrated that different extraction methods had no significant effect on the morphology of CNCs, but contributed to the different aspect ratio values, which might affect their reinforcement efficiency in composite films [40].

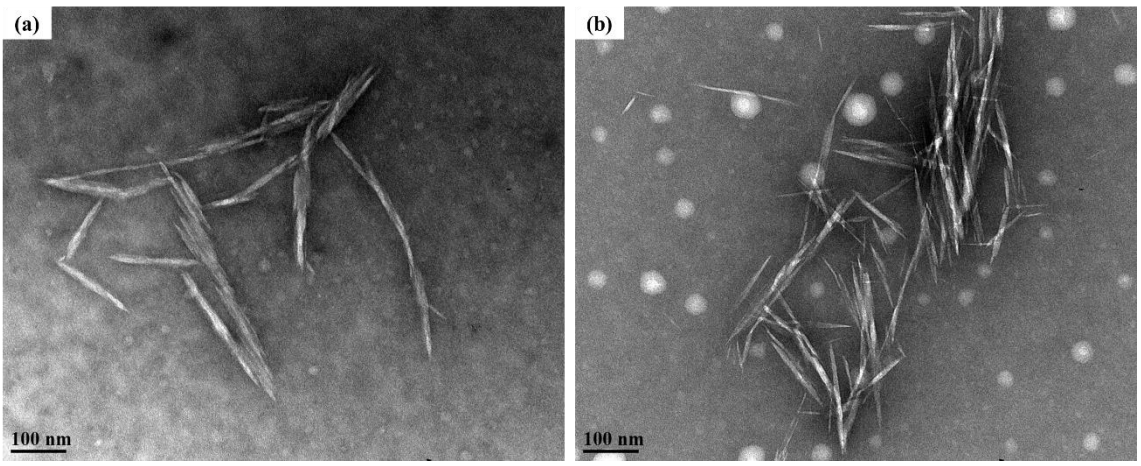

Figure 3.2. Transmission electron microscopy (TEM) images (×110,000 magnification) of HCNCs (a) and TCNCs (b).

X-ray diffraction was used to evaluate the crystalline type and index of textile waste and CNCs. As shown in Figure 3.3, all the samples exhibited the same diffraction peaks at 15.0°, 16.4°, and 22.5°, corresponding to the $(1\bar{1}0)$, (110), and (200) lattice planes of cellulose I_β, respectively [41]. This indicated that sulfuric acid hydrolysis and three-step oxidation did not alter the crystalline structure of cellulose [24]. However, the crystallinity index of TCNCs and HCNCs was 89.05% and 89.99%, respectively, which showed a remarkable increase compared with that of textile waste (73.42%). This was because the amorphous region of cotton fibers was effectively removed during CNC extraction.

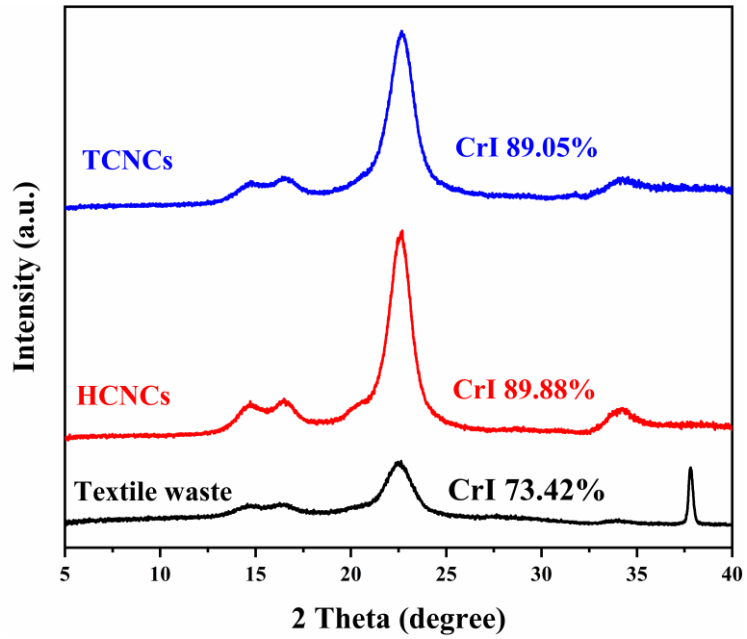

Figure 3.3. X-ray diffraction (XRD) patterns and crystallinity index (CrI) of textile waste, HCNCs, and TCNCs.

The FT-IR spectra of TCNCs and HCNCs are shown in Figure 3.4 (a). Both of them exhibited similar characteristic absorption peaks. For example, the broad peak at 3336 cm^{-1} was related to the stretching vibration of OH groups and the inter-chain hydrogen bonds [42]. The peak at 2900 cm^{-1} was attributed to the stretching vibration of C–H, and the peaks at 1427 cm^{-1}, 1371 cm^{-1}, and 1315 cm^{-1} were attributed to the bending of C–H, CH_2, and OH, respectively, which were typical for polysaccharides. The peak at 1160 cm^{-1} was characteristic of the asymmetric vibration of (C–O–C), and those at 1055 cm^{-1} and 1031 cm^{-1} were associated with C–O–C pyranose ring (antisymmetric in phase ring) stretching vibration [43]. The peak at 893 cm^{-1} was characteristic of cellulose with β-glycoside bonds of glucose ring [36]. Especially, the characteristic peaks of cellulose I_β appeared at 3290 and 3336 cm^{-1}, and the peak at 1427 cm^{-1} is attributable to the crystalline absorption [44]. The absorbance ratio of the bands at 1427 and 893 cm^{-1} (A_{1427}/A_{893}), adopted as the crystallinity index, is closely related to the portion of the

cellulose I structure [45]. Despite the use of different extraction methods, the ratios of A_{1427}/A_{893} were comparable, which indicated the similar crystallinity [46]. This result was in accordance with that of the XRD test. It was noticed that the only new peak of TCNCs existed at 1616 cm^{-1}, which was assigned to the asymmetric vibration of –COO–. This indicated the successful extraction of CNCs with carboxyl groups by three-step oxidization [47].

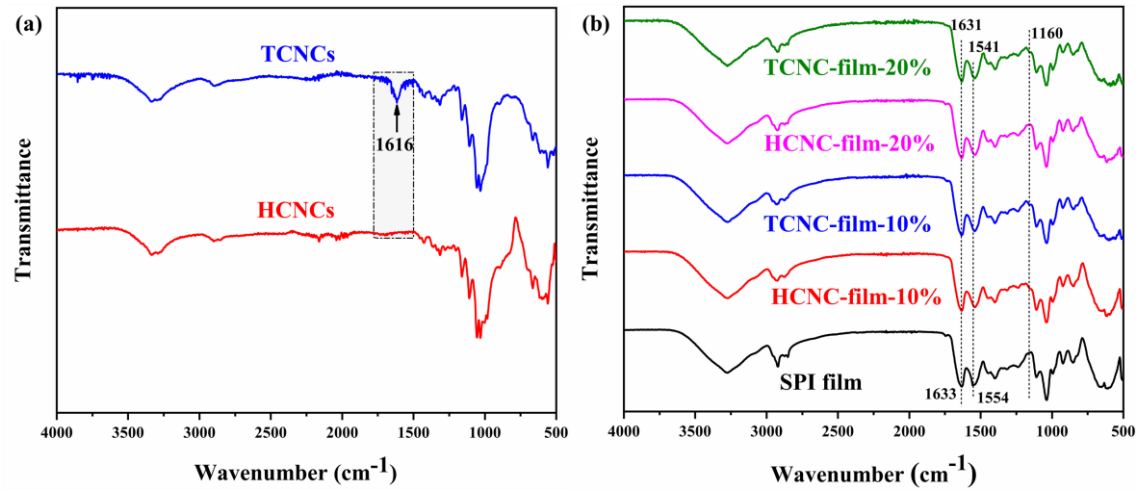

Figure 3.4. Fourier-transform infrared spectroscopy (FT-IR) spectra of (a) HCNCs and TCNCs, and (b) SPI and SPI/CNC films.

Figure 3.4 (b) displays the FT-IR spectra of SPI and SPI/CNC films. The peak at 2922 cm^{-1} was assigned to the C–H stretching, and the characteristic peak of cellulose appeared at 1160 cm^{-1}. The main characteristic peaks of SPI were illustrated at 1633 cm^{-1}, 1554 cm^{-1}, and 1238 cm^{-1}, presenting the Amide I (C–O stretching), Amide II (N–H bending), and Amide III (C–H and N–H stretching), respectively [48]. It was worth noting that the peaks of Amides I and Amide II showed a slight shift in terms of the CNC addition, indicating that there might be more exposed polar groups, and the bindings between the peptide chains increased. Li et al. suggested that the FT-IR peak shift at 1626 cm^{-1} and 1537 cm^{-1} with the addition of CNCs was

the result of the molecular hydrogen bonding formed between protein and CNCs. That would result in an improvement in the mechanical properties [49]. There was no obvious change in the peak at 3275 cm^{-1}. It was likely that some interactions among SPI were disrupted, and new bonding formed between SPI and CNCs, which were both reflected in FT-IR intensity [50].

Optical transmittance of SPI and SPI/CNC films is presented in Figure 3.5 (a). Evidently, the plain SPI film presented the highest transmittance among all the samples. The addition of CNCs into SPI film lessened its transparency, which decreased with the increasing amount of CNCs. This was because of the scattering or obstruction of light by the dispersed CNCs in SPI film, which was consistent with previous reports [51,52]. It was noted that, for the composite films containing the same content of CNCs, the transmittance at 600 nm of TCNC-film was higher than that of HCNC-film. This might be because of the better dispersion of TCNCs in water caused by the negatively charged carboxyl groups. However, despite the decreasing transmittance, the printed text under the films was still clearly visible, as shown in Figure 3.5 (b–f).

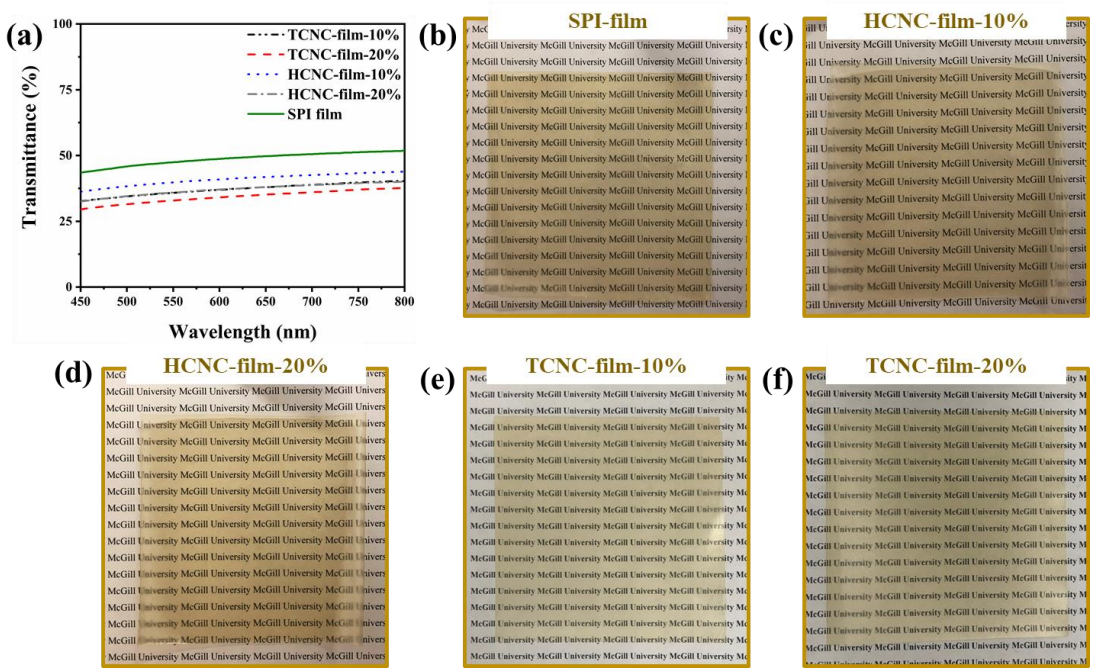

Figure 3.5. Optical transmittance (a) and photos (b–f) of SPI and SPI/CNC films.

As depicted in Figure 3.6, the SPI/CNC films had an obviously lower WVP compared with the plain SPI film ($p < 0.05$). With the addition of 10% and 20% TCNCs, the WVP of SPI film significantly reduced from $1.62 \pm 0.15 \times 10^{-6}$ g m^{-1} h^{-1} Pa^{-1} to $1.25 \pm 0.02 \times 10^{-6}$ g m^{-1} h^{-1} Pa^{-1} and $1.16 \pm 0.02 \times 10^{-6}$ g m^{-1} h^{-1} Pa^{-1}, respectively. A similar decrease in WVP values was also observed for HCNC-films. This indicated that both HCNCs and TCNCs derived from textile waste could enhance the water vapor barrier property of SPI film by decreasing the pathway of water molecules to transfer through the film [52]. However, the WVP differences between films containing 10% and 20% CNCs were not significant ($p > 0.05$).

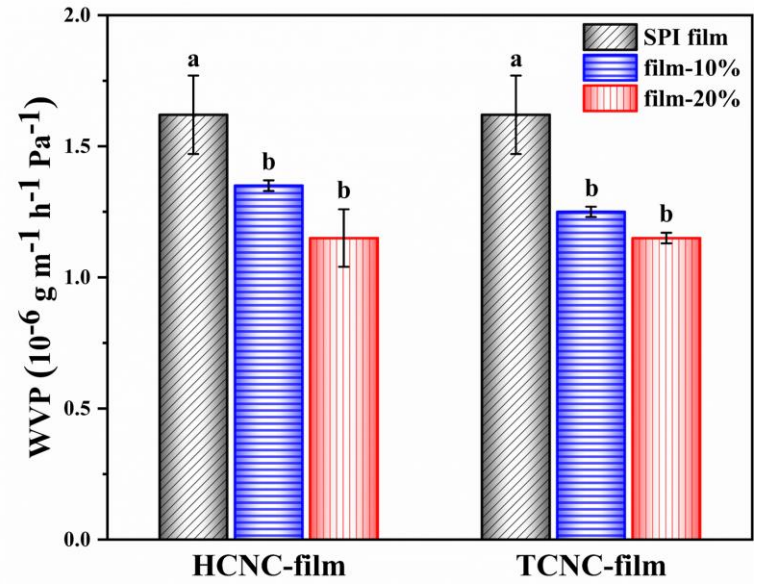

Figure 3.6. Water vapor permeability (WVP) of SPI and SPI/CNC films. Different letters on the tops of the columns indicate significant difference ($p < 0.05$) in terms of CNC content.

The mechanical properties of SPI and SPI/CNC films were tested to evaluate the reinforcing effects of HCNCs and TCNCs derived from textile waste. As shown in Figure 3.7 (d), all the samples exhibited an initial linear elastic behavior followed by continuous growth in the slope on account of plastic deformation. After that, there was a plateau until the critical values of stress and strain were eventually reached, and the films broke [53]. It was worth noting that the addition of CNCs, both HCNCs and TCNCs, made an important contribution to mechanical properties. For example, the tensile strength of SPI films containing 10% and 20% HCNCs significantly increased from 2.60 ± 0.42 MPa to 4.66 ± 0.26 MPa and 5.39 ± 0.11 MPa, respectively. This was because of the addition of rigid rod-like nanofillers in SPI films [21]. TCNCs showed an even better reinforcing effect compared with HCNCs. The tensile strength and Young's modulus of TCNC-film-20% were 8.81 ± 0.18 MPa and 4.02 ± 0.34 MPa, which were 3.39- and 9.80-fold of those of SPI film (2.60 ± 0.42 MPa and 0.41 ± 0.12 MPa),

respectively. This was because of the higher aspect ratio and better dispersion of TCNCs in water and SPI film, leading to a faster and uniform diffusion of stress [54]. On the other hand, the elongation at break of SPI/CNC films presented a significant decrease with the addition of CNCs, because the reinforcement restricted the mobility of protein molecules [55]. It was worth noting that the different CNC contents led to a significantly increased tensile strength ($p < 0.05$), but the change in elongation at break was not obvious ($p > 0.05$).

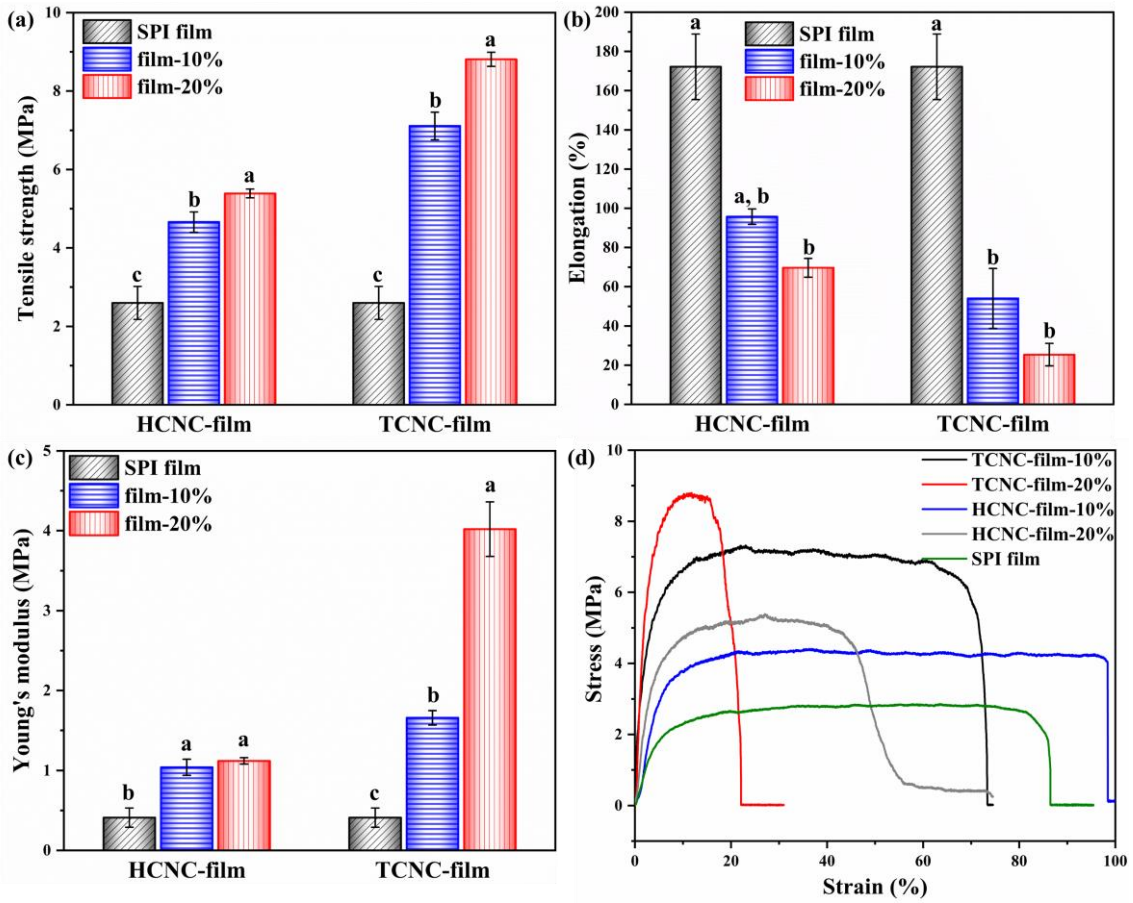

Figure 3.7. Tensile strength (a), elongation at break (b), Young's modulus (c), and stress–strain curves (d) of SPI and SPI/CNC films. Different letters on the tops of the columns indicate significant difference ($p < 0.05$) in terms of CNC content.

Table 3.1. Physical properties of soy protein isolate (SPI) and SPI/cellulose nanocrystal (CNC) films. WVP, water vapor permeability.

Samples	Tensile Strength (MPa)	Elongation at Break (%)	Young's Modulus (MPa)	WVP (10^{-6} g m^{-1} h^{-1} Pa^{-1})	Transmittance (%, 600 nm)
SPI film	2.6 ± 0.42	172.15 ± 16.69	0.41 ± 0.12	1.62 ± 0.15	48.7
HCNC-film-10%	4.66 ± 0.26	95.74 ± 3.93	1.04 ± 0.10	1.35 ± 0.02	40.9
HCNC-film-20%	5.39 ± 0.11	69.69 ± 4.80	1.12 ± 0.04	1.15 ± 0.11	37.1
TCNC-film-10%	7.11 ± 0.35	54.06 ± 15.27	1.66 ± 0.09	1.25 ± 0.02	37.0
TCNC-film-20%	8.81 ± 0.18	25.37 ± 5.77	4.02 ± 0.34	1.15 ± 0.02	34.1

3.5. Conclusions

Two kinds of CNCs with different functional groups were successfully extracted from textile waste through sulfuric acid hydrolysis and three-step oxidization. TEM and XRD results revealed that both HCNCs and TCNCs had the rod-like shape and cellulose I_β crystalline structure, with a high crystallinity index of 89.88% and 89.05%, respectively. A relatively higher aspect ratio was observed for TCNCs (17.10 ± 12.85) compared with HCNCs (10.00 ± 3.39). Those results demonstrated that textile waste materials offer a potential feedstock for the extraction of CNCs. Their application in reinforcing SPI film was investigated and summarized in Table 3.1. The SPI/CNC films maintained the high transparency with the addition of 20% CNCs. Besides, the WVP of HCNC-film-20% and TCNC-film-20% presented a significant decrease by around 29%. The mechanical property tests indicated that the tensile strength and

Young's modulus of the composite films were remarkably improved. When adding 20% CNCs, the tensile strength of HCNC-film and TCNC-film was 2.07-fold and 3.39-fold higher than that of SPI film, and their Young's modulus showed 1.73-fold and 8.80-fold increases. This work reported the possibilities of directly extracting CNCs from textile waste, contributing to solving the cellulosic waste disposal problem, and the derived CNCs showed significant potential in food packaging application.

3.6. References

1. Racho, P.; Waiwong, W. Modified textile waste for heavy metals removal. *Energy Rep.* 2020, *6*, 927–932.
2. Canada, W.R.W.i. Textiles Waste: The Facts. Availabe online: https://wrwcanada.com/en/get-involved/resources/textiles-themed-resources/textiles-waste-facts (accessed on 4 April 2020).
3. Gardetti, M.A.; Muthu, S.S. *The UN Sustainable Development Goals for the Textile and Fashion Industry*; Springer: Berlin, Germany, 2020.
4. Cay, A.; Yanik, J.; Akduman, C.; Duman, G.; Ertas, H. Application of textile waste derived biochars onto cotton fabric for improved performance and functional properties. *J. Clean Prod.* 2020, *251*, 119664.
5. Xu, Z.; Gu, S.; Sun, Z.; Zhang, D.; Zhou, Y.; Gao, Y.; Qi, R.; Chen, W. Synthesis of char-based adsorbents from cotton textile waste assisted by iron salts at low pyrolysis temperature for Cr(VI) removal. *Environ. Sci. Pollut.* 2020, *27*, 11012–11025.
6. Sukhavattanakul, P.; Manuspiya, H. Fabrication of hybrid thin film based on bacterial cellulose nanocrystals and metal nanoparticles with hydrogen sulfide gas sensor ability. *Carbohydr. Polym.* 2020, *230*, 115566.
7. Huang, S.T.; Liu, X.H.; Chang, C.Y.; Wang, Y.X. Recent developments and prospective

food-related applications of cellulose nanocrystals: A review. *Cellulose* 2020, *27*, 2991–3011.

8. Favier, V.; Chanzy, H.; Cavaille, J.Y. Polymer nanocomposites reinforced by cellulose whiskers. *Macromolecules* 1995, *28*, 6365–6367.
9. Darpentigny, C.; Molina-Boisseau, S.; Nonglaton, G.; Bras, J.; Jean, B. Ice-templated freeze-dried cryogels from tunicate cellulose nanocrystals with high specific surface area and anisotropic morphological and mechanical properties. *Cellulose* 2019, *27*, 233–247.
10. Zhao, G.M.; Du, J.; Chen, W.M.; Pan, M.Z.; Chen, D.Y. Preparation and thermostability of cellulose nanocrystals and nanofibrils from two sources of biomass: Rice straw and poplar wood. *Cellulose* 2019, *26*, 8625–8643.
11. Ambrosio-Martin, J.; Fabra, M.J.; Lopez-Rubio, A.; Lagaron, J.M. Melt polycondensation to improve the dispersion of bacterial cellulose into polylactide via melt compounding: Enhanced barrier and mechanical properties. *Cellulose* 2015, *22*, 1201–1226.
12. Jiang, Q.; Xing, X.; Jing, Y.; Han, Y. Preparation of cellulose nanocrystals based on waste paper via different systems. *Int. J. Biol. Macromol.* 2020, *149*, 1318–1322.
13. Nagarajan, K.J.; Balaji, A.N.; Kasi Rajan, S.T.; Ramanujam, N.R. Preparation of bio-eco based cellulose nanomaterials from used disposal paper cups through citric acid hydrolysis. *Carbohydr. Polym.* 2020, *235*, 115997.
14. Sirvio, J.; Hyvakko, U.; Liimatainen, H.; Niinimaki, J.; Hormi, O. Periodate oxidation of cellulose at elevated temperatures using metal salts as cellulose activators. *Carbohydr. Polym.* 2011, *83*, 1293–1297.
15. Gao, H.M.; Duan, B.; Lu, A.; Deng, H.B.; Du, Y.M.; Shi, X.W.; Zhang, L.N. Fabrication of cellulose nanofibers from waste brown algae and their potential application as milk thickeners. *Food Hydrocolloids* 2018, *79*, 473–481.
16. Gestranius, M.; Stenius, P.; Kontturi, E.; Sjoblom, J.; Tammelin, T. Phase behaviour and

droplet size of oil-in-water pickering emulsions stabilised with plant-derived nanocellulosic materials. *Colloids Surf. A* 2017, *519*, 60–70.

17. Leung, A.C.W.; Hrapovic, S.; Lam, E.; Liu, Y.L.; Male, K.B.; Mahmoud, K.A.; Luong, J.H.T. Characteristics and properties of carboxylated cellulose nanocrystals prepared from a novel one-step procedure. *Small* 2011, *7*, 302–305.
18. Li, B.; Xu, W.; Kronlund, D.; Maattanen, A.; Liu, J.; Smatt, J.-H.; Peltonen, J.; Willfor, S.; Mu, X.; Xu, C. Cellulose nanocrystals prepared via formic acid hydrolysis followed by TEMPO-mediated oxidation. *Carbohydr. Polym.* 2015, *133*, 605–612.
19. Zhang, Y.; Karimkhani, V.; Makowski, B.; Samaranayake, G.; Rowan, S. Nanoemulsions and nanolatexes stabilized by hydrophobically functionalized cellulose nanocrystals. *Macromolecules* 2017, *16*, 6032–6042.
20. Wang, Z.; Yao, Z.; Zhou, J.; Zhang, Y. Reuse of waste cotton cloth for the extraction of cellulose nanocrystals. *Carbohydr. Polym.* 2017, *157*, 945–952.
21. Wang, Y.; Cao, X.; Zhang, L. Effects of cellulose whiskers on properties of soy protein thermoplastics. *Macromol. Biosci.* 2006, *6*, 524–531.
22. Ko, S.W.; Soriano, J.P.E.; Lee, J.Y.; Unnithan, A.R.; Park, C.H.; Kim, C.S. Nature derived scaffolds for tissue engineering applications: Design and fabrication of a composite scaffold incorporating chitosan-g-d,l-lactic acid and cellulose nanocrystals from Lactuca sativa L. cv green leaf. *Int. J. Biol. Macromol.* 2018, *110*, 504–513.
23. Yang, H.; Tejado, A.; Alam, N.; Antal, M.; van de Ven, T.G. Films prepared from electrosterically stabilized nanocrystalline cellulose. *Langmuir* 2012, *28*, 7834–7842.
24. Amoroso, L.; Muratore, G.; Ortenzi, M.A.; Gazzotti, S.; Limbo, S.; Piergiovanni, L. Fast production of cellulose nanocrystals by hydrolytic-oxidative microwave-assisted treatment. *Polymers* 2020, *12*, 68.
25. Xia, C.; Wang, L.; Dong, Y.; Zhang, S.; Shi, S.Q.; Cai, L.; Li, J. Soy protein isolate-based

films cross-linked by epoxidized soybean oil. *RSC Adv.* 2015, *5*, 82765–82771.

26. Li, K.; Jin, S.; Han, Y.; Li, J.; Chen, H. Improvement in functional properties of soy protein isolate-based film by cellulose nanocrystal-graphene artificial nacre nanocomposite. *Polymers* 2017, *9*, 321.
27. Park, S.; Baker, J.O.; Himmel, M.E.; Parilla, P.A.; Johnson, D.K. Cellulose crystallinity index: Measurement techniques and their impact on interpreting cellulase performance. *Biotechnol. Biofuels* 2010, *3*, 10.
28. Ye, H.M.; Wang, C.S.; Zhang, Z.Z.; Yao, S.F. Effect of cellulose nanocrystals on the crystallization behavior and enzymatic degradation of poly(butylene adipate). *Carbohydr. Polym.* 2018, *189*, 99–106.
29. Fitch-Vargas, P.R.; Aguilar-Palazuelos, E.; Zazueta-Morales, J.D.; Vega-Garcia, M.O.; Valdez-Morales, J.E.; Martinez-Bustos, F.; Jacobo-Valenzuela, N. Physicochemical and microstructural characterization of corn starch edible films obtained by a combination of extrusion technology and casting technique. *J. Food Sci.* 2016, *81*, E2224–E2232.
30. Zhang, C.; Ma, Y.; Zhao, X.; Ma, D. Development of soybean protein-isolate edible films incorporated with beeswax, span 20, and glycerol. *J. Food Sci.* 2010, *75*, C493–C497.
31. Yu, H.Y.; Yang, X.Y.; Lu, F.F.; Chen, G.Y.; Yao, J.M. Fabrication of multifunctional cellulose nanocrystals/poly(lactic acid) nanocomposites with silver nanoparticles by spraying method. *Carbohydr. Polym.* 2016, *140*, 209–219.
32. Yu, Z.; Sun, L.; Wang, W.; Zeng, W.; Mustapha, A.; Lin, M. Soy protein-based films incorporated with cellulose nanocrystals and pine needle extract for active packaging. *Ind. Crops. Prod.* 2018, *112*, 412–419.
33. Abd Hamid, S.B.; Chowdhury, Z.Z.; Karim, M.Z.; Ali, M.E. Catalytic isolation and physicochemical properties of nanocrystalline cellulose (NCC) using HCl-FeCl3 system combined with ultrasonication. *BioResources* 2016, *11*, 3840–3855.

34. Beltramino, F.; Roncero, M.B.; Vidal, T.; Valls, C. A novel enzymatic approach to nanocrystalline cellulose preparation. *Carbohydr. Polym.* 2018, *189*, 39–47.

35. Ding, M.C.; Li, C.W.; Chen, F.S. Isolation and characterization of cellulose nanocrystals from cloth hairs and evaluation of their compatibility with PLLA. *Cellulose* 2017, *24*, 4785–4792.

36. Hemmati, F.; Jafari, S.M.; Kashaninejad, M.; Barani Motlagh, M. Synthesis and characterization of cellulose nanocrystals derived from walnut shell agricultural residues. *Int. J. Biol. Macromol.* 2018, *120*, 1216–1224.

37. Ojala, J.; Sirvio, J.A.; Liimatainen, H. Nanoparticle emulsifiers based on bifunctionalized cellulose nanocrystals as marine diesel oil-water emulsion stabilizers. *Chem. Eng. J.* 2016, *288*, 312–320.

38. Marett, J.; Aning, A.; Foster, E.J. The isolation of cellulose nanocrystals from pistachio shells via acid hydrolysis. *Ind. Crops Prod.* 2017, *109*, 869–874.

39. Mascheroni, E.; Rampazzo, R.; Ortenzi, M.A.; Piva, G.; Bonetti, S.; Piergiovanni, L. Comparison of cellulose nanocrystals obtained by sulfuric acid hydrolysis and ammonium persulfate, to be used as coating on flexible food-packaging materials. *Cellulose* 2016, *23*, 779–793.

40. Lim, W.L.; Gunny, A.A.N.; Kasim, F.H. Overview of cellulose nanocrystals: Extraction, physicochemical properties and applications. *IOP Conf. Ser. Mater. Sci. Eng.* 2019, *670*, 12058.

41. Gong, X.; Wang, Y.; Tian, Z.; Zheng, X.; Chen, L. Controlled production of spruce cellulose gels using an environmentally "green" system. *Cellulose* 2014, *21*, 1667–1678.

42. Ilharco, L.M.; Garcia, A.R.; daSilva, J.L.; Ferreira, L.F.V. Infrared approach to the study of adsorption on cellulose: Influence of cellulose crystallinity on the adsorption of benzophenone. *Langmuir* 1997, *13*, 4126–4132.

43. Lei, W.Q.; Fang, C.Q.; Zhou, X.; Yin, Q.; Pan, S.F.; Yang, R.; Liu, D.H.; Ouyang, Y. Cellulose nanocrystals obtained from office waste paper and their potential application in PET packing materials. *Carbohydr. Polym.* 2018, *181*, 376–385.
44. Kafle, K.; Greeson, K.; Lee, C.; Kim, S.H. Cellulose polymorphs and physical properties of cotton fabrics processed with commercial textile mills for mercerization and liquid ammonia treatments. *Text Res. J.* 2014, *84*, 1692–1699.
45. Oh, S.Y.; Yoo, D.I.; Shin, Y.; Seo, G. FTIR analysis of cellulose treated with sodium hydroxide and carbon dioxide. *Carbohydr Res* 2005, *340*, 417–428.
46. Alves, L.; Medronho, B.F.; Antunes, F.E.; Romano, A.; Miguel, M.G.; Lindman, B. On the role of hydrophobic interactions in cellulose dissolution and regeneration: Colloidal aggregates and molecular solutions. *Colloid Surface A* 2015, *483*, 257–263.
47. Gong, X.Y.; Wang, Y.X.; Chen, L.Y. Enhanced emulsifying properties of wood-based cellulose nanocrystals as Pickering emulsion stabilizer. *Carbohydr. Polym.* 2017, *169*, 295–303.
48. Ansarifar, E.; Shahidi, F.; Mohebbi, M.; Ramezanian, N.; Koocheki, A.; Mohamadian, A. Optimization of limonene microencapsulation based on native and fibril soy protein isolate by VIKOR method. *Lwt-Food Sci. Technol.* 2019, *115*, 107884.
49. Li, K.; Jin, S.; Chen, H.; He, J.; Li, J. A high-performance soy protein isolate-based nanocomposite film modified with microcrystalline cellulose and Cu and Zn nanoclusters. *Polymers* 2017, *9*, 167.
50. Carpine, D.; Dagostin, J.L.A.; de Andrade, E.F.; Bertan, L.C.; Mafra, M.R. Effect of the natural surfactant Yucca schidigera extract on the properties of biodegradable emulsified films produced from soy protein isolate and coconut oil. *Ind. Crops Prod.* 2016, *83*, 364–371.
51. Cao, J.; Sun, X.; Lu, C.; Zhou, Z.; Zhang, X.; Yuan, G. Water-soluble cellulose acetate from

waste cotton fabrics and the aqueous processing of all-cellulose composites. *Carbohydr. Polym.* 2016, *149*, 60–67.

52. Yadav, M.; Chiu, F.C. Cellulose nanocrystals reinforced kappa-carrageenan based UV resistant transparent bionanocomposite films for sustainable packaging applications. *Carbohydr. Polym.* 2019, *211*, 181–194.
53. Alvarez-Castillo, E.; Bengoechea, C.; Guerrero, A. Composites from by-products of the food industry for the development of superabsorbent biomaterials. *Food Bioprod. Process.* 2020, *119*, 296–305.
54. Wang, Y.; Chen, L. Cellulose nanowhiskers and fiber alignment greatly improve mechanical properties of electrospun prolamin protein fibers. *ACS Appl. Mater. Interfaces* 2014, *6*, 1709–1718.
55. Xu, X.Y.; Song, K.L.; Xing, B.; Hu, W.F.; Ke, Q.F.; Zhao, Y. Thermal-tenacity-enhanced and biodegradable textile sizes from cellulose nanocrystals reinforced soy protein for effective yarn coating. *Ind. Crops Prod.* 2019, *140*, 111701.

Connecting Text

In chapter 3, we demonstrated the possibility of directly extracting CNCs from textile waste and their effects on improving the mechanical strength and water vapor barrier property of SPI films. Chapter 4 aimed to modify the obtained CNCs and incorporate them into commercial plastic films as antibacterial nanofillers. Firstly, CNCs were modified with methacrylamide, and the antibacterial capacity of the modified CNCs was assessed. Secondly, the modified CNCs were incorporated into cellulose acetate and poly(vinyl chloride) films as antibacterial nanofillers. Thirdly, the effects of modified CNCs on the antibacterial, mechanical, and optical properties were investigated.

Chapter 4. Modification of Cellulose Nanocrystals as Antibacterial Nanofillers to Fabricate Rechargeable Nanocomposite Films for Active Packaging

4.1. Abstract

Growing food safety concerns have required the development of functional films incorporated with antibacterial nanofillers for active packaging, and cellulose nanocrystals (CNCs) are promising candidates due to their unique morphology and availability for modification. Herein, this study aims to develop an approach to producing functional CNCs that can be easily incorporated into commercial plastic films as antibacterial nanofillers for active packaging. Particularly, CNCs extracted from cotton textile waste were selected as the model and modified with methacrylamide (MAM). Cellulose acetate (CA) and polyvinyl chloride (PVC) were chosen as film-forming agents, and the modified CNCs (MAM-CNCs) were incorporated by the solution casting method. Addition of MAM-CNCs significantly improved the mechanical and UV barrier properties of CA and PVC films. After chlorination, the composite films with 3% MAM-CNCs exhibited excellent antibacterial efficacy against common foodborne pathogens, e.g., higher than 6-log reduction of *Staphylococcus aureus* and *Escherichia coli* after 1 hour of contact at 37 °C. Moreover, this antibacterial capacity could be recharged by chlorination without affecting the mechanical performance of plastic films. Therefore, this work reveals the potential of utilizing modified CNCs to fabricate functional packaging materials.

4.2. Introduction

To address global climate change and plastic pollution, nanocellulose - the most abundant crystalline polysaccharide nanomaterial on Earth - is expected to be used this century to fabricate high-tech materials and products because of its CO_2-accumulating nature [1]. Cellulose

nanocrystals (CNCs), usually separated from plants, animals, and bacteria, are one type of cellulose nanomaterials and display great properties, such as high crystallinity, nontoxicity, biocompatibility, and large specific surface area. In addition, CNCs possess abundant hydroxyl groups available for further modification, facilitating various potential applications [2]. For instance, Yao and colleagues [3] investigated surface modification of CNCs through self-polymerization of dopamine and their application as reinforcing agents in cellulose acetate (CA) membrane. It was found that the modification enhanced the dispersion and interfacial adhesion of CNCs, which improved the mechanical properties and filtration and antifouling performances of CA films. Wang and Chen [4] reported that the surface-modified CNCs could be uniformly dispersed in the electrospun prolamin protein fibers, and a percolating network of these rigid nanofillers subsequently formed to facilitate a faster diffusion of stress when the modified CNC content reached 3 wt%. Numerous studies used CNCs to reinforce packaging materials for the improved mechanical, barrier, and thermal properties [5-7]. It will further broaden its scope of application if CNC-based nanofillers with multi-functions can be developed.

Contamination of food by bacterial pathogens is one of the biggest concerns in the food industry as it can result in serious human illnesses and death [8]. Antibacterial packaging has become an important strategy in controlling foodborne disease by hindering microbial growth, contributing to reducing food contamination and protecting consumer health [9]. A convenient approach to developing antibacterial packaging is to incorporate active fillers in the polymer matrix [10]. In this regard, CNC-based nanomaterials could be promising candidates due to their

non-fossil-based renewability, biodegradability, and high reactivity for surface modification [11]. The feasibility of extracting CNCs from cotton waste through sulfuric acid hydrolysis has been proved in our previous work, and the obtained CNCs demonstrated a comparable aspect ratio to those from cotton linters [12]. Therefore, we aimed at selecting CNCs derived from cotton waste as a model and modifying them with methacrylamide (MAM) to investigate their potential as antibacterial nanofillers in different polymer films in the current study. MAM is a precursor of N-halamines, which were used for the modification of cellulose due to their high efficacy against various microorganisms and rechargeability [13]. CA and poly(vinyl chloride) (PVC) were selected as models to make plastic films because the former is one of the most widely used cellulose derivative plastics with excellent optical and mechanical properties [14], and the latter is a common plastic in the polyethylene "family" that has low cost, easy processability, and broad applications [15]. The effect of modified CNCs on the mechanical and optical properties of CA and PVC films was investigated, and the antibacterial property and rechargeability of composite materials were evaluated with two common foodborne pathogens, *Staphylococcus aureus* ATCC 6538 and *Escherichia coli* K12, as the targets.

4.3. Materials and Methods

4.3.1. Materials

Waste cotton clothes were kindly provided by Renaissance (Montreal, Canada). Sulfuric acid (H_2SO_4, 95.0-98.0%), sodium hydroxide (NaOH, ≥98%), methacrylamide (MAM, 98%), sodium persulfate (≥98%), sodium thiosulfate (99%), cellulose acetate (CA, average M_n ~30,000 by GPC), and dimethylacetamide (DMAc, 99.8%) were purchased from Sigma-

Aldrich (Oakville, ON, Canada) and used without further treatment. Commercial polyvinyl chloride (PVC) films were produced by Polyvinyl Films, Inc. (MA, USA). Luria–Bertani (LB) medium was purchased from Becton Dickinson (Franklin Lakes, NJ, USA). Phosphate-buffered saline (10× PBS) was obtained from VWR International (Mississauga, ON, Canada).

4.3.2. Extraction and modification of CNCs

CNCs were extracted from cotton textile waste by sulfuric acid hydrolysis according to our previous work [12]. Briefly, 5.00 g of cotton clothes were mixed with 100.00 g H_2SO_4 solution (60 wt%) and stirred for 1 hour at room temperature. Then, 1 L cold water was added to stop the hydrolysis process. CNCs were washed until pH 6 and coded as HCNCs. For the modification, 1.80 g NaOH was added in 50.00 g of HCNC suspension (10 wt%) under stirring. Then, 5.00 g MAM and 0.03 g sodium persulfate were added and stirred until MAM and sodium persulfate were completely dissolved. The reaction was conducted at 65 ℃ for 5 hours. After that, the product was washed with distilled water to remove unreacted MAM and sodium persulfate and named as MAM-CNCs.

4.3.3. Preparation of composite films

CA and PVC films with the addition of MAM-CNCs were prepared by solvent casting method. CA and MAM-CNCs were added in acetic acid aqueous solution (85 wt%) and stirred at room temperature for 24 hours, while PVC and MAM-CNCs were dispersed in DMAc overnight. The resultant suspensions were filled into the mold and dried at 180 ℃ for 2 hours. The composite films were coded as Neat CA, CA-1% MAM-CNC, CA-3% MAM-CNC, CA-5% MAM-CNC, Neat PVC, PVC-1% MAM-CNC, PVC-3% MAM-CNC, and PVC-5% MAM-

CNC, corresponding to the MAM modified CNC content (based on the dry plastic content) of 0, 1, 3, and 5 wt %, respectively.

4.3.4. Characterizations

4.3.4.1. X-ray diffraction (XRD)

XRD patterns of HCNCs and MAM-CNCs were obtained using an Empyrean 3 (Malvern Panalytical Ltd., UK) X-ray diffractometer in a Bragg Brentano configuration, with Cu Kα radiation between 4° and 40°. The crystallinity index (CrI) was determined by the peak height method [16] in terms of Equation (1):

$$CrI\ (\%) = \frac{I_{(200)} - I_{am}}{I_{(200)}} \times 100\% \qquad \text{Equation (1)}$$

where $I_{(200)}$ is the diffraction intensity of the (200) crystallographic plane at around $2\theta = 22.5°$, and I_{am} is the diffraction intensity of the amorphous fraction at approximately $2\theta = 18.5°$.

4.3.4.2. Fourier-transform infrared (FT-IR) spectroscopy

FT-IR spectra of HCNCs, MAM-CNCs, and composite films were obtained by using a Varian Excalibur 3100 FT-IR spectrometer (Varian, Melbourne, Australia) equipped with an attenuated total reflectance (ATR) accessory (Specac, UK). The spectra were collected as the average of 72 scans with a resolution of 2 cm^{-1}, using the empty accessory as blank. Spectral collection was carried out at 650-4000 cm^{-1}.

4.3.4.3. ^{13}C solid-state nuclear magnetic resonance (NMR) spectroscopy

The solid-state NMR spectra of HCNCs and MAM-CNCs were collected by a Varian VNMRS (now Agilent, Santa Clara, CA, USA) spectrometer operating at 399.9 MHz for ^{1}H and 100.5 MHz for ^{13}C using a 7.5 mm Varian Chemagnetics double-resonance probe. The sample was

spun at 3 kHz, and TOSS was used to suppress spinning sidebands. The number of scans was 12288, and the recycle delay was 4 s. The cross-polarization technique with a contact time of 2 ms was applied to record the spectra, and the spectra were referenced using the carbonyl signal of glycine at 176.4 ppm.

Furthermore, NMR spectra were used to evaluate the degree of crystallinity of the HCNCs and MAM-CNCs. The crystallinity index was calculated by Equation (2) [17]:

$$CrI\ (\%) = \frac{A_c}{A_c + A_a} \times 100\% \qquad \text{Equation (2)}$$

where A_c and A_a represented the fitted signal intensity of crystalline and amorphous regions, respectively.

4.3.4.4. Mechanical properties

The mechanical properties of composite films were tested using an eXpert 7601 Single Column testing machine (ADMIT, USA) at 25 ℃ according to standard ASTM D882. The initial grip separation distance was set as 20 mm, and the separation speed was 20 mm/min. The dimension of film specimens was 60 mm × 10 mm (length × width), with the thicknesses of about 0.2 mm for CA films and 0.1 mm for PVC films. The thickness of the films was measured by a Traceable digital caliper (Fisher Scientific, ON, Canada).

4.3.4.5. Optical transmittance

The optical transmittance of composite films was measured using a DU 800 UV-Vis spectrophotometer (Beckman Coulter, USA) in the wavelength range of 200-800 nm. The spectra were recorded with air as background. The blocking percentages for UVB (280–315 nm) and UVA (315-400 nm) were calculated by Equations (3) and (4), respectively [18]:

$$UVB\ blocking\ (\%) = 100 - \frac{\sum_{280\ nm}^{315\ nm} T_\lambda \times \Delta\lambda}{\sum_{280\ nm}^{315\ nm} \Delta\lambda} \quad \text{Equation (3)}$$

$$UVA\ blocking\ (\%) = 100 - \frac{\sum_{315\ nm}^{400\ nm} T_\lambda \times \Delta\lambda}{\sum_{315\ nm}^{400\ nm} \Delta\lambda} \quad \text{Equation (4)}$$

where T_λ is the average spectral transmittance of the films, $\Delta\lambda$ is the measured wavelength interval (nm), and λ is the wavelength.

4.3.4.6. Water vapor permeability (WVP)

WVP of composite films was evaluated by the gravimetric method according to Zhang and others [19]. Films were sealed on a glass jar containing anhydrous calcium chloride. Then, the jars were placed in a desiccator filled with distilled water at 25 ℃. The weight of the jars was measured periodically. WVP value was calculated using Equation (5):

$$WVP = \frac{\Delta m \times n}{A \times t \times \Delta p} \quad \text{Equation (5)}$$

where Δm is the change in jar weight (g), n is the film thickness (m), A is the exposed area of the film (m^2), t is the time (hour), and Δp is the partial pressure difference existed between the two sides of film sample (Pa).

4.3.4.7. Antibacterial test

MAM-modified CNCs and composite films were endowed with antibacterial property by chlorination and coded as MAM-CNC-Cl, CA-MAM-CNC-Cl, and PVC-MAM-CNC-Cl. In brief, the samples were chlorinated by soaking in a 5% sodium hypochlorite solution at pH 7 and stirred at room temperature for 2 hours. After that, the chlorine-charged samples were washed thoroughly with distilled water to remove the unbonded chlorine. The chlorine content of MAM-CNC-Cl was determined by iodometric titration [20].

The antibacterial activities were evaluated by using *S. aureus* ATCC 6538 and *E. coli* K12 as

the model microbes to separately represent Gram-positive and Gram-negative bacteria. Both bacterial strains were preserved at -80 °C in LB broth containing 20% glycerol (v/v). For routine cultivation, *S. aureus* and *E. coli* were grown on LB agar plates at 37 °C in an aerobic condition. Overnight bacterial culture was prepared by cultivating *S. aureus* and *E. coli* individually in 4 mL of LB broth at 37 °C with constant shaking to achieve a concentration of ca. 8 log. Then, the bacterial inoculums were prepared by diluting the overnight culture with PBS to a certain concentration for further experiment.

The antibacterial efficacy of HCNCs, HCNC after chlorination (HCNC-Cl), MAM-CNCs (as control), and MAM-CNC-Cl was evaluated by mixing 20 mL of CNC suspension and 200 μL of bacterial inoculum to a final concentration of 10^5 CFU/mL [21]. The mixture was incubated for 1 hour with constant shaking, and then 500 μL of the upper suspension was added to a sterile glass tube containing 4.0 mL of PBS and 500 μL of sterile sodium thiosulfate. Then, the mixed solution was vortexed and serially diluted. Addition of sodium thiosulfate did not affect bacterial cell viability (data not shown). Finally, 10 μL of the diluted solution was transferred to LB agar plate. After 24 hours of incubation at 37 ℃, the number of colonies on the plate was enumerated to calculate the log reduction.

The effect of composite films against *S. aureus* and *E. coli* was tested by following the modified AATCC test method 100 [22], where neat CA and PVC films (without any CNCs), neat films treated with the same chlorination procedure, and films with MAM-CNCs served as control groups. Briefly, 20 μL of bacterial suspension (~10^6 CFU/mL) was added onto the surface of the film (2 cm × 2 cm) and then covered with another film to enable sufficient contact. After 1

hour contact, 4 mL of sterile sodium thiosulfate was added and vortexed for 2 min to rinse off bacteria. The rinsing solution was then serially diluted for the aforementioned plating assay. The zone of inhibition was evaluated using the disc diffusion method [23]. *S. aureus* and *E. coli* were grown in LB broth for 16 hours and adjusted to 10^8 CFU/mL; then a sterile swab was used to evenly spread the bacterial suspension on the surface of the LBA plate. The film specimens (diameter of 6 mm) with or without MAM-CNCs were placed over the surface of the inoculated plate. The plates were incubated at 37 °C for 24 hours, and the bacterial inhibition zone was measured to evaluate the antibacterial activity of the prepared films.

4.3.4.8. Rechargeability

To evaluate the rechargeability, selected composite films (CA-3% MAM-CNC and PVC-3% MAM-CNC) were first chlorinated for 2 hours and then fully quenched with sodium thiosulfate solution. The films were recharged by chlorination for 2 hours, and the antibacterial activity and mechanical performance were measured as described above.

4.3.5. Statistical analysis

All experiments were carried out in triplicate and reported as mean ± SD (standard deviation). One-way analysis of variance (ANOVA) was applied to statistical analysis, followed by LSD post-hoc analysis at the confidence level of 0.05. All of the analyses were carried out by using IBM SPSS Statistics 26 software.

4.4. Results and Discussion

4.4.1. Structure of modified CNCs

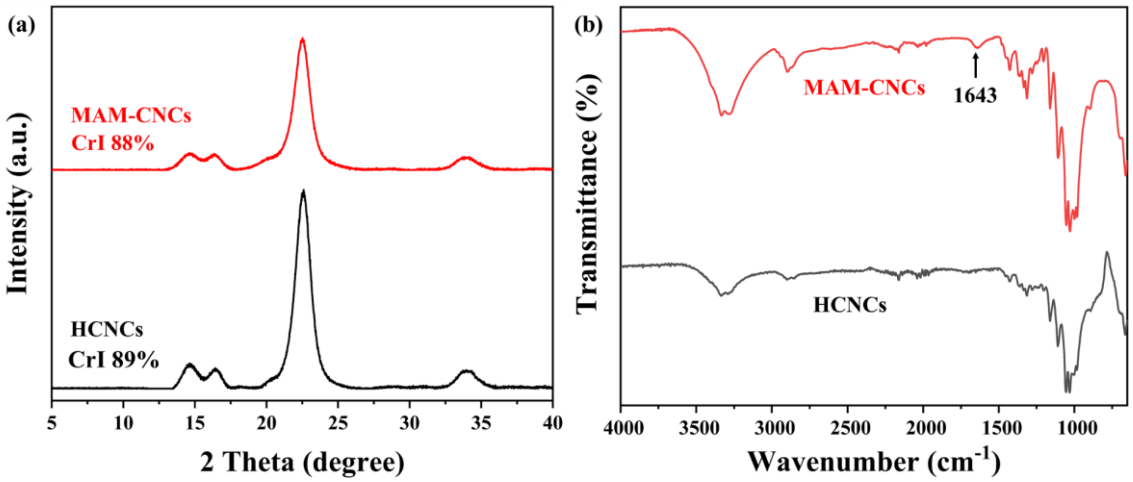

Figure 4.1. XRD patterns and crystallinity index (a) and FT-IR spectra (b) of HCNCs and MAM-CNCs.

The structure of CNCs before and after MAM modification was studied. Figure 4.1 (a) presents the XRD patterns and crystallinity of HCNCs and MAM-CNCs. It was obvious that two diffraction patterns were quite similar with three peaks at 14.6°, 16.4°, and 22.5°, corresponding to the (1$\bar{1}$0), (110), and (200) crystallographic planes of cellulose I_β [24]. Both HCNCs and MAM-CNCs had a high crystallinity index (CrI) of 89% and 88%, respectively. The results suggested that the chemical modification had little effect on the crystalline structure of CNCs derived from cotton waste. As shown in Figure 4.1 (b), FT-IR spectra of HCNCs and MAM-CNCs exhibited analogous characteristic peaks of cellulose. Specifically, in the region of 3600-3000 cm^{-1}, there was a broad band due to stretching vibration of O-H and inter-chain hydrogen bonds. A broad absorption band around 2900 cm^{-1} was assigned to the stretching vibration of the aliphatic C-H bond. Besides, the typical bands of cellulose were observed: C-H bending at 1427 cm^{-1}, CH_2 bending at 1371 cm^{-1}, O-H bending at 1315 cm^{-1}, asymmetric

vibration of C-O-C at 1160 cm^{-1}, and C-O-C pyranose ring stretching vibration at 1055 cm^{-1} and 1031 cm^{-1}. The band at 893 cm^{-1} was associated with cellulose with β-glycoside bonds of the glucose ring, also known as the amorphous absorption band. The absorbance ratio of the bands at 1427 and 893 cm^{-1} for HCNCs and MAM-CNCs, regarded as empirical crystallinity index, were comparable, suggesting similar crystallinity [25]. The typical stretching vibrations of N-H and C-N in modified CNCs at around 3376 and 1401 cm^{-1} overlapped with the characteristic bands of cellulose [26], but the appearance of the band at 1643 cm^{-1} was attributed to the stretching vibration of amide carbonyl C=O bond. Besides, the C=C bond of MAM monomer was opened after modification, leading to the disappearance of the band at 1600 cm^{-1} [27].

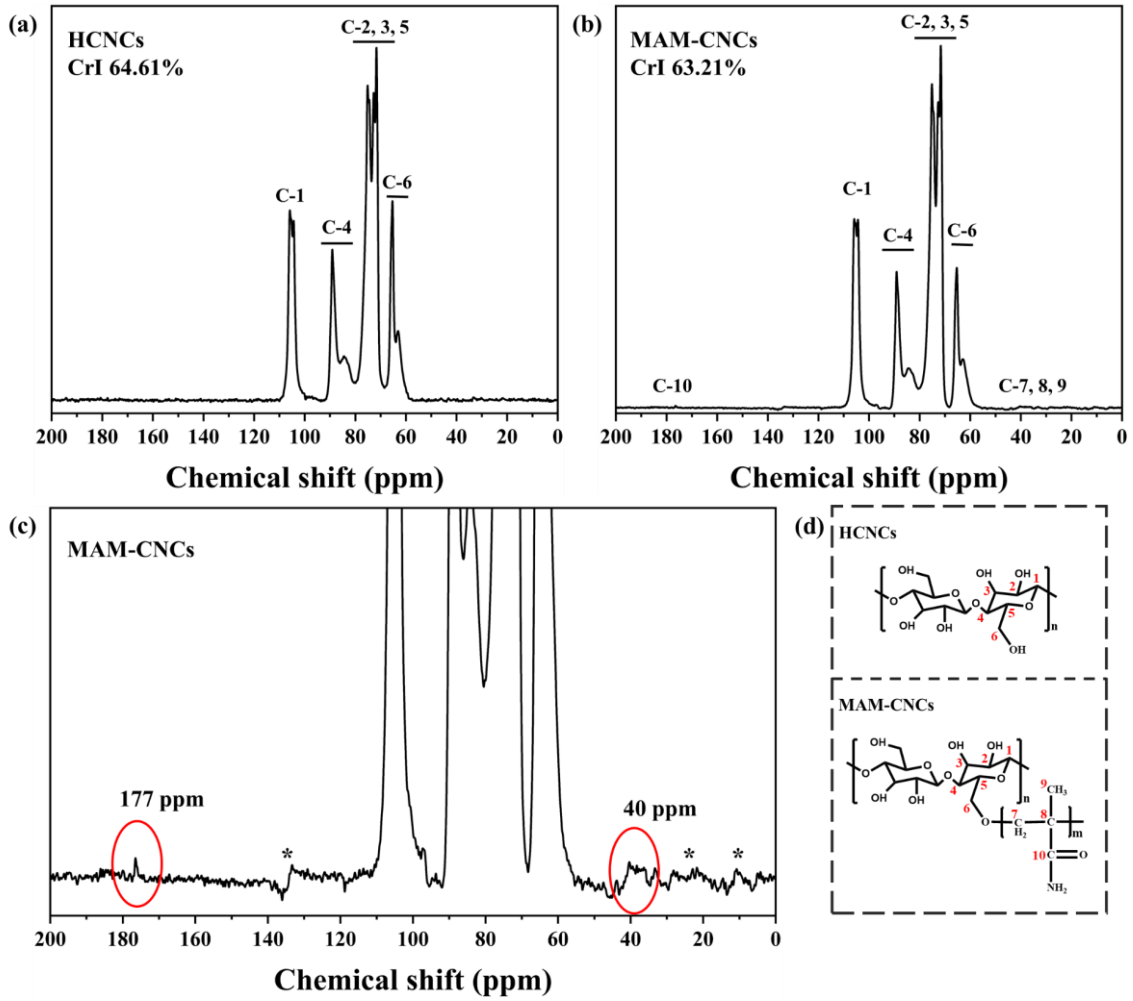

Figure 4.2. ^{13}C solid-state NMR spectra (a-c) and molecular structures (d) of HCNCs and MAM-CNCs.

^{13}C solid-state NMR spectra were acquired to further explain the chemical modification of CNCs. As shown in Figure 4.2 (a, b), both spectra display the typical peaks of cellulose in the range of 110-60 ppm, which were assigned to the carbons in anhydroglucose units [28]. In detail, the signals at 110-100 ppm were attributed to C-1, and the features between 68 and 80 ppm were assigned to C-2, C-3, and C-5 collectively. The peaks centered at 91-80 ppm were assigned to C-4, representing the β-(1-4) linkage. C-4 peak exhibited a doublet at 89 and 84 ppm, attributing to the crystalline and amorphous regions, respectively. The chemical shift ranging 68-60 ppm corresponded to C-6 atom, and C-6 resonance for the crystalline and

amorphous regions was at 65 and 63 ppm. Both HCNCs and MAM-CNCs spectra presented doublets at C-1, C-4, and C-6, corresponding to NMR resonance peaks of cellulose I_β crystalline structure [29]. Although the CrI values were much lower than those obtained from XRD data, they showed a similar trend that the CrI of HCNCs and MAM-CNCs were quite similar (64.61 and 63.21%). The result was coincided with the study conducted by Agarwal and coauthors [17] and could be attributed to the differences in the principle of measurement and analysis approach [30]. As shown in Figure 4.2 (c), the new peak at 177 ppm was attributed to the carbonyl carbons (C-10), and the broad peak at around 40 ppm was assigned to the methylene and methyl carbons (C-7, 8, 9) [31]. Moreover, the absence of the peaks at 122 and 138 ppm was related to the opening of C=C bond of MAM monomer. Similar FTIR and NMR results have been reported, which could confirm the successful modification of HCNCs with MAM [26,20,32,33].

4.4.2. Structure and properties of composite films

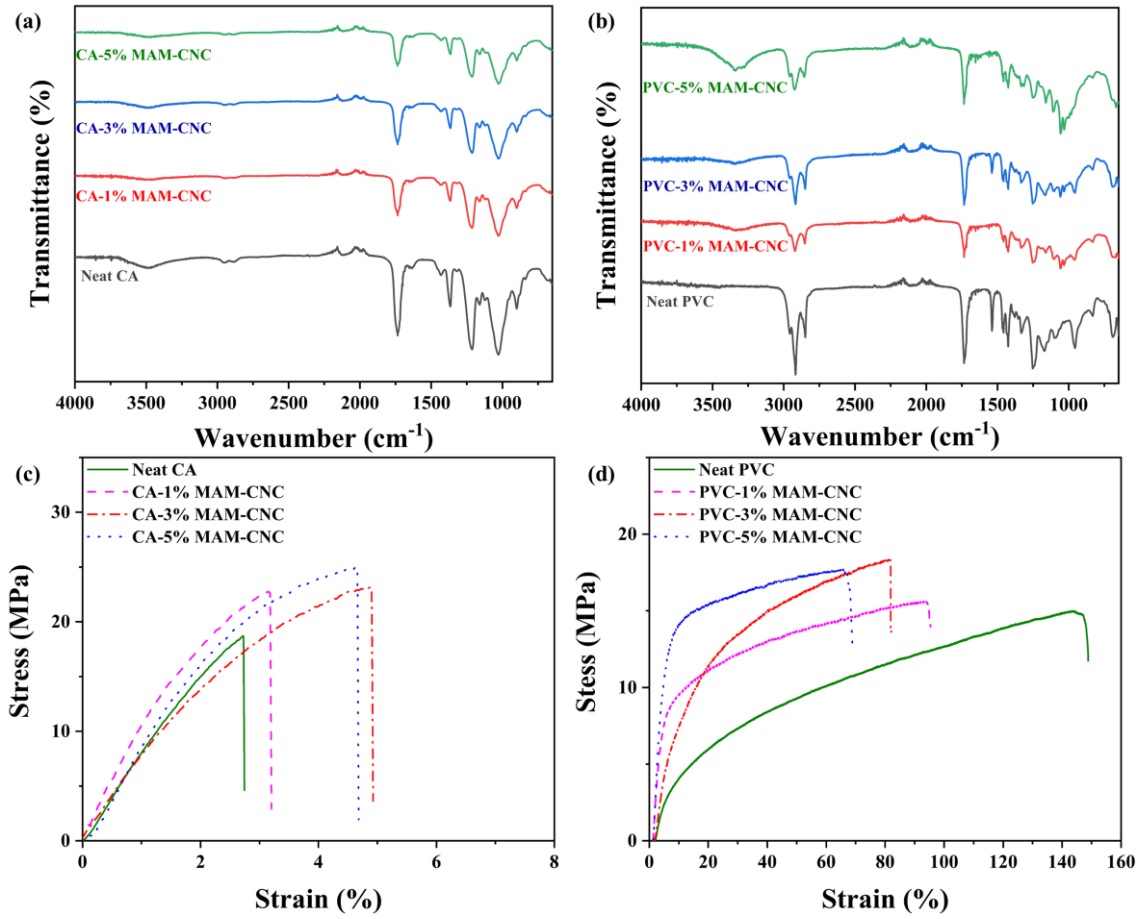

Figure 4.3. FT-IR spectra (a, b) and stress-strain curves (c, d) of the composite films.

The chemical structure of CA-based and PVC-based composite films was analyzed by FT-IR spectroscopy. As shown in Figure 4.3 (a, b), all CA films displayed the same characteristic peaks at 3486, 2950, 2882, 1735, and 1365 cm^{-1}, which were ascribed to O-H stretching, aliphatic C-H asymmetric, C=O stretching, and CH_2 scissoring, respectively [34]. The two peaks at 1213 and 1028 cm^{-1} corresponded to the asymmetric and symmetric stretching of C-O-C bonds, respectively [35]. The spectra of MAM-CNCs overlapped with those of CA so that no additional peaks could be observed [36]. Neat PVC showed characteristic peaks at 2919 cm^{-1} for C-H stretching, 1425 cm^{-1} for CH_2-Cl angular deformation, 1332 cm^{-1} for CH_2 angular

deformation, 1252 cm^{-1} for Cl-CH out of plane angular deformation, 956 cm^{-1} for out-of-plane trans deformation, and 833 cm^{-1} for C-Cl bond stretching [37]. The sharp peak at 1734 cm^{-1} was attributed to the additives of the commercial PVC film [38]. The addition of MAM-CNCs was confirmed by the typical peaks at 1055 cm^{-1} and 1031 cm^{-1} for C-O-C pyranose ring stretching vibration.

The effect of MAM-CNCs on the mechanical properties of CA and PVC films was analyzed. It was evident in Figure 4.3 (c) that the CA films followed brittle fracture [39]. Increasing loading of MAM-CNCs resulted in the improvement of tensile strength and elongation at break. For example, the tensile strength and elongation of CA-5% MAM-CNCs were 24.07 ± 0.96 MPa and 5.78 ± 1.80% in comparison with 17.87 ± 0.84 MPa and 2.58 ± 0.95% for the neat CA film, which were significantly increased by 35 and 124%, respectively. This might be explained by the good dispersion of nanofillers and interfacial adhesion between the modified nanocellulose and CA. Similar effects were observed in other CNC reinforced CA composite films [34, 40]. The adjusted hydrophobicity of modified CNCs and the similar chemical structure of modified CNCs and CA enabled the good interfacial compatibility [34, 41], contributing to the effective stress transfer at the interface and delaying the stretching failure [42, 43].PVC films displayed a typical ductile curve characterized by a plastic deformation region [44]. As listed in Table 4.1, addition of MAM-CNCs significantly improved the tensile strength but reduced the elongation. This result was in agreement with the previous reports [45, 46]. The presence of MAM-CNCs could reduce the PVC chain mobility and prevent from uncoiling, making the composite films less stretchable [45].

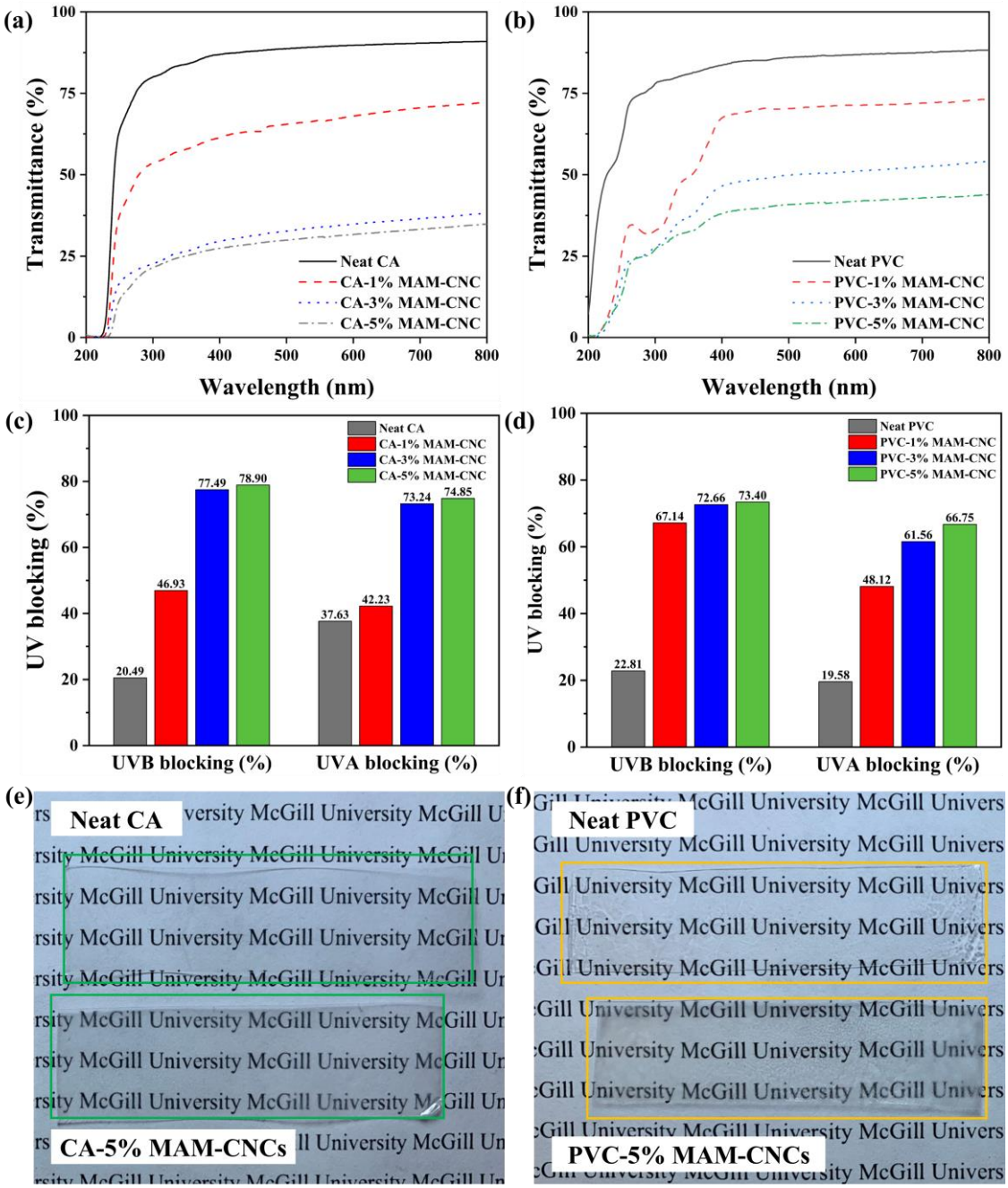

Figure 4.4. Optical transmittance spectra (a, b), UV blocking percentages (c, d), and photographs (e, f) of CA-based and PVC-based films.

High transparency and UV shielding capacity of the composite films are desirable characteristics in the food packing and medical industries. Figure 4.4 (a, b) displays the UV-vis transmittance spectra of CA-based and PVC-based films containing different MAM-CNCs contents. Both neat CA and neat PVC films exhibited limited UV blocking capacity, although

they possessed a high visible light transmittance of ~90%. Addition of MAM-CNCs reduced the UV-vis light transmittance of the films. Particularly, the CA-3% MAM-CNCs exhibited the reduction of 57.00 and 35.61% in UVB and UVA transmittance compared to the neat CA film, and the increase of 44.33 and 28.54% in UVB and UVA blocking capacities was observed in PVC-1% MAM-CNCs. These results were mainly attributed to the conjugated bond of the modified CNCs, which exhibited a strong absorption effect on ultraviolet radiation [47]. For both CA and PVC composite films, the transmittance of visible light at 600 nm decreased. Nonetheless, the digital images of CA-5% MAM-CNCs and PVC-5% MAM-CNCs in Figure 4.4 (e, f) were visually uniform, and the letters under the films were still visible. Therefore, incorporation of MAM-CNCs in packaging materials prevents the damage caused by UV light and displays the products in the package.

WVP is another important feature of packaging materials since the presence of water is crucial to microbial growth and chemical reactions. The WVP values of CA-MAM-CNCs and PVC-MAM-CNCs films are summarized in Table 4.1. A relatively low content of MAM-CNCs (1%) did not change the WVP values too much, but a further increase (3 and 5%) of nanofillers significantly reduced the permeability. For example, neat CA and PVC films had the WVP values of $6.72 \pm 0.83\times10^{-7}$ g $m^{-1}h^{-1}Pa^{-1}$ and $3.86 \pm 0.23\times10^{-7}$ g $m^{-1}h^{-1}Pa^{-1}$, respectively, which decreased to $4.24 \pm 0.43\times10^{-7}$ and $2.27 \pm 0.23\times10^{-7}$ g $m^{-1}h^{-1}Pa^{-1}$ when the content of MAM-CNCs was 5%. This could be attributed to the incorporated nanofillers in the film matrices, making the tortuous pathway for hindering the permeation of water molecules [48, 49].

Table 4.1. Physical properties of CA-based films and PVC-based films. Means within a column with different letters were significantly different ($p < 0.05$) within the same sample groups.

Samples	Tensile strength (MPa)	Elongation at break (%)	WVP (10^{-7} g $m^{-1}h^{-1}Pa^{-1}$)
Neat CA	17.87 ± 0.84^{b}	$2.58\%\pm0.95^{b}$	6.72 ± 0.83^{a}
CA-1% MAM-CNC	22.79 ± 0.04^{a}	$3.18\%\pm0.18^{a, b}$	$5.45\pm0.79^{a, b}$
CA-3% MAM-CNC	23.58 ± 0.45^{a}	$5.58\%\pm0.88^{a, b}$	4.54 ± 1.87^{b}
CA-5% MAM-CNC	24.07 ± 0.96^{a}	$5.78\%\pm1.80^{a}$	4.24 ± 0.43^{b}
Neat PVC	14.01 ± 0.67^{b}	$157.28\%\pm25.50^{a}$	3.86 ± 0.23^{a}
PVC-1% MAM-CNC	14.33 ± 1.18^{b}	$95.25\%\pm11.06^{b}$	$3.41\pm0.23^{a, b}$
PVC-3% MAM-CNC	19.15 ± 3.48^{a}	$84.57\%\pm16.70^{b}$	$2.73\pm0.45^{b, c}$
PVC-5% MAM-CNC	19.91 ± 1.22^{a}	$76.16\%\pm11.62^{b}$	2.27 ± 0.23^{c}

4.4.3. Antibacterial properties of modified CNCs and composite films

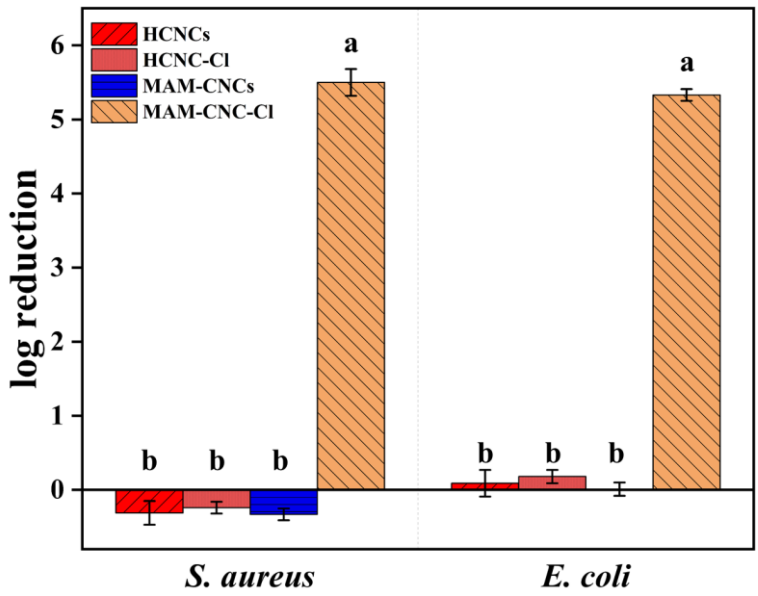

Figure 4.5. Antibacterial efficiency of HCNCs, HCNC-Cl, MAM-CNCs, and MAM-CNC-Cl against *S. aureus* and *E. coli*. Statistical significance ($p < 0.05$) between different CNC samples was indicated by different letters.

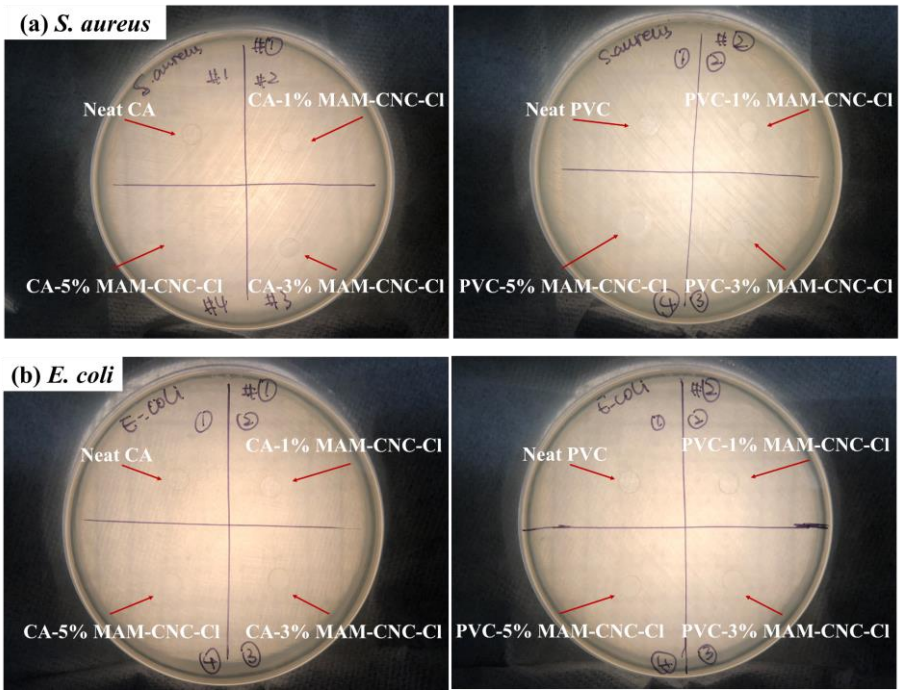

Figure 4.6. Images of inhibition zone against *S. aureus* (a) and *E. coli* (b) observed after 24 hours of incubation with CA films (left) and PVC films (right).

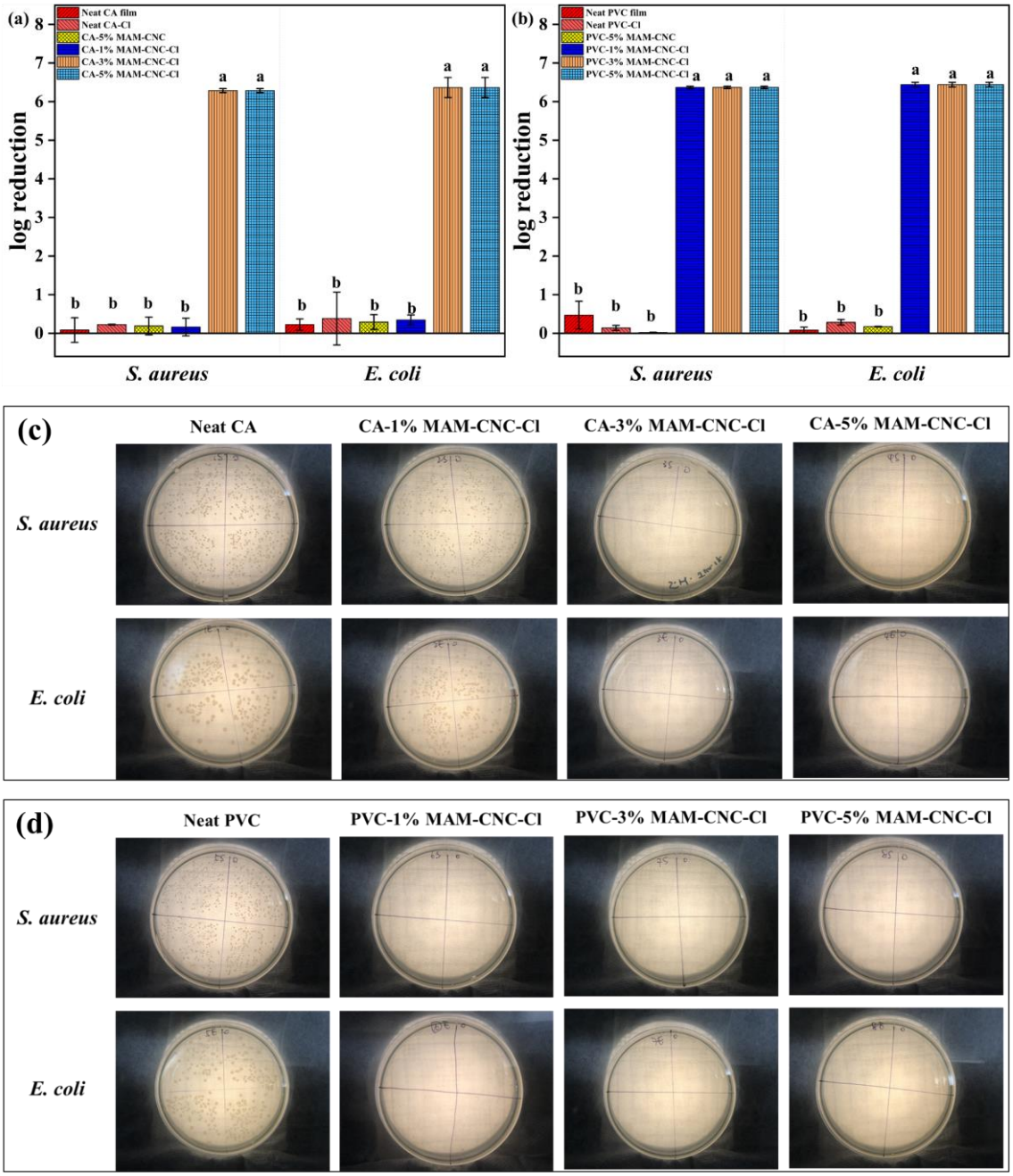

Figure 4.7. Antibacterial efficiency of CA films (a) and PVC films (b) with different treatments against *S. aureus* and *E. coli* after 1 hour incubation. Different letters on the tops of the columns indicate significant differences ($p < 0.05$) within the same sample groups. Photos of *S. aureus* and *E. coli* colonies grew on LBA plates upon 1 hour exposure to CA films (c) and PVC films (d).

HCNCs and MAM-CNCs before and after chlorination were incubated with *S. aureus* and *E. coli* at the concentration of ~10^5 CFU/mL. As shown in Figure 4.5, the control groups, including HCNCs, HCNC-Cl, and MAM-CNCs, didn't have any obvious effects on the growth of *S. aureus* and *E. coli*. In contrast, MAM-CNC-Cl with 0.04% oxidative chlorine could completely inactivate 5.50 log of *S. aureus* and 5.33 log of *E. coli* within 1 hour of contact. The excellent antibacterial efficacy of MAM-CNC-Cl was related to the transformation from N-H to N-Cl after chlorination, and the oxidative chlorine could transfer to the surface of the microbes, rupture their cell structure, and inactivate the cells [50].

The antibacterial activity of composite films was first investigated by the qualitative inhibition zone test through the disk diffusion method. After 24 hours of incubation, no inhibition zone could be seen even for the composite films after chlorination (Figure 4.6). Generally, the inhibition zone appears around the test product if the antimicrobial agent leaches into the agar and then inhibits bacterial proliferation [51]. This observation indicated that no or minimal release of modified CNCs occurred into the nutrient agar. Compared to our previously reported photobactericidal CNC nanofillers that were modified by rose Bengal and obviously diffused from the materials to the culture media [52], the limited migration of MAM-CNC nanofillers is important to ensure food safety when they are applied in primary food packaging [53]. Therefore, plate assay was performed where both *S. aureus* and *E. coli* were incubated on the surface of the composite films, and the neat films were used as control samples. As shown in Figure 4.7, neither the neat polymer films with/without chlorination nor the MAM-CNC films without chlorination treatment caused any significant reduction ($p > 0.05$) of both bacterial strains. As

shown in Figure 4.7 (a, c), there was even no significant effect on CA-1% MAM-CNC-Cl films after the 1 hour exposure, but a significant reduction was observed after these two bacterial strains were exposed to chlorine-charged CA-3% MAM-CNC and CA-5% MAM-CNC films. Specifically, 6.29 log reduction for *S. aureus* and 6.37 log reduction for *E. coli* were identified for the treatment of CA-3% MAM-CNC-Cl and CA-5% MAM-CNC-Cl. With only 1% MAM-CNC, the PVC composite film after chlorination could reduce 6.37 log of *S. aureus* and 6.44 log of *E. coli*. The excellent antibacterial efficacy was mainly due to the introduction of active chlorine on the chlorinated MAM-CNC, which could deactivate bacteria upon contact [54]. This bactericidal effect was also better than those of rose Bengal modified CNCs [52], CNCs grafted with 3-pentadecylphenol [55], and bacteriocin immobilized CNCs [56]. These results indicated that the MAM-CNCs are promising antibacterial nanofillers for different polymeric materials.

4.4.4. Rechargeability of composite films

Benefiting from the incorporated N-halamine structure, the antibacterial activity of composite films could be easily regenerated. CA-3% MAM-CNC and PVC-3% MAM-CNC were selected as the model samples to investigate the effect of recharge on antibacterial and mechanical properties. The films were chlorinated for 2 hours and then completely quenched with thiosulfate solution. Afterward, the films were recharged with oxidative chlorine again. As shown in Table 4.2, the recharged films could still reduce 6.39 log of *S. aureus* reduction and 6.38 log of *E. coli* upon 1 hour contact. At the same time, the tensile strength and elongation of recharged films presented no significant changes ($p > 0.05$) in comparison to those of CA-3% MAM-CNC and PVC-3% MAM-CNC films. The rechargeability is one of the unique

characteristics that distinguish the N-halamine modified cellulose nanofillers from other CNC modifications, such as quaternary ammonium compounds, aminoalkyl, aldehyde, and bacteriophage-modified cellulose nanostructures [53], and it will benefit the reuse of antibacterial packaging materials and reduce the cost and waste.

Table 4.2. Antibacterial and mechanical properties of CA-3% MAM-CNC-Cl, recharged CA-3% MAM-CNC-Cl, PVC-3% MAM-CNC-Cl, and recharged PVC-3% MAM-CNC-Cl. Two-tailed Student's t-test was performed within the same sample groups.

Samples	Log reduction		Tensile strength (MPa)	Elongation at break (%)
	S. aureus [1]	*E. coli* [2]		
CA-3% MAM-CNC-Cl	6.29±0.05	6.37±0.26	23.58±0.45	5.58±0.88
Recharged CA-3% MAM-CNC-Cl	6.39±0.06	6.38±0.06	23.22±1.94	4.93±0.61
PVC-3% MAM-CNC-Cl	6.37±0.03	6.44±0.06	19.15±3.48	84.57±16.70
Recharged PVC-3% MAM-CNC-Cl	6.39±0.06	6.38±0.06	16.01±0.73	78.68±29.31

[1, 2] inoculum concentrations around 10^6 CFU/mL

4.5. Conclusions

In this study, CNCs were successfully modified with N-halamine and applied as antibacterial nanofillers for CA and PVC films. The modification was verified by FT-IR and solid-state NMR. After chlorination, MAM-CNC-Cl showed a high antibacterial efficacy (99.999%) against both *S. aureus* and *E. coli*. With the addition of 5%-MAM-CNCs, CA and PVC films exhibited the improved UVB and UVA blocking capacity (37-58% and 47-50%), significantly

reduced WVP values (-37 and -41%), and dramatically increased tensile strength (34 and 42%), while retaining the acceptable transparency. More importantly, the incorporated MAM-CNCs hardly leach out from the plastic films, and the nanocomposite films with limited amounts of MAM-CNC (3% for CA and 1% for PVC) could result in the complete inactivation of *S. aureus* and *E. coli* at a concentration of 10^6 CFU/mL after 1 hour contact. This antibacterial activity could be fully recharged by chlorination without affecting the mechanical performance of the nanocomposite films. Therefore, this work demonstrates the promising applications of CNC-based functional nanofillers in active packaging.

4.6. References

1. Peng, N., Huang, D., Gong, C., Wang, Y., Zhou, J., & Chang, C. (2020). Controlled arrangement of nanocellulose in polymeric matrix: From reinforcement to functionality. *ACS Nano*, *14*(12), 16169-16179.
2. Huang, S., Liu, X., Chang, C., & Wang, Y. (2020). Recent developments and prospective food-related applications of cellulose nanocrystals: A review. *Cellulose*, *27*(6), 2991-3011.
3. Yao, A., Yan, Y., Tan, L., Shi, Y., Zhou, M., Zhang, Y., Zhu, P., & Huang, S. (2021). Improvement of filtration and antifouling performance of cellulose acetate membrane reinforced by dopamine modified cellulose nanocrystals. *Journal of Membrane Science*, *637*, 119621.
4. Wang, Y., & Chen, L. (2014). Cellulose nanowhiskers and fiber alignment greatly improve mechanical properties of electrospun prolamin protein fibers. *ACS Applied Materials & Interfaces*, *6*(3), 1709-1718.

5. Perumal, A., Sellamuthu, P., Nambiar, R., & Sadiku, E. (2018). Development of polyvinyl alcohol/chitosan bio-nanocomposite films reinforced with cellulose nanocrystals isolated from rice straw. *Applied Surface Science*, *449*, 591-602.
6. Niinivaara, E., Desmaisons, J., Dufresne, A., Bras, J., & Cranston, E. (2021). Thick polyvinyl alcohol films reinforced with cellulose nanocrystals for coating applications. *ACS Applied Nano Materials*, *4*(8), 8015-8025.
7. Rojas-Lema, S., Nilsson, K., Trifol, J., Langton, M., Gomez-Caturla, J., Balart, R., Garcia-Garcia, D., & Moriana, R. (2021). Faba bean protein films reinforced with cellulose nanocrystals as edible food packaging material. *Food Hydrocolloids*, *121*, 107019.
8. Zhou, C., Koshani, R., O'Brien, B., Ronholm, J., Cao, X., & Wang, Y. (2021). Bio-inspired mechano-bactericidal nanostructures: a promising strategy for eliminating surface foodborne bacteria. *Current Opinion in Food Science*, *39*, 110-119.
9. Bahrami, A., Delshadi, R., Assadpour, E., Jafari, S., & Williams, L. (2020). Antimicrobial-loaded nanocarriers for food packaging applications. *Advances in Colloid and Interface Science*, *278*, 102140.
10. Videira-Quintela, D., Guillén, F., Martin, O., & Montalvo, G. (2022). Antibacterial LDPE films for food packaging application filled with metal-fumed silica dual-side fillers. *Food Packaging and Shelf Life*, *31*, 100772.
11. Ahmad, H. (2021). Celluloses as support materials for antibacterial agents: a review. *Cellulose*, *28* (5), 2715-2761.
12. Huang, S., Tao, R., Ismail, A., & Wang, Y. (2020). Cellulose nanocrystals derived from

textile waste through acid hydrolysis and oxidation as reinforcing agent of soy protein film. *Polymers*, *12*(4), 958.

13. Hu, J., Li, R., Zhu, S., Zhang, G., & Zhu, P. (2021). Facile preparation and performance study of antibacterial regenerated cellulose carbamate fiber based on N-halamine. *Cellulose*, *28*(8), 4991-5003.
14. Laroque, D., de Aragao, G., de Araújo, P., & Carciofi, B. (2021). Active cellulose acetate-carvacrol films: Antibacterial, physical and thermal properties. *Packaging Technology and Science, 34,* 463-474.
15. Zampino, D., Mancuso, M., Zaccone, R., Ferreri, T., Borzacchiello, A., Zeppetelli, S., Dattilo, S., Ussia, M., Ferreri, L., Carbone, D., Recca, G., & Puglisi, C. (2021). Thermo-mechanical, antimicrobial and biocompatible properties of PVC blends based on imidazolium ionic liquids. *Materials Science and Engineering: C*, *122*, 111920.
16. Park, S., Baker, J., Himmel, M., Parilla, P., & Johnson, D. (2010). Cellulose crystallinity index: measurement techniques and their impact on interpreting cellulase performance. *Biotechnology for Biofuels*, *3*(1), 1-10.
17. Agarwal, U., Reiner, R., Ralph, S., Catchmark, J., Chi, K., Foster, E., Hunt, C., Baez, C., Ibach, R., & Hirth, K. (2021). Characterization of the supramolecular structures of cellulose nanocrystals of different origins. *Cellulose*, *28*(3), 1369-1385.
18. Song, Y., Chen, S., Chen, Y., Xu, Y., & Xu, F. (2021). Biodegradable and transparent films with tunable UV-blocking property from Lignocellulosic waste by a top-down approach. *Cellulose*, *28*(13), 8629-8640.

19. Zhang, X., Wei, Y., Chen, M., Xiao, N., Zhang, J., & Liu, C. (2020). Development of functional chitosan-based composite films incorporated with hemicelluloses: Effect on physicochemical properties. *Carbohydrate Polymers*, *246*, 116489.

20. Zhang, S., Li, L., Ren, X., & Huang, T. (2020). N-halamine modified multiporous bacterial cellulose with enhanced antibacterial and hemostatic properties. *International Journal of Biological Macromolecules*, *161*, 1070-1078.

21. Tang, X., Xu, H., Shi, Y., Wu, M., Tian, H., & Liang, J. (2020). Porous antimicrobial starch particles containing N-halamine functional groups. *Carbohydrate Polymers*, *229*, 115546.

22. Xu, D., Wang, S., Hu, J., Liu, Y., Jiang, Z., & Zhu, P. (2021). Enhancing antibacterial and flame-retardant performance of cotton fabric with an iminodiacetic acid-containing N-halamine. *Cellulose*, *28*(5), 3265-3277.

23. Zhang, X., Zhang, Q., Xue, Y., Wang, Y., Zhou, X., Li, Z., & Li, Q. (2021). Simple and green synthesis of calcium alginate/AgCl nanocomposites with low-smoke flame-retardant and antimicrobial properties. *Cellulose*, *28*(8), 5151-5167.

24. Gong, J., Li, J., Xu, J., Xiang, Z., & Mo, L. (2017). Research on cellulose nanocrystals produced from cellulose sources with various polymorphs. *RSC Advances*, *7*(53), 33486-33493.

25. Oh, S., Yoo, D., Shin, Y., & Seo, G. (2005). FTIR analysis of cellulose treated with sodium hydroxide and carbon dioxide. *Carbohydrate Research*, *340*(3), 417-428.

26. Derkaoui, S., Belbachir, M., Haoue, S., Zeggai, F., Rahmouni, A., & Ayat, M. (2019). Homopolymerization of methacrylamide by anionic process under effect of Maghnite-Na^+

(Algerian MMT). *Journal of Organometallic Chemistry*, *893*, 52-60.

27. Rosace, G., Colleoni, C., Trovato, V., Iacono, G., & Malucelli, G. (2017). Vinylphosphonic acid/methacrylamide system as a durable intumescent flame retardant for cotton fabric. *Cellulose*, *24*(7), 3095-3108.
28. Surov, O., Voronova, M., & Zakharov, A. (2021). Synthesis and properties of cellulose nanocrystal conjugates with reactive dyes. *Cellulose*, *28*(10), 6269-6285.
29. Atalla, R., & Vanderhart, D. (1984). Native cellulose: a composite of two distinct crystalline forms. *Science*, *223*(4633), 283-285.
30. Park, S., Johnson, D., Ishizawa, C., Parilla, P., & Davis, M. (2009). Measuring the crystallinity index of cellulose by solid state ^{13}C nuclear magnetic resonance. *Cellulose*, *16*(4), 641-647.
31. Fardioui, M., Mekhzoum, M., & Bouhfid, R. (2021). Photoluminescent biocomposite films of chitosan based on styrylbenzothiazolium-g-cellulose nanocrystal for anti-counterfeiting applications. *International Journal of Biological Macromolecules*, *184*, 981-989.
32. Kong, X., Zhang, S., Wang, Y., Liu, Y., Li, R., Ren, X., & Huang, T. (2019). Antibacterial polyvinyl alcohol films incorporated with N-halamine grafted oxidized microcrystalline cellulose. *Composites Communications, 15*, 25-29.
33. Zhang, Y., Yin, M., Lin, X., Ren, X., Huang, T., & Kim, I. S. (2019). Functional nanocomposite aerogels based on nanocrystalline cellulose for selective oil/water separation and antibacterial applications. *Chemical Engineering Journal, 371*, 306-313.
34. Cheng, M., Qin, Z., Hu, J., Liu, Q., Wei, T., Li, W., Ling, Y., & Liu, B. (2021). Facile

one−step preparation of acetylated cellulose nanocrystals and their reinforcing function in cellulose acetate film with improved interfacial compatibility. *Cellulose*, *28*(4), 2137-2148.

35. Gobalu, K., Vasudevan, M., Gopinath, S., Perumal, V., & Ovinis, M. (2021). Molybdenum disulphide/cellulose acetate nanofiber composite on screen printed electrodes for detecting cardiac troponin by electrical impedance spectroscopy. *Cellulose*, *28*(9), 5761-5774.
36. Ang, M., Devanadera, K., Duena, A., Luo, Z., Chiao, Y., Millare, J., Aquino, R., Huang, S., & Lee, K. (2021). Modifying cellulose acetate mixed-matrix membranes for improved oil–water separation: Comparison between sodium and organo-montmorillonite as particle additives. *Membranes*, *11*(2), 80.
37. Patil, S., & Jena, H. (2021). Performance assessment of polyvinyl chloride films plasticized with Citrullus lanatus seed oil based novel plasticizer. *Polymer Testing*, *101,* 107271.
38. Coltro, L., Pitta, J., & Madaleno, E. (2013). Performance evaluation of new plasticizers for stretch PVC films. *Polymer Testing*, *32*(2), 272-278.
39. Senthil Muthu Kumar, T., Rajini, N., Jawaid, M., Varada Rajulu, A., & Winowlin Jappes, J. (2018). Preparation and properties of cellulose/tamarind nut powder green composites. *Journal of Natural Fibers*, *15*(1), 11-20.
40. Cao, J., Sun, X., Lu, C., Zhou, Z., Zhang, X., & Yuan, G. (2016). Water-soluble cellulose acetate from waste cotton fabrics and the aqueous processing of all-cellulose composites. *Carbohydrate Polymers*, *149*, 60-67.
41. Jiang, M., Zhang, J., Wang, Y., Ahmad, I., Guo, X., Cao, L., Chen, Y., Gan, L., & Huang, J. (2021). Covalent-bond-forming method to reinforce rubber with cellulose nanocrystal

based on the thiol-ene click reaction. *Composites Communications*, *27*, 100865.

42. Sharma, A., Mandal, T., & Goswami, S. (2021). Fabrication of cellulose acetate nanocomposite films with lignocelluosic nanofiber filler for superior effect on thermal, mechanical and optical properties. *Nano-Structures & Nano-Objects*, *25*, 100642.
43. Chen, K., Yu, J., Huang, J., Tang, Q., Li, H., & Zou, Z. (2021). Improved mechanical, water vapor barrier and UV-shielding properties of cellulose acetate films with flower-like metal-organic framework nanoparticles. *International Journal of Biological Macromolecules*, *167*, 1-9.
44. Mendoza, D., Browne, C., Raghuwanshi, V., Mouterde, L., Simon, G., Allais, F., & Garnier, G. (2021). Phenolic ester-decorated cellulose nanocrystals as UV-absorbing nanoreinforcements in polyvinyl alcohol films. *ACS Sustainable Chemistry & Engineering*, *9*(18), 6427-6437.
45. Ahmed, R., Ibrahiem, A., El-Bayoumi, A., & Atta, M. (2021). Structural, mechanical, and dielectric properties of polyvinylchloride/graphene nano platelets composites. *International Journal of Polymer Analysis and Characterization*, *26*(1), 68-83.
46. Hajibeygi, M., & Jafarzadeh, H. (2020). Effects of phosphorus-containing aromatic polyamide and organo-modified hydroxyapatite nanoparticles on the thermal, combustion and mechanical properties of polyvinyl chloride. *Polymer Bulletin*, *77*(8), 4259-4287.
47. Li, F., Yu, H. Y., Li, Y., Abdalkarim, S., Zhu, J., & Zhou, Y. (2021). "Soft-rigid" synergistic reinforcement of PHBV composites with functionalized cellulose nanocrystals and amorphous recycled polycarbonate. *Composites Part B: Engineering*, *206*, 108542.

48. Júnior, L., da Silva, R., Vieira, R., & Alves, R. (2021). Water vapor sorption and permeability of sustainable alginate/collagen/SiO_2 composite films. *LWT*, *152*, 112261.

49. Gan, P., Sam, S., Abdullah, M., Omar, M., & Tan, W. (2021). Water resistance and biodegradation properties of conventionally-heated and microwave-cured cross-linked cellulose nanocrystal/chitosan composite films. *Polymer Degradation and Stability*, *188*, 109563.

50. Bu, D., Zhou, Y., Yang, C., Feng, H., Cheng, C., Zhang, M., Xu, Z., Xiao, L., Liu, Y., & Jin, Z. (2021). Preparation of quaternarized N-halamine-grafted graphene oxide nanocomposites and synergetic antibacterial properties. *Chinese Chemical Letters, 32*(11), 3509-3513.

51. Spieser, H., Denneulin, A., Deganello, D., Gethin, D., Koppolu, R., & Bras, J. (2020). Cellulose nanofibrils and silver nanowires active coatings for the development of antibacterial packaging surfaces. *Carbohydrate Polymers*, *240*, 116305.

52. Koshani, R., Zhang, J., van de Ven, T., Lu, X., & Wang, Y. (2021). Modified hairy nanocrystalline cellulose as photobactericidal nanofillers for food packaging application. *ACS Sustainable Chemistry & Engineering*, *9*(31), 10513-10523.

53. Tavakolian, M., Jafari, S., & van de Ven, T. (2020). A review on surface-functionalized cellulosic nanostructures as biocompatible antibacterial materials. *Nano-Micro Letters*, *12*, 73.

54. Ren, X., Akdag, A., Zhu, C., Kou, L., Worley, S., & Huang, T. (2009). Electrospun polyacrylonitrile nanofibrous biomaterials. *Journal of Biomedical Materials Research.*

Part A, *91*(2), 385-390.

55. Shin, H., Kim, S., Kim, J., Kong, S., Lee, Y., & Lee, J. (2022). Preparation of 3-pentadecylphenol-modified cellulose nanocrystal and its application as a filler to polypropylene nanocomposites having improved antibacterial and mechanical properties. *Journal of Applied Polymer Science*, *139*(13), 51848.
56. Bagde, P., & Nadanathangam, V. (2019). Mechanical, antibacterial and biodegradable properties of starch film containing bacteriocin immobilized crystalline nanocellulose. *Carbohydrate Polymers*, *222*, 115021.

Connecting Text

In the previous chapter, CNCs obtained from textile waste were modified with N-halamine and applied as antibacterial nanofillers for cellulose acetate and poly(vinyl chloride) films. Chapter 5 aimed to investigate the effects of different antibacterial modifications of CNCs on the performance of active compostable packaging materials. The PLA films were selected as a model, and CNCs were modified with methacrylamide, quaternary ammonium salt, and zinc oxide, respectively. The effects of three different modified CNCs on antibacterial activity, mechanical properties, gas barrier property, and compost disintegrability of PLA films were compared.

Chapter 5. Construction of Compostable Packaging with Antibacterial Property and Improved Performance using Sprayed Coatings of Modified Cellulose Nanocrystals

5.1. Abstract

Increasing concerns about food safety and the environment have facilitated the development of eco-friendly antibacterial packaging. This study aimed to demonstrate a facile way to fabricate active packaging materials with modified cellulose nanocrystals (CNCs) and compare the effects of different modified CNCs on the performance of compostable materials. Polylactic acid (PLA) film was selected as a model, and CNCs were modified with methacrylamide, cetyltrimethylammonium bromide, and zinc oxide, respectively, and then applied on the surface of PLA films by spray-coating. All modified CNCs showed excellent antibacterial activity against *S. aureus* and *E. coli* (>99.999%). The effects of different CNC modifications on the performance of PLA films were investigated. Compared to neat PLA films, PLA/CNC films exhibited improved mechanical strength with maintained flexibility, lower gas permeability, and faster compost disintegration rate, and extended the shelf life of wrapped pork samples from 3 days to more than 10 days. Therefore, this work will also facilitate the applications of PLA materials in eco-friendly packaging.

5.2. Introduction

Foodborne diseases are global public health concerns that cause considerable socioeconomic implications. In fact, the problem is caused by consuming food contaminated with microorganisms or chemical substances that result in over 200 diseases (Gao et al., 2022). According to the estimation of the World Health Organization, foodborne diseases lead to over 420,000 deaths annually, with 40% being children under five (WHO, 2020). Among the solutions to reduce foodborne diseases, antibacterial packaging is an important approach to

controlling foodborne pathogens during transportation and storage. At the same time, the increasing environmental concerns about non-degradable plastics bring awareness of "green" packaging materials. Numerous research efforts have been made to promote the applications of biodegradable polymers, which include polysaccharides, proteins of animal or plant origin, lipids, and polyesters from microbial sources (Fonseca-García et al., 2021; Omerović et al., 2021). Among them, polylactic acid (PLA) has been reported as a promising candidate to replace the fossil-based plastic, due to its renewability, biodegradability, facial processing, and biocompatibility (Ma et al., 2022; Shojaeiarani et al., 2022). PLA has the largest market share in the biodegradable plastic field, estimated for a market of $6.5 billion by 2025 (Shojaeiarani et al, 2020). Various PLA based antimicrobial packaging materials have been developed by the incorporation of functional agents such as metal oxide (Zhang et al., 2021), lignin (Cerro et al., 2021), chitosan (Kongkaoroptham et al., 2021), and essential oil (Fiore et al, 2021). For instance, Jiang et al. (Jiang et al., 2022) prepared antibacterial membranes based on PLA, polybutylene adipate terephthalate, carboxymethyl cellulose, and silver, which showed the effective antibacterial property against *Staphylococcus aureus* (*S. aureus*) and *Escherichia coli* (*E. coli*). However, the poor mechanical and barrier properties of PLA films limited their applications in food packaging due to the low crystallinity of PLA (Beauson et al., 2022; Sharafi et al., 2022).

Cellulose nanocrystals (CNCs) have received noticeable attention owing to their unique morphology, high mechanical strength, and broad functionalization capacities (Huang et al., 2020). Numerous studies focused on the reinforcing effects of CNCs on the mechanical

properties of packaging films (Niinivaara et al., 2021; Rojas-Lema et al., 2021; Salmieri et al., 2014a, 2014b). To further broaden the application scope of CNCs, recent research investigated the modifications of CNCs with multifunctions and applied them as functional nanofillers of packaging materials. For example, Koshani et al. (Koshani et al., 2021) synthesized the antibacterial hairy CNCs with the conjugated photosensitizer rose bengal, which could inactivate over 80% of both *Listeria monocytogenes* and *Salmonella enterica* serotype Typhimurium upon normal light irradiation. Shin et al. (Shin et al., 2022) prepared the functionalized CNCs by grafting 3-pentadecylphenol that showed the antibacterial property of 99.99% against *E. coli*. However, these nanofillers needed to be incorporated when the packaging materials were formed, and the effects of different modified CNCs on compostable packaging have been seldom compared.

Packaging materials based on biopolymers will help reduce the negative effect on the environment, while the antibacterial property can better protect food products and decrease food waste. In this study, we hypothesized that (i) a sprayed coating of modified CNCs could improve the performance of PLA films, and (ii) the effects were related to the different modifications of CNCs. CNCs derived from waste textile were selected as a model and modified with N-halamine (methacrylamide, MAM), quaternary ammonium salt (CTAB), and metal oxide (ZnO), respectively. The modified CNCs were spray-coated on the surface of PLA films, and their effects on the properties (antibacterial activity, mechanical properties, gas barrier properties, and compost disintegrability) of PLA films were investigated. Moreover, the preservation of pork loin with CNC-coated or uncoated PLA films was monitored.

5.3. Materials and Methods

5.3.1. Materials

Waste cotton clothes were kindly provided by Renaissance (Montreal, QC, Canada). CNCs were directly extracted from textile waste by using sulfuric acid hydrolysis, according to our previous work (Huang et al., 2020). Cetyltrimethylammonium bromide (CTAB, ≥98%), zinc acetate dihydrate (>95%), sodium hydroxide (NaOH, ≥97.0%), methacrylamide (MAM, 98%), sodium persulfate (≥98%), sodium thiosulfate anhydrous (≥98%), tetrahydrofuran (THF, >95%), and glacial acetic acid (≥99.7% w/w) were purchased from Fisher Scientific (Ottawa, ON, Canada) and used without further treatment. Pellet PLA (Ingeo 4043D grade, >98%, density of 1.24 g/cc) was purchased from NatureWorks (Minnetonka, MN, USA). Luria–Bertani (LB) medium and tryptic soy agar (TSA) were purchased from Becton, Dickinson and Company (Franklin Lakes, NJ, USA), and phosphate-buffered saline (10× PBS) was obtained from VWR International (Mississauga, ON, Canada).

5.3.2. Modification of CNCs

MAM-modified CNCs were prepared according to the method reported by Liu et al. (Liu et al., 2017) with some modifications. The desired amount of NaOH was added into 50.00 g of CNC aqueous suspension (10 wt%), and then 5.00 g MAM and 0.03 g sodium persulfate were added and stirred at room temperature for 20 min. The reaction was conducted at 65 °C (in a water bath) for 5 hours. After that, the product was washed with distilled water to remove unreacted MAM and sodium persulfate and coded as MAM-CNCs.

The preparation of CTAB-modified CNCs was carried out according to the method described

by Ranjbar et al. (Ranjbar et al., 2020). Briefly, 40.00 g of CNC aqueous suspension (5 wt%) was slowly added to 20.00 g of CTAB solution (5 wt%). The mixture was stirred at room temperature for 2 hours. Then, the modified CNCs were washed with distilled water to remove the unbounded CTAB and coded as CTAB-CNCs.

The zinc oxide-modified CNCs were synthesized by using zinc acetate as the zinc precursor and NaOH as a reducing agent, according to a previous report (Badawy et al., 2021) with some modifications. In brief, zinc acetate solution (50.00 g, 10 wt%) was mixed with CNC aqueous suspension (50.00 g, 2.5 wt%) and stirred at 80 ℃ for 1 hour. Then, NaOH solution (50 mL, 0.1 mol/L) was added dropwise to the mixture, and the suspension showed a milky color. The reaction continued at 80 ℃ for 2 hours under stirring. The obtained samples were well-washed with distilled water and coded as ZnO-CNCs.

5.3.3. Preparation of PLA/CNC composite films

PLA films were prepared by dissolving 0.8 g PLA pellets in 10 mL THF, and the solution was filled into a glass mold and dried at 25 ℃ for 12 hours. After washing with distilled water, the modified CNCs were centrifugated (7000 g, 30 min, Eppendorf centrifuge 5430, NRW, Germany), dispersed in acetic acid (2 w/v%), and then sprayed on the surface of PLA films (length × width × thickness: 8 cm × 6 cm × 0.15 mm). The PLA/CNC composite films were dried in the fume hood for 24 hours and coded as PLA-CC4, PLA-CC8, PLA-ZC4, PLA-ZC8, PLA-MC4, and PLA-MC8, corresponding to the CTAB-CNCs, ZnO-CNCs, and MAM-CNCs contents (based on the dry weight of PLA) of 4 and 8 wt%, respectively. The films were stored at 25 ℃ and 50% relative humidity for 3 days prior to analysis.

5.3.4. Characterizations

5.3.4.1. Fourier-transform infrared (FTIR) spectroscopy

FTIR spectra of modified CNCs and PLA/CNC composite films were obtained by using a Cary 630 FTIR spectrometer with an attenuated total reflectance sampling module (Agilent technologies, Inc., USA). The spectra were collected in the range of 4000-650 cm^{-1} as the average of 64 scans with a resolution of 2 cm^{-1}, using the empty accessory as blank.

5.3.4.2. X-ray diffraction (XRD)

XRD patterns of pristine and modified CNCs were obtained using an Empyrean 3 (Malvern Panalytical Ltd., UK) X-ray diffractometer in a Bragg Brentano configuration, with Cu Kα radiation between 4° and 80°. The crystallinity index (CrI) was determined by the peak height method (Park et al., 2010) in terms of Equation (1):

$$CrI\ (\%) = \frac{I_{(200)} - I_{am}}{I_{(200)}} \times 100\% \qquad \text{Equation (1)}$$

where $I_{(200)}$ is the maximum diffraction intensity associated with surface areas of crystalline cellulose, and I_{am} is the diffraction intensity of an amorphous cellulose fraction.

5.3.4.3. UV-vis spectroscopy

UV-vis spectra of pristine CNC and ZnO-CNC suspensions were collected on a DU 800 UV-Vis spectrophotometer (Beckman Coulter, USA) in the wavelength range of 200-400 nm against distilled water as blank.

5.3.4.4. Zeta potential measurement

The surface charge of pristine and modified CNCs was measured using the NanoBrook Omni zeta potential analyzer (Brookhaven Instruments Corporation, USA). Triplicate measurements

were taken at 25 ℃ after the samples were conditioned for 300 seconds.

5.3.4.5. Transmission electron microscopy (TEM)

The morphology of modified CNCs was observed using the Talos F200X G2 TEM (Thermo Fisher Scientific, USA). A tiny drop of diluted CNC suspension was deposited on a carbon-coated copper grid. After air drying at room temperature, the sample was imaged on TEM at a voltage of 200 kV.

5.3.4.6. Scanning electron microscopy (SEM)

The surface morphology of PLA/CNC composite films was observed by Hitachi TM1000 SEM (NJ, USA), operating at an acceleration voltage of 4 kV. The film samples were sputtered with 4 nm gold-platinum prior to observation and photographing.

5.3.4.7. Antibacterial test

Two strains were used for the antibacterial testing, namely *S. aureus* ATCC 6538 (Gram-positive) and *E. coli* K12 (Gram-negative). Each strain was prepared from -80 °C 20% glycerol stock and streaked for isolation on LB agar plates. The plates were incubated at 37 °C overnight, and isolated colonies were picked for inoculation of 4 mL LB broth at 37 °C with constant shaking. After 16 hours, a concentration of ca. 8 log for each bacterial culture was achieved, and the bacterial inoculums were prepared by diluting the culture with PBS to a certain concentration for further experiments.

The antibacterial efficacy of modified CNCs was evaluated by mixing 20 mL of CNC suspension and 200 μL of bacterial inoculum to a final concentration of 10^5 CFU/mL (Tang et al., 2020). The mixture was incubated for 1 hour with constant shaking, and then the upper

suspension was used for serial dilution using PBS. After that, the diluted solution was spread onto the surface of LB agar plate and incubated at 37 °C for 24 hours. The colonies on the plate were enumerated to calculate the log reduction.

The antibacterial activity of PLA/CNC composite films against *S. aureus* and *E. coli* was analyzed by a modified AATCC 100 test method (Xu et al., 2021). The composite films with a thickness of 0.15 mm were cut into 2 cm × 2 cm. Then, 20 μL of bacterial suspension (~10^6 CFU/mL) was sandwiched between two films to enable sufficient contact. After 1 hour of contact, 4 mL of sterile sodium thiosulfate was added and vortexed to rinse off bacteria. The rinsing solution was serially diluted for the plating assay.

The zone of inhibition was measured using the disc diffusion method (Zhang et al., 2021). *S. aureus* and *E. coli* suspensions with a concentration of around 10^8 CFU/mL were evenly spread on the LB agar plates, and the composite films (diameter of 6 mm) were placed over the surface of the inoculated plate. The plates were incubated at 37 ℃ for 24 hours, and the bacterial inhibition zone was measured.

5.3.4.8. Mechanical properties

The mechanical properties of PLA/CNC composite films were tested using an eXpert 7601 single column testing machine (ADMIT, USA) at 25 ℃ according to the standard ASTM D882. The dimension of film specimens was 60 mm × 10 mm × 0.15 mm (length × width × thickness). The initial grip separation distance was set as 20 mm, and the separation speed was 20 mm/min. The thickness of the films was measured by a Traceable digital caliper (Fisher Scientific, ON, Canada).

5.3.4.9. Gas barrier properties

Water vapor permeability (WVP) was determined using a water vapor permeability tester (model 3/61, Mocon, Inc., USA) at 37 ℃ and 90% relative humidity (RH). WVP values were calculated using Equation (2) (Zhou et al., 2022):

$$WVP = \frac{WVTR \times n}{\Delta p} \quad \text{Equation (2)}$$

where n is the film thickness (m), and Δp is the partial pressure difference across the films (Pa). The oxygen transmission rate (OTR) of PLA/CNC composite films was determined at 23 ℃ and 0% RH using an oxygen permeability tester (model 2/22, Mocon, Inc., USA).

5.3.4.10. Water contact angle

The water contact angle was tested by a contact angle meter (Future digital scientific, Co. USA) using the sessile drop method. The water droplet (5 μL) was placed on the film surface, and the image was immediately captured and analyzed with the goniometer at room temperature. Each measurement was performed on a different spot of the film, and the results were based on the average of three measurements.

5.3.4.11. Disintegration under composting conditions

The disintegration performance of PLA/CNC composite films was tested following the ISO-20200 standard (ISO, 2015). Briefly, solid synthetic waste was prepared by mixing 40% sawdust, 30% rabbit feed, 10% ripe compost, 10% corn starch, 5% saccharose, 4% corn oil, and 1% urea together. After that, the dry waste was mixed with water in 45:55 ratio. The composite films were cut into 25 mm × 25 mm and buried at 6 cm depth in composting reactor containing synthetic wet waste. The reactor was then put in an air-circulation oven at 58 ± 2 ℃,

and water was added periodically to maintain the humidity in the compost. The films were recovered from the reactor at different times (3, 7, 10, and 14 days), dried, and weighed. The weight loss of the films was calculated using Equation (3) (Cerro et al., 2021):

$$Weight\ loss\ (\%) = \frac{m_i - m_d}{m_i} \times 100\% \quad \text{Equation (3)}$$

where m_i and m_d were the initial dry mass and residue dry mass of tested samples, respectively.

5.3.4.12. Meat preservation test

Pork loin was selected as a food model and purchased from a local market. The pork was cut into 1 cm × 1 cm × 1 cm portions and randomly divided into five groups. The test groups were packaged with PLA/CNC composite films, and the control groups were either unpackaged or wrapped with neat PLA films. The samples were placed on the trays and stored at 4 ℃. The total viable count (TVC) values were determined at 0, 1, 3, 5, 7, and 10 days of storage according to the method reported by Zhong et al. (Zhong et al., 2021). Briefly, the pork samples were transferred aseptically to a stomacher bag and added with PBS solution. The mixture was homogenized for 2 minutes using a lab stomacher blender (Seward, UK). Then, serial dilutions were prepared with PBS, spread on TSA plates, and incubated at 37 ℃ for 48 hours. The experiments were performed in triplicate, and the results of TVC were reported as CFU/g.

5.3.5. Statistical analysis

The experiments were carried out in triplicate, and data were presented as the mean ± standard deviation. The statistical analysis of the data was carried out through a one-way analysis of variance (ANOVA) using IBM SPSS Statistics 26 software, and the differences between means were analyzed by LSD post-hoc analysis at the confidence level of 0.05.

5.4. Results and Discussion

5.4.1. Structure of modified CNCs

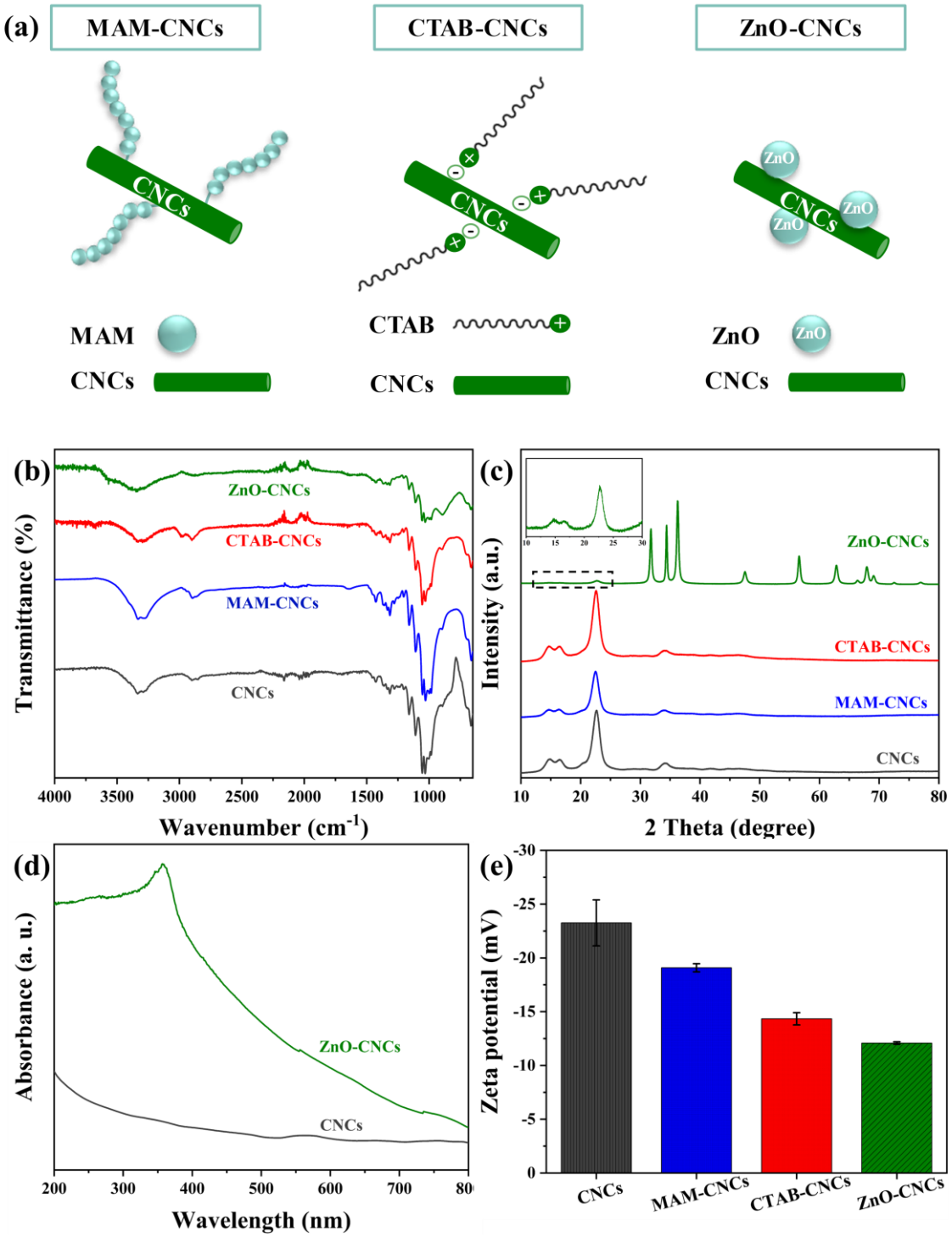

Figure 5.1. (a) Illustration, (b) FTIR spectra, (c) XRD patterns, (d) UV-vis spectra, and (e) zeta potential of pristine and modified CNCs.

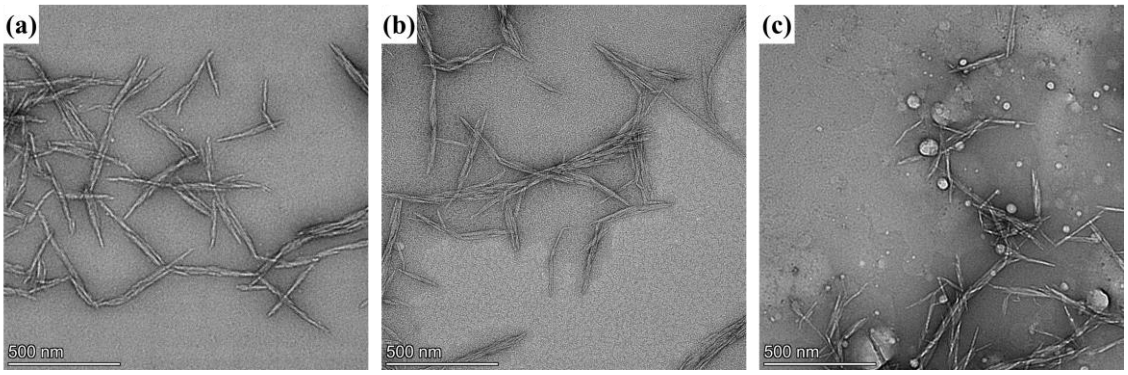

Figure 5.2. TEM images of (a) MAM-CNCs, (b) CTAB-CNCs, and (c) ZnO-CNCs.

Figure 5.1 (a) illustrates the different modified CNCs, and their chemical structures were analyzed by FTIR (Figure 5.1 (b)). The FTIR spectrum of unmodified CNCs showed the characteristic peaks at 3338 cm^{-1}, 2893 cm^{-1}, 1427 cm^{-1}, 1371 cm^{-1}, 1315 cm^{-1}, 1160 cm^{-1}, 1055 cm^{-1}, 1031 cm^{-1}, and 893 cm^{-1}, corresponding to O-H stretching, C-H stretching, C-H bending, CH_2 bending, O-H bending, asymmetric vibration of C-O-C, pyranose ring stretching, and β-glycoside bonds of the glucose ring, respectively. After the modification with MAM, the FTIR spectrum of MAM-CNCs showed a significant new peak at 1643 cm^{-1} assigned to amide carbonyl C=O bond. Besides, the peak at 1600 cm^{-1} attributed to C=C bond of MAM was not observed in MAM-CNCs, indicating that the residue of unreacted MAM monomer was removed from the product. Proof of the successful modification of MAM onto CNCs was interpreted in comparison with the previous report (Rosace et al., 2017). Compared to original CNCs, only slight changes of FTIR spectrum were observed for CTAB-CNCs. Strong C-H stretching at 2984 cm^{-1} and 2900 cm^{-1}, corresponding to the long-chain alkyl group of CTAB, suggested the presence of CTAB on CNCs and the absence of direct chemical bonding (Ranjbar et al., 2020). For ZnO-CNCs, no changes were found in the FTIR spectrum (Sharma et al., 2019), but a new and strong characteristic peak at 365 nm appeared in the UV-vis spectrum

(Figure 5.1 (d)), ascribed to the basic bandgap absorption of ZnO (Xiao et al., 2020). It has been reported that hydrogen bonds and electrostatic attraction are two potential interactions between CNCs and ZnO (Fu et al., 2015; Sharma et al., 2019; Zhao et al., 2017). The XRD patterns of pristine and modified CNCs are shown in Figure 5.1 (c). All the samples exhibited similar diffraction peaks at 14.6° ($1\bar{1}0$), 16.4° (110), and 22.5° (200), ascribed to cellulose I_β crystal structure (Duarte Urueña et al., 2021). ZnO-CNCs also showed the peaks at 31.8°, 34.5°, 36.2°, 47.8°, 56.5°, 62.8°, and 68.0°, corresponding to (100), (002), (101), (102), (110), (103), and (112) of the ZnO crystal structure, respectively (Elfeky et al., 2020). The surface charges of the modified CNCs are shown in Figure 5.1 (e). The original CNCs had a zeta potential value of around -23 mV, which was similar to the samples from sago frond wastes prepared by sulfuric acid hydrolysis (Arnata et al., 2020; Asadi et al., 2021). After surface modification, MAM-CNCs showed similar surface charges with CNCs. The electrostatic interaction between CTAB and CNCs resulted in the reduced negative charges of CNCs (Baggio et al., 2022), while ZnO-CNCs had the least charges due to the attracted ZnO (Badawy et al., 2021; Guan et al., 2019). Figure 5.2 shows the morphologies of modified CNCs, which had a typical rod-like shape with an average length of 158 nm and a diameter of 10 nm, without obvious aggregation (Badawy et al., 2021; Gahrooee et al., 2021; Li et al., 2020). The particle size of ZnO in Figure 5.2 (c) was 36±16 nm, which was similar to the reported ones (Elfeky et al., 2020; Lizundia et al., 2018).

5.4.2. Antibacterial activity

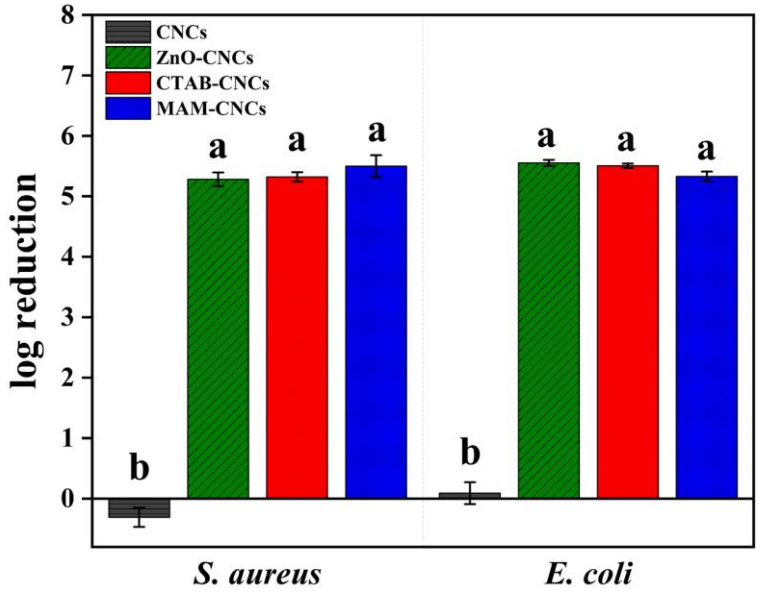

Figure 5.3. Antibacterial efficiency of pristine and modified CNCs against *S. aureus* and *E. coli*. Statistical significance ($p < 0.05$) between different CNC samples was indicated by different letters.

The pristine and modified CNCs were cultivated with Gram-positive (*S. aureus*) and Gram-negative (*E. coli*) bacteria to evaluate their antibacterial activity. For MAM-CNCs, chlorination treatment with sodium hydrochloride was conducted to convert the N-H bond to oxidative chlorine, which activated the antibacterial capacity of MAM-CNCs (Chang et al., 2018). In contrast, ZnO-CNCs and CTAB-CNCs did not require any pre-treatment. As shown in Figure 5.3, the original CNCs did not exhibit any effect against both *S. aureus* (-0.31 log) and *E. coli* (0.09 log), which was consistent with a previous report (Zhou et al., 2022). At the same time, significant antibacterial efficiency ($p < 0.05$) was observed in all modified CNC samples, with >99.999% reduction for both strains. After the chlorination treatment, MAM-CNCs could generate active chlorine that transferred to cell membranes and resulted in cell death (Kong et

al., 2019). CTAB-CNCs could change the bacterial membrane permeability or bacterial surface electrostatic balance after contact, ultimately leading to cell death (Xie et al., 2011). As for ZnO-CNCs, several probable routes have been proposed to explain their bactericidal mechanism. The released ion mediated killing was one of the possible mechanisms, where the released Zn^{2+} entered the bacterial cells, leading to inhibited DNA replication. ZnO might also attach and induce deformation of the bacterial cell wall (Ahmad, 2021; Roy & Rhim, 2019; Zhang et al., 2021).

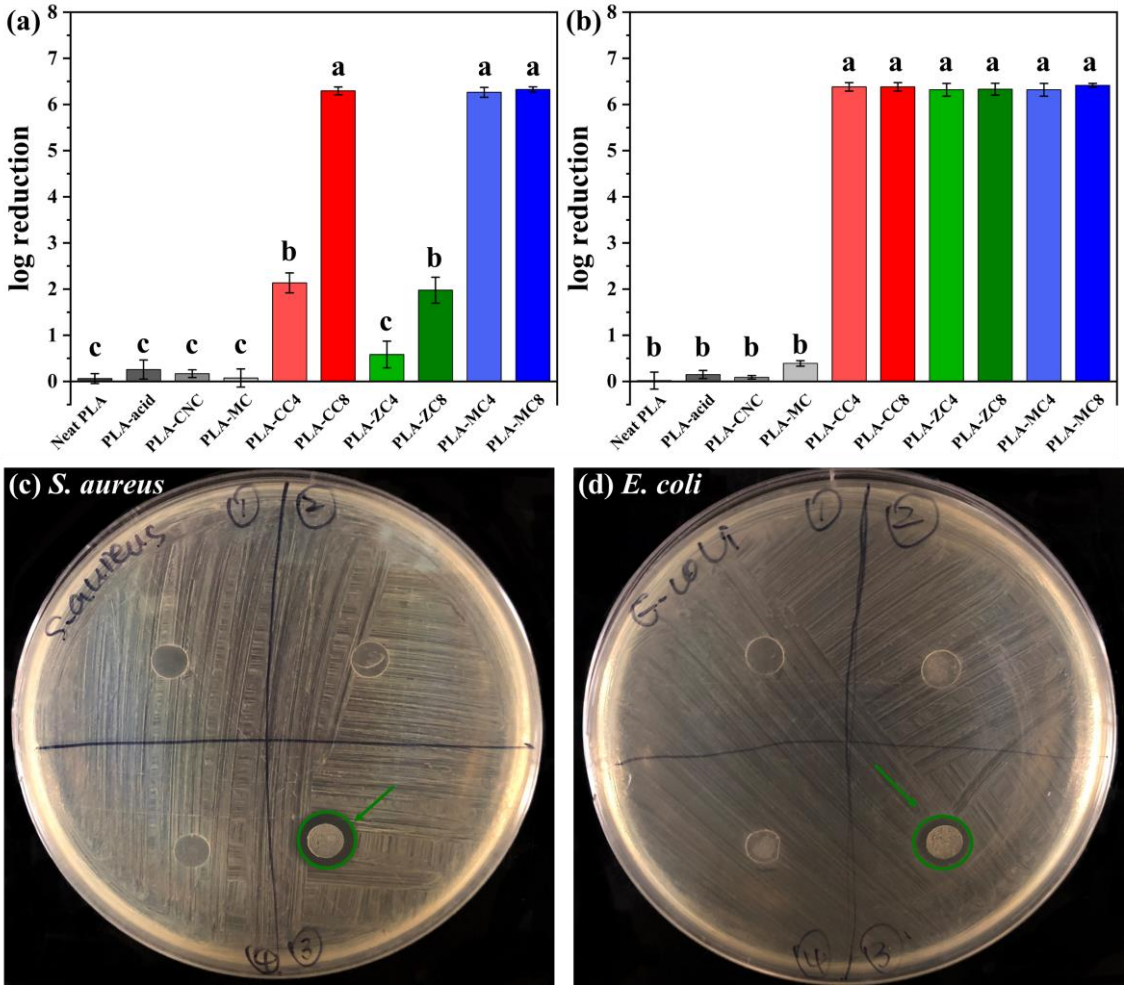

Figure 5.4. (a, b) Antibacterial activity and (c, d) images of inhibition zone of PLA/CNC composite films against *S. aureus* and *E. coli*. Means with different letters on the column top were significantly different ($p < 0.05$).

As shown in Figure 5.4 (a, b), the control groups, including neat PLA film, neat PLA films treated with acetate acid, PLA film with pristine CNC coating, and PLA film with MAM-CNC coating (without chlorination), did not show any antibacterial activity against either *S. aureus* or *E. coli*. On the contrary, all the antibacterial CNC coatings exhibited obvious effects, depending on the types of bacteria and CNC modifications, as well as the amount of CNC derivatives. Particularly, PLA-CC composite films displayed an increasing log reduction of *S. aureus* from 2.14 to 6.29 with increasing CNC contents, while PLA-MC showed high antibacterial efficiency against *S. aureus* even with low coating mass. However, the antibacterial activity of PLA-ZC for *S. aureus* was not as high as the other two coatings. In the case of *E. coli*, all three CNC coatings showed significant antibacterial efficiencies (>99.9999%) upon 1 hour of contact. It meant that CTAB-CNC and ZnO-CNC coatings had a stronger influence upon the Gram-negative bacteria than the Gram-positive strains, and the chlorinated MAM-CNCs showed excellent antibacterial activity for both types of bacteria. Similar results have reported that *E. coli* was less resistant to the antibacterial agents (e.g., ZnO nanoparticles) than the Gram-positive bacteria (Shankar et al., 2018; Zhang et al., 2017). In one aspect, the Gram-positive *S. aureus* consists of a thicker cell wall than that of the Gram-negative *E. coli*; in another aspect, the Gram-positive bacteria could form aggregates to protect the internal cells from the antibacterial agents (Pantani et al., 2013). Based on the antibacterial efficiencies, PLA-CC8, PLA-ZC8, and PLA-MC8 were selected for the following tests. The inhibition zones of neat and coated PLA films are shown in Figure 5.4 (c, d). No obvious inhibition zone was observed in neat PLA, PLA-CC8, and PLA-MC8 films for both *S. aureus* and *E. coli*,

suggesting little or no release of the antibacterial agents from the coatings to the agar plates. On the contrary, PLA-ZC8 films exhibited similar inhibition rings (~10 mm) against *S. aureus* and *E. coli*, which was due to the release of ZnO and/or Zn^{2+} ions (Pantani et al., 2013; Wahid et al., 2019).

5.4.3. Structure of PLA/CNC composite films

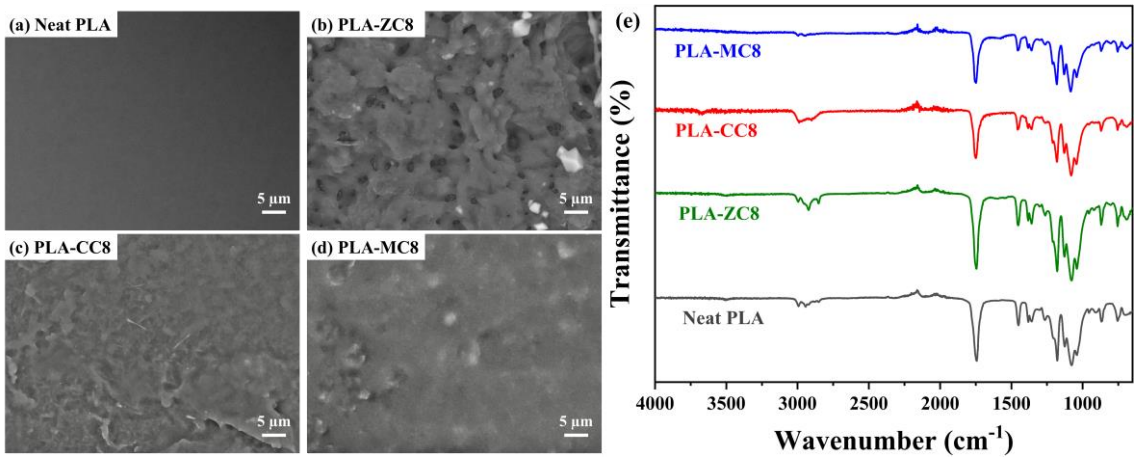

Figure 5.5. SEM images (a-d) and FTIR spectra (e) of neat and coated PLA films.

The surface morphology of neat and coated PLA films was observed by SEM. Figure 5.5 (a) displays the smooth and homogeneous surface of neat PLA without cracks or holes. The addition of coating solutions (acetic acid) resulted in the eroded surfaces, and the modified CNCs were combined with the polymeric matrix. It explained the little or no release of CNCs from the films to the agar plates. FTIR analysis of the composite films was carried out to study the molecular structures. As shown in Figure 5.5, the peaks of neat PLA film at 2994 cm^{-1} and 2943 cm^{-1} were associated with the C-H asymmetric and symmetric stretching in $-CH_3$ groups. The peak at 1743 cm^{-1} corresponded to the C=O stretching vibration of the ester groups. The peaks between 1450 cm^{-1} and 1357 cm^{-1} represented asymmetric and symmetric bending of C-H bond in the methyl groups, while the peaks at 1178 cm^{-1} and 1077 cm^{-1} were related to the

C-O-C symmetric and asymmetric stretching (Doganay et al., 2016). With the addition of CNC coatings, no new characteristic peaks or obvious shift of peaks were observed. It indicated that no new covalent bonds were formed after the incorporation of modified CNCs.

5.4.4. Mechanical and barrier properties of PLA/CNC composite films

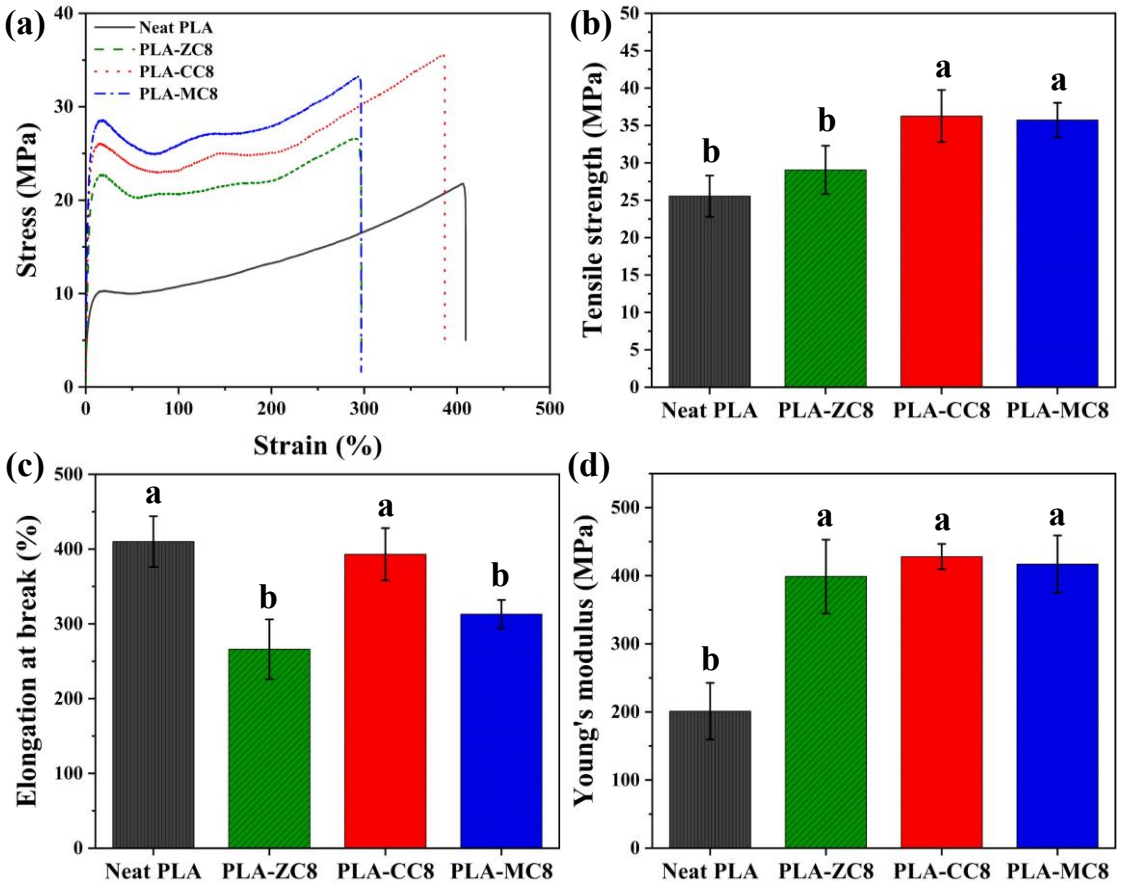

Figure 5.6. (a) Stress-stain curves, (b) tensile strength, (c) elongation at break, and (d) Young's modulus of neat and coated PLA films. Means with different letters on the column top were significantly different ($p < 0.05$).

Mechanical properties of neat and coated PLA films were measured, and the representative stress-strain curves are shown in Figure 5.6 (a). Their thicknesses did not have any significant difference, and all the films exhibited similar curves, beginning with elastic deformation and following by plastic deformation. Obvious yielding points were observed, which define the

limitation of the elastic behavior and the beginning of the plastic behavior (Beauson et al., 2022). For the neat PLA films, the stress at the yielding point was ~10 MPa and the films fractured at the strain of ~400%. For all types of coated PLA films, an increase in yield strength was clearly observed (20-30 MPa), suggesting their improved resistance to loading before permanent deformation (Aghajani et al., 2018). Figure 5.6 (b-d) shows the variations of tensile strength, elongation at break, and Young's modulus of PLA films with different CNC coatings. All the coatings significantly increased the Young's modulus, and PLA-CC8 and PLA-MC8 had an improved tensile strength, but only PLA-CC8 could maintain the ductility of the neat PLA films. The increase in mechanical strength could be explained that the surface coating well combined with the polymeric matrix and acted as a scaffold (Gulzar et al., 2022). The retained ductility of PLA-CC8 might be attributed to the good interfacial compatibility, which contributed to effective stress transfer and delaying the stretching failure (Dehnad et al., 2014; Jin et al., 2020).

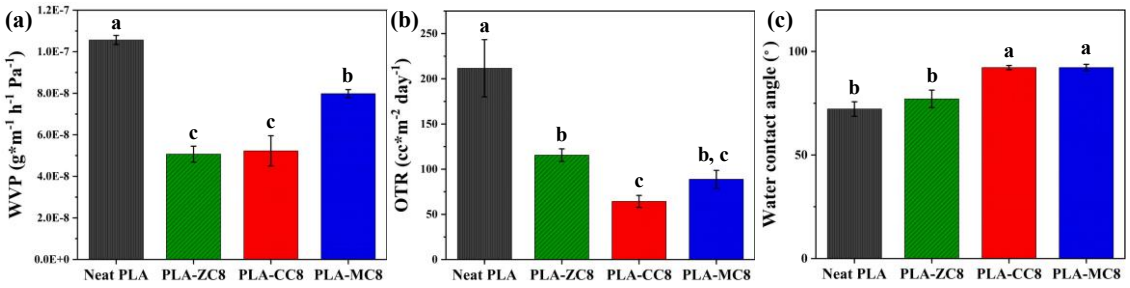

Figure 5.7. (a) WVP, (b) OTR, and (c) water contact angle of neat and coated PLA films. Means with different letters on the top of the columns were significantly different ($p < 0.05$).

The water vapor and oxygen barrier properties of neat and coated PLA films are important to their potential applications in packaging. As shown in Figure 5.7 (a, b), the neat PLA film had an average WVP value of 1.06×10^{-7} g $m^{-1}h^{-1}Pa^{-1}$ and OTR value of 211.72 cc $m^{-2}day^{-1}$, while

the permeability of PLA/CNC composite films significantly ($p < 0.05$) decreased. Particularly, PLA-CC8 showed the lowest WVP and OTR values of 5.22×10^{-8} g $m^{-1}h^{-1}Pa^{-1}$and 64.34 cc $m^{-2}day^{-1}$, respectively. It was because the modified CNCs tightly combined with PLA after solution coating and formed a dense layer on the surface of the films (Zhou et al., 2021). These values were relatively lower than those reported previously; for example, the WVP value of PLA/ZnO composite films was around 7×10^{-8} g $m^{-1}h^{-1}Pa^{-1}$ (Shankar et al., 2018), and the poly(ethylene furanoate)/PLA films had an OTR value of 144 cc $m^{-2}day^{-1}$ (Fredi et al., 2022). Figure 5.7 (c) shows the water contact angle of neat and coated PLA films. As expected, the neat PLA film had a hydrophilic surface with a contact angle of around 74.2° (Vilarinho et al., 2021). A slight increase ($p > 0.05$) in contact angle of PLA-ZC8 was observed, which might be due to the hydrophobic nature of ZnO (Roy & Rhim, 2019). The surface hydrophobicity of PLA-CC8 and PLA-MC8 films was significantly higher than that of the neat PLA film. It could be explained by the existence of long carbon chains on the modified CNCs (Ly & Mekonnen, 2020).

5.4.5. Compost disintegrability

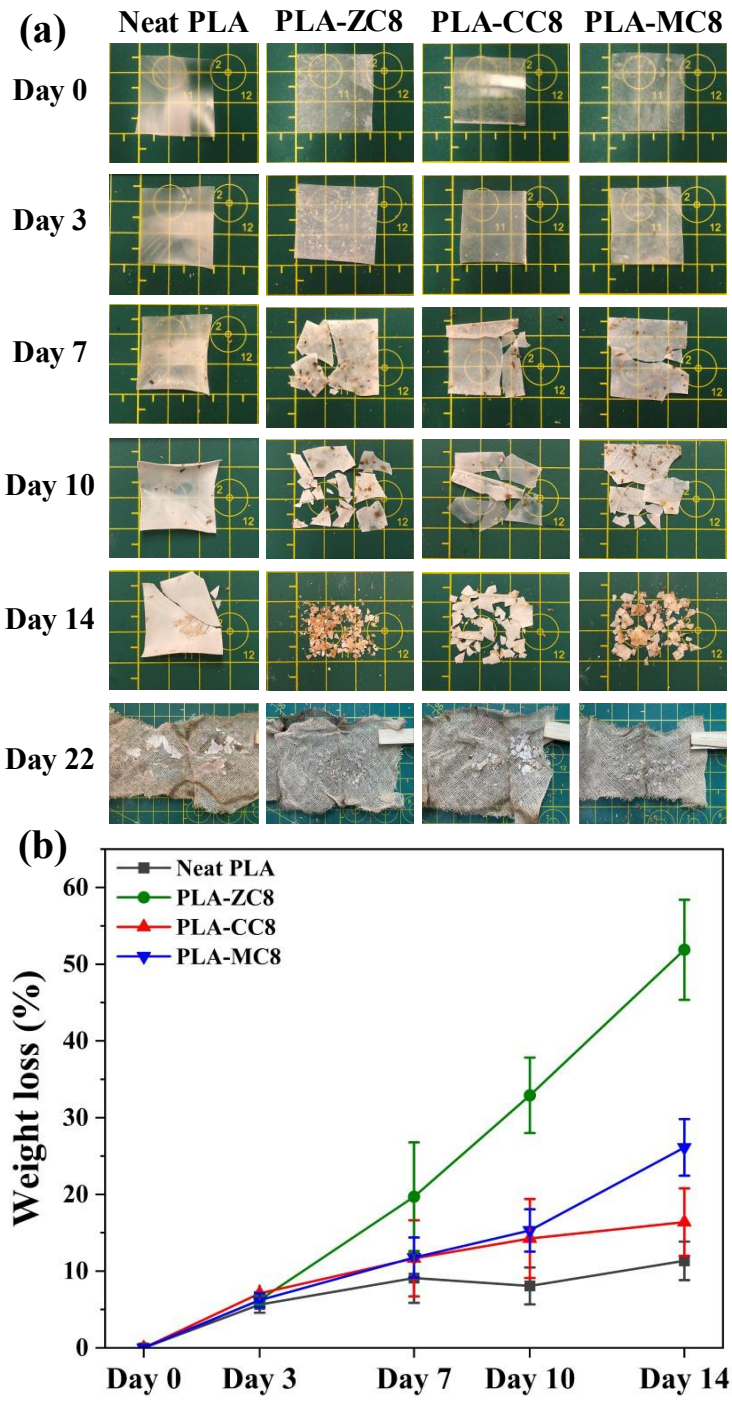

Figure 5.8. (a) Photos and (b) weight loss of neat and coated PLA films after incubating under composting conditions.

PLA films hold great potential for "green" packaging materials because of their degradable character under specific conditions (Rojas et al., 2021). In this regard, the effect of CNC

coatings on the disintegrability of PLA films under composting conditions was investigated. As shown in Figure 5.8 (a), no particular alterations were observed after 3 days for all the samples. The PLA/CNC composite films became opaque, and the fragmentation started after 7 days. Compared to neat PLA film, the fragmentation of CNC coated PLA films was more obvious on day 10 and day 14. The weight loss showed a similar trend (Figure 5.8 (b)). All the films exhibited a gradual increase in weight loss under composting conditions. Especially after 14 days, the weight loss of PLA-ZC8, PLA-MC8, and PLA-CC8 films was about 51.88%, 26.12%, and 16.38%, respectively, against 11.34% for the neat PLA film. To be noted, only a few tiny fragments were recovered on day 22, so it was difficult to weigh and calculate the weight loss. The results revealed a faster disintegration rate of PLA/CNC composite films, and it was consistent with reported results that CNCs acted as a source of energy and carbon and facilitated the initiation of disintegration (Degli-Innocenti, 2021; Lizundia et al., 2018; Sun et al., 2022).

5.4.6. Preservation of pork

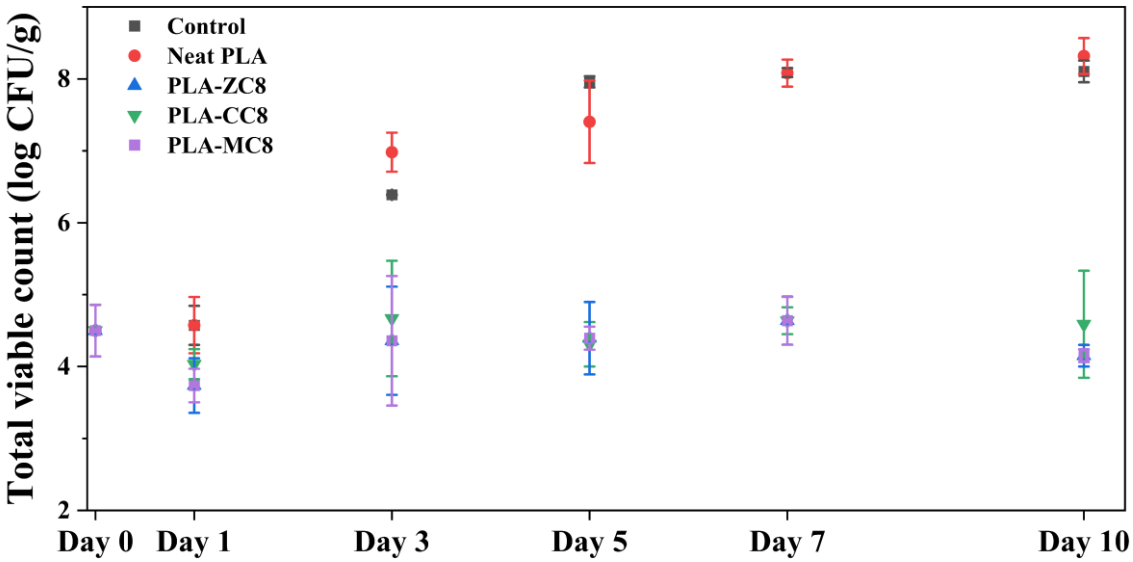

Figure 5.9. Total viable counts of pork samples during storage at 4 ℃.

Pork is a commonly consumed red meat worldwide, containing rich sources of certain protein, vitamins, and minerals. However, cross-contamination happens frequently during the production. Herein, pork was chosen as a model for evaluating the packaging performance. The initial TVC value of 4.50 log CFU/g in the raw pork was similar to a reported value (Vargas Romero et al., 2021). As shown in Figure 5.9, the total viable population of the microorganism in pork samples (unpackaged and wrapped with neat PLA film) rapidly increased during the storage period. The permissible limit of the overall microorganism in fresh meat should be less than 5×10^6 CFU/g, as regulated by European Commission No. 2073/2005 (Commission, 2005). Therefore, both the control sample and neat PLA group exceeded the limit after 3 days of cold storage (about 6.39 and 6.98 log CFU/g). It was worth noting that all PLA/CNC composite film wrapped pork samples had delayed bacteria growth, and their TVC values were lower than 5×10^6 CFU/g after storage at 4 ℃ for 10 days. No significant difference was observed among the three coatings, which indicated the sufficient antibacterial activity of all these modified CNCs for extended shelf life of fresh pork.

5.5. Conclusions

This work demonstrated a convenient method to fabricate compostable packaging films with antibacterial activity. The effects of sprayed coatings of three types of modified CNCs (CTAB-CNCs, ZnO-CNCs, and MAM-CNCs) on the structure and properties of PLA films were revealed. Especially, ZnO-CNC coated PLA films exhibited prominent disintegration behavior. After incubating under composting conditions for 14 days, a weight loss of 51.88% was recorded, which was over 5 times higher than the neat PLA film. CTAB-CNC coating

significantly increased the tensile strength and Young's modulus without affecting the ductility, and at the same time, showed the improvement of 51% and 70% in water vapor and oxygen barrier properties, respectively. MAM-CNC coated PLA films had the most effective antibacterial capacity against both Gram-positive and Gram-negative bacteria. With a small amount of coating, PLA-MC4 films could inactivate >99.9999% of *S. aureus* and *E. coli* upon 1 hour of contact. After all, three PLA/CNC composite films could significantly extend the shelf life of wrapped pork from 3 days to more than 10 days. Further investigations are expected to ensure that the biocompatibility inherent to PLA films is retained after coating. Hopefully, this strategy of spray coating with modified CNCs could be applied in other plastic and paper-based packaging materials.

5.6. References

Aghajani, M., Wang, M., Cox, L. M., Killgore, J. P., Greenberg, A. R., & Ding, Y. (2018). Influence of support-layer deformation on the intrinsic resistance of thin film composite membranes. *Journal of Membrane Science, 567*, 49-57. https://doi.org/10.1016/j.memsci.2018.09.031

Ahmad, H. (2021). Celluloses as support materials for antibacterial agents: a review. *Cellulose, 28*(5), 2715-2761. https://doi.org/10.1007/s10570-021-03703-2

Arnata, I. W., Suprihatin, S., Fahma, F., Richana, N., & Sunarti, T. C. (2020). Cationic modification of nanocrystalline cellulose from sago fronds. *Cellulose, 27*(6), 3121-3141. https://doi.org/10.1007/s10570-019-02955-3

Asadi, H., Ghalei, S., Handa, H., & Ramasamy, R. P. (2021). Cellulose nanocrystal reinforced silk fibroin coating for enhanced corrosion protection and biocompatibility of Mg-based alloys for orthopedic implant applications. *Progress in Organic Coatings, 161*, 106525. https://doi.org/10.1016/j.porgcoat.2021.106525

Badawy, A. A., Ghanem, A. F., Yassin, M. A., Youssef, A. M., & Rehim, M. H. A. (2021).

Utilization and Characterization of Cellulose Nanocrystals Decorated with Silver and Zinc Oxide Nanoparticles for Removal of Lead Ion from Wastewater. *Environmental Nanotechnology, Monitoring & Management*, *16*, 100501. https://doi.org/10.1016/j.enmm.2021.100501

Baggio, G. M., Camani, P. H., & Rosa, D. S. (2022). Concentration and carbon chain length effects of cationic surfactant in enzymatic production of cellulose nanostructures. *Journal of Molecular Liquids, 346*, 118231. https://doi.org/10.1016/j.molliq.2021.118231

Beauson, J., Schillani, G., Van der Schueren, L., & Goutianos, S. (2022). The effect of processing conditions and polymer crystallinity on the mechanical properties of unidirectional self-reinforced PLA composites. *Composites Part A: Applied Science and Manufacturing, 152*, 106668. https://doi.org/10.1016/j.compositesa.2021.106668

Cerro, D., Bustos, G., Villegas, C., Buendia, N., Truffa, G., Godoy, M. P., Rodriguez, F., Rojas, A., Galotto, M.J., Constandil, L., & Torres, A. (2021). Effect of supercritical incorporation of cinnamaldehyde on physical-chemical properties, disintegration and toxicity studies of PLA/lignin nanocomposites. *International Journal of Biological Macromolecules, 167*, 255-266. https://doi.org/10.1016 /j.ijbiomac.2020.11.140

Chang, D., Li, Z., Wang, X., Zhu, C., Dong, A., & Gao, G. (2018). N-Halamine polymer from bipolymer to amphiphilic terpolymer with enhancement in antibacterial activity. *Colloids and Surfaces B: Biointerfaces, 163*, 402-411. https://doi.org/10.1016/j.colsurfb.2018.01.013

Commission Regulation (EC) No 2073/2005 of 15 November 2005 on microbiological criteria for foodstuffs. (2005). https://eur-lex.europa.eu/legal-content/EN/ALL/?uri=CELEX%3A32005R2073

Degli-Innocenti, F. (2021). Is composting of packaging real recycling? *Waste Management, 130*, 61-64. https://doi.org/10.1016/j.wasman.2021.05.017

Dehnad, D., Emam-Djomeh, Z., Mirzaei, H., Jafari, S.-M., & Dadashi, S. (2014). Optimization of physical and mechanical properties for chitosan–nanocellulose biocomposites. *Carbohydrate Polymers, 105*, 222-228. https://doi.org/10.1016/j.carbpol.2014.01.094

Doganay, D., Coskun, S., Kaynak, C., & Unalan, H. E. (2016). Electrical, mechanical and thermal properties of aligned silver nanowire/polylactide nanocomposite films. *Composites*

Part B: Engineering, 99, 288-296. https://doi.org/10.1016/j.compositesb.2016.06.044

Duarte Urueña, G., Ribeiro, K. C., Prestes, E., Pinheiro, L. A., & Carvalho, B. M. (2021). Extraction of Cellulose Nanocrystal from Multilayer Packaging Residues Composed of a Mixture of Eucalyptus and Pine Fibers. *Waste and Biomass Valorization, 12*(10), 5763-5777. https://doi.org/10.1007/s12649-021-01383-4

Elfeky, A. S., Salem, S. S., Elzaref, A. S., Owda, M. E., Eladawy, H. A., Saeed, A. M., Awad, M.A., Abou-Zeid, R.E., & Fouda, A. (2020). Multifunctional cellulose nanocrystal /metal oxide hybrid, photo-degradation, antibacterial and larvicidal activities. *Carbohydrate Polymers, 230*, 115711. https://doi.org/10.1016/j.carbpol.2019.115711

Fiore, A., Park, S., Volpe, S., Torrieri, E., & Masi, P. (2021). Active packaging based on PLA and chitosan-caseinate enriched rosemary essential oil coating for fresh minced chicken breast application. *Food Packaging and Shelf Life, 29*, 100708. https://doi.org/10.1016/j.fpsl.2021.100708

Fonseca-García, A., Jiménez-Regalado, E. J., & Aguirre-Loredo, R. Y. (2021). Preparation of a novel biodegradable packaging film based on corn starch-chitosan and poloxamers. *Carbohydrate Polymers*, *251*, 117009. https://doi.org/10.1016/j.carbpol.2020.117009

Fredi, G., Dorigato, A., Dussin, A., Xanthopoulou, E., Bikiaris, D.N., Botta, L., Fiore, V. and Pegoretti, A. (2022). Compatibilization of Polylactide/Poly (ethylene 2, 5-furanoate)(PLA/PEF) Blends for Sustainable and Bioderived Packaging. *Molecules, 27*(19), 6371. https://doi.org/10.3390/molecules27196371

Fu, F., Li, L., Liu, L., Cai, J., Zhang, Y., Zhou, J., & Zhang, L. (2015). Construction of Cellulose Based ZnO Nanocomposite Films with Antibacterial Properties through One-Step Coagulation. *ACS Applied Materials & Interfaces, 7*(4), 2597-2606. https://doi.org/10.1021/am507639b

Gahrooee, T. R., Abbasi Moud, A., Danesh, M., & Hatzikiriakos, S. G. (2021). Rheological characterization of CNC-CTAB network below and above critical micelle concentration (CMC). *Carbohydrate Polymers, 257*, 117552. https://doi.org/10.1016/j.carbpol.2020.117552

Gao, P., Cha, R., Luo, H., Xu, Y., Zhang, P., Han, L., Wang, X., Zhang, Z., & Jiang, X. (2022).

Development of antimicrobial oxidized cellulose film for active food packaging. *Carbohydrate Polymers*, *278*, 118922. https://doi.org/10.1016/j.carbpol.2021.118922

Guan, Y., Yu, H.-Y., Abdalkarim, S. Y. H., Wang, C., Tang, F., Marek, J., Chen, W.L., Militky, J., & Yao, J.-M. (2019). Green one-step synthesis of ZnO/cellulose nanocrystal hybrids with modulated morphologies and superfast absorption of cationic dyes. *International Journal of Biological Macromolecules, 132*, 51-62. https://doi.org/10.1016/j.ijbiomac.2019.03.104

Gulzar, S., Tagrida, M., Nilsuwan, K., Prodpran, T., & Benjakul, S. (2022). Electrospinning of gelatin/chitosan nanofibers incorporated with tannic acid and chitooligosaccharides on polylactic acid film: Characteristics and bioactivities. *Food Hydrocolloids, 133*, 107916. https://doi.org/10.1016/j.foodhyd.2022.107916

Huang, S., Liu, X., Chang, C., & Wang, Y. (2020). Recent developments and prospective food-related applications of cellulose nanocrystals: a review. *Cellulose, 27*(6), 2991-3011. https://doi.org/10.1007/s10570-020-02984-3

Huang, S., Tao, R., Ismail, A., & Wang, Y. (2020). Cellulose Nanocrystals Derived from Textile Waste through Acid Hydrolysis and Oxidation as Reinforcing Agent of Soy Protein Film. *Polymers, 12*(4), 958. https://doi.org/10.3390/polym12040958

International Organization for Standardization. (2015). *Plastics-Determination of the degree of disintegration of plastic materials under simulated composting conditions in a laboratory-scale test* (ISO 20200:2015). https://www.iso.org/standard/63 367.html

Jiang, S., Li, Q., Wang, F., Wang, Z., Cao, X., Shen, X., & Yao, Z. (2022). Highly effective and sustainable antibacterial membranes synthesized using biodegradable polymers. *Chemosphere, 291*, 133106. https://doi.org/10.1016/j.chemosphere.2021.133106

Jin, K., Tang, Y., Zhu, X., & Zhou, Y. (2020). Polylactic acid based biocomposite films reinforced with silanized nanocrystalline cellulose. *International Journal of Biological Macromolecules, 162*, 1109-1117. https://doi.org/10.1016/j.ijbiomac.2020.06.201

Kong, X., Zhang, S., Wang, Y., Liu, Y., Li, R., Ren, X., & Huang, T.-S. (2019). Antibacterial polyvinyl alcohol films incorporated with N-halamine grafted oxidized microcrystalline cellulose. *Composites Communications, 15*, 25-29. https://doi.org/10.1016/j.coco.2019.0

6.005

Kongkaoroptham, P., Piroonpan, T., & Pasanphan, W. (2021). Chitosan nanoparticles based on their derivatives as antioxidant and antibacterial additives for active bioplastic packaging. *Carbohydrate Polymers*, *257*, 117610. https://doi.org/10.1016/j.carbpol.2020.117610

Koshani, R., Zhang, J., van de Ven, T. G. M., Lu, X., & Wang, Y. (2021). Modified Hairy Nanocrystalline Cellulose as Photobactericidal Nanofillers for Food Packaging Application. *ACS Sustainable Chemistry & Engineering, 9*(31), 10513-10523. https://doi.org/10.1021/acssuschemeng.1c02289

Li, M.-C., Wu, Q., Han, J., Mei, C., Lei, T., Lee, S.-y., & Gwon, J. (2020). Overcoming Salt Contamination of Bentonite Water-Based Drilling Fluids with Blended Dual-Functionalized Cellulose Nanocrystals. *ACS Sustainable Chemistry & Engineering, 8*(31), 11569-11578. https://doi.org/10.1021/acssuschemeng.0c02774

Liu, Y., Li, L., Pan, N., Wang, Y., Ren, X., Xie, Z., Buschle-Diller, G., & Huang, T.-S. (2017). Antibacterial cellulose acetate films incorporated with N-halamine-modified nano-crystalline cellulose particles. *Polymers for Advanced Technologies, 28*(4), 463-469. https://doi.org/10.1002/pat.3906

Lizundia, E., Goikuria, U., Vilas, J. L., Cristofaro, F., Bruni, G., Fortunati, E., Armentano, I., Visai, L., & Torre, L. (2018). Metal Nanoparticles Embedded in Cellulose Nanocrystal Based Films: Material Properties and Post-use Analysis. *Biomacromolecules, 19*(7), 2618-2628. https://doi.org/10.1021/acs.biomac.8b00243

Ly, M., & Mekonnen, T. H. (2020). Cationic surfactant modified cellulose nanocrystals for corrosion protective nanocomposite surface coatings. *Journal of Industrial and Engineering Chemistry, 83*, 409-420. https://doi.org/10.1016/j.jiec.2019.12.014

Ma, X., Wu, N., Liu, P., & Cui, H. (2022). Fabrication of highly efficient phenylphosphorylated chitosan bio-based flame retardants for flammable PLA biomaterial. *Carbohydrate Polymers*, *287*, 119317. https://doi.org/10.1016/j.carbpol.2022.119317

Niinivaara, E., Desmaisons, J., Dufresne, A., Bras, J., & Cranston, E. D. (2021). Thick Polyvinyl Alcohol Films Reinforced with Cellulose Nanocrystals for Coating Applications. *ACS Applied Nano Materials*. https://doi.org/10.1021/acsanm.1c01244

Omerović, N., Djisalov, M., Živojević, K., Mladenović, M., Vunduk, J., Milenković, I., Gadjanski, I., & Vidić, J. (2021). Antimicrobial nanoparticles and biodegradable polymer composites for active food packaging applications. *Comprehensive Reviews in Food Science and Food Safety, 20*(3), 2428-2454. https://doi.org/10.1111/1541-4337.12727

Pantani, R., Gorrasi, G., Vigliotta, G., Murariu, M., & Dubois, P. (2013). PLA-ZnO nanocomposite films: Water vapor barrier properties and specific end-use characteristics. *European Polymer Journal, 49*(11), 3471-3482. https://doi.org/10.1016/j.eurpolymj.2013.08.005

Park, S., Baker, J. O., Himmel, M. E., Parilla, P. A., & Johnson, D. K. (2010). Cellulose crystallinity index: measurement techniques and their impact on interpreting cellulase performance. *Biotechnol Biofuels, 3*(1), 10. https://doi.org/10.1186/1754-6834-3-10

Ranjbar, D., Raeiszadeh, M., Lewis, L., MacLachlan, M. J., & Hatzikiriakos, S. G. (2020). Adsorptive removal of Congo red by surfactant modified cellulose nanocrystals: a kinetic, equilibrium, and mechanistic investigation. *Cellulose, 27*(6), 3211-3232. https://doi.org/10.1007/s10570-020-03021-z

Rojas-Lema, S., Nilsson, K., Trifol, J., Langton, M., Gomez-Caturla, J., Balart, R., Garcia-Garcia, D. and Moriana, R. (2021). Faba bean protein films reinforced with cellulose nanocrystals as edible food packaging material. *Food Hydrocolloids, 121*, 107019. https://doi.org/10.1016/j.foodhyd.2021.107019

Rojas, A., Velásquez, E., Patiño Vidal, C., Guarda, A., Galotto, M. J., & López de Dicastillo, C. (2021). Active PLA Packaging Films: Effect of Processing and the Addition of Natural Antimicrobials and Antioxidants on Physical Properties, Release Kinetics, and Compostability. *Antioxidants, 10*(12), 1976. https://doi.org/10.3390/antiox10121976

Rosace, G., Colleoni, C., Trovato, V., Iacono, G., & Malucelli, G. (2017). Vinylphosphonic acid/methacrylamide system as a durable intumescent flame retardant for cotton fabric. *Cellulose, 24*(7), 3095-3108. https://doi.org/10.1007/s10570-017-1294-x

Roy, S., & Rhim, J.-W. (2019). Carrageenan-based antimicrobial bionanocomposite films incorporated with ZnO nanoparticles stabilized by melanin. *Food Hydrocolloids, 90*, 500-507. https://doi.org/10.1016/j.foodhyd.2018.12.056

Salmieri, S., Islam, F., Khan, R.A., Hossain, F.M., Ibrahim, H.M., Miao, C., Hamad, W.Y. and

Lacroix, M. (2014a). Antimicrobial nanocomposite films made of poly(lactic acid)-cellulose nanocrystals (PLA-CNC) in food applications: part A—effect of nisin release on the inactivation of Listeria monocytogenes in ham. *Cellulose, 21*(3), 1837-1850. https://doi.org/10.1007/s10570-014-0230-6

Salmieri, S., Islam, F., Khan, R.A., Hossain, F.M., Ibrahim, H.M., Miao, C., Hamad, W.Y. and Lacroix, M. (2014b). Antimicrobial nanocomposite films made of poly(lactic acid)–cellulose nanocrystals (PLA–CNC) in food applications—part B: effect of oregano essential oil release on the inactivation of Listeria monocytogenes in mixed vegetables. *Cellulose, 21*(6), 4271-4285. https://doi.org/10.1007/s10570-014-0406-0

Shankar, S., Wang, L.-F., & Rhim, J.-W. (2018). Incorporation of zinc oxide nanoparticles improved the mechanical, water vapor barrier, UV-light barrier, and antibacterial properties of PLA-based nanocomposite films. *Materials Science and Engineering: C, 93*, 289-298. https://doi.org/10.1016/j.msec.2018.08.002

Sharafi Zamir, S., Fathi, B., Ajji, A., Robert, M., & Elkoun, S. (2022). Crystallinity and Gas Permeability of Poly (Lactic Acid)/Starch Nanocrystal Nanocomposite. *Polymers, 14*(14), 2802. https://doi.org/10.3390/polym14142802

Sharma, P. R., Sharma, S. K., Antoine, R., & Hsiao, B. S. (2019). Efficient Removal of Arsenic Using Zinc Oxide Nanocrystal-Decorated Regenerated Microfibrillated Cellulose Scaffolds. *ACS Sustainable Chemistry & Engineering, 7*(6), 6140-6151. https://doi.org/10.1021/acssuschemeng.8b06356

Shin, H., Kim, S., Kim, J., Kong, S., Lee, Y., & Lee, J.-C. (2022). Preparation of 3-pentadecylphenol-modified cellulose nanocrystal and its application as a filler to polypropylene nanocomposites having improved antibacterial and mechanical properties. *Journal of Applied Polymer Science, 139*(13), 51848. https://doi.org/10.1002/app.51848

Shojaeiarani, J., Bajwa, D. S., Stark, N. M., Bergholz, T. M., & Kraft, A. L. (2020). Spin coating method improved the performance characteristics of films obtained from poly(lactic acid) and cellulose nanocrystals. *Sustainable Materials and Technologies, 26*, e00212. https://doi.org/10.1016/j.susmat.2020.e00212

Shojaeiarani, J., Shirzadifar, A., Shine, C., & Reisi, A. M. (2022). Hybrid nanocomposite packaging films from cellulose nanocrystals, zinc sulfide quantum dots reinforced

polylactic acid with fluorescent and antibacterial properties. *Polymer Engineering & Science, 62*, 1562-1570.https://doi.org/10.1002/pen.25944

Sun, C., Li, C., Li, H., Liu, M., Zheng, H., Tan, H., Wang, Y., & Zhang, Y. (2022). Modified Cellulose Nanocrystals Enhanced the Compatibility Between PLA and PBAT to Prepare a Multifunctional Composite Film. *Journal of Polymers and the Environment, 30*, 3139–3149. https://doi.org/10.1007/s10924-022-02422-4

Tang, X., Xu, H., Shi, Y., Wu, M., Tian, H., & Liang, J. (2020). Porous antimicrobial starch particles containing N-halamine functional groups. *Carbohydrate Polymers, 229*, 115546. https://doi.org/10.1016/j.carbpol.2019.115546

Vargas Romero, E., Lim, L. T., Suarez Mahecha, H., & Bohrer, B. M. (2021). The Effect of Electrospun Polycaprolactone Nonwovens Containing Chitosan and Propolis Extracts on Fresh Pork Packaged in Linear Low-Density Polyethylene Films. *Foods, 10*(5), 1110. https://doi.org/10.3390/foods10051110

Vilarinho, F., Stanzione, M., Buonocore, G. G., Barbosa-Pereira, L., Sendón, R., Vaz, M. F., & Sanches Silva, A. (2021). Green tea extract and nanocellulose embedded into polylactic acid film: Properties and efficiency on retarding the lipid oxidation of a model fatty food. *Food Packaging and Shelf Life, 27*, 100609. https://doi.org/1 0.1016/j.fpsl.2020.100609

Wahid, F., Duan, Y. X., Hu, X. H., Chu, L. Q., Jia, S. R., Cui, J. D., & Zhong, C. (2019). A facile construction of bacterial cellulose/ZnO nanocomposite films and their photocatalytic and antibacterial properties. *International Journal of Biological Macromolecules, 132*, 692-700. https://doi.org/10.1016/j.ijbiomac.2019.03.240

World Health Organization. (2020). Food safety. World Health Organization. Retrieved August 31, 2022, from https://www.who.int/news-room/fact-sheets/detail/food-safety

Xiao, Y., Liu, Y., Kang, S., Wang, K., & Xu, H. (2020). Development and evaluation of soy protein isolate-based antibacterial nanocomposite films containing cellulose nanocrystals and zinc oxide nanoparticles. *Food Hydrocolloids, 106*, 105898. https://doi.org/10.1016/j. foodhyd.2020.105898

Xie, D., Weng, Y., Guo, X., Zhao, J., Gregory, R. L., & Zheng, C. (2011). Preparation and evaluation of a novel glass-ionomer cement with antibacterial functions. *Dental Materials, 27*(5), 487-496. https://doi.org/10.1016/j.dental.2011.02.006

Xu, D., Wang, S., Hu, J., Liu, Y., Jiang, Z., & Zhu, P. (2021). Enhancing antibacterial and flame-retardant performance of cotton fabric with an iminodiacetic acid-containing N-halamine. *Cellulose, 28*(5), 3265-3277. https://doi.org/10.1007/s10570-021-03716-x

Zhang, H., Hortal, M., Jordá-Beneyto, M., Rosa, E., Lara-Lledo, M., & Lorente, I. (2017). ZnO-PLA nanocomposite coated paper for antimicrobial packaging application. *LWT, 78*, 250-257. https://doi.org/10.1016/j.lwt.2016.12.024

Zhang, R., Lan, W., Ji, T., Sameen, D. E., Ahmed, S., Qin, W., & Liu, Y. (2021). Development of polylactic acid/ZnO composite membranes prepared by ultrasonication and electrospinning for food packaging. *LWT, 135*, 110072. https://doi.org/10.1016/j.lwt.2020.110072

Zhang, X., Zhang, Q., Xue, Y., Wang, Y., Zhou, X., Li, Z., & Li, Q. (2021). Simple and green synthesis of calcium alginate/AgCl nanocomposites with low-smoke flame-retardant and antimicrobial properties. *Cellulose*, *28*(8), 5151-5167. https:// doi.org/10.1007/s10570-021-03825-7

Zhao, S.-W., Zheng, M., Zou, X.-H., Guo, Y., & Pan, Q.-J. (2017). Self-Assembly of Hierarchically Structured Cellulose@ZnO Composite in Solid–Liquid Homogeneous Phase: Synthesis, DFT Calculations, and Enhanced Antibacterial Activities. *ACS Sustainable Chemistry & Engineering, 5*(8), 6585-6596. https://doi.org/10.1021/acssuschemeng.7b00842

Zhong, C., Hou, P.-F., Li, Y.-X., Yang, W.-Y., Shu, M., & Wu, G.-P. (2021). Characterization, antioxidant and antibacterial activities of gelatin film incorporated with protocatechuic acid and its application on beef preservation. *LWT, 151*, 112154. https://doi.org/10.1016/j.lwt.2021.112154

Zhou, C., Girouard, F., O'Brien, B., Ronholm, J., & Wang, Y. (2022). Construction of chevaux-de-frise from cellulose nanocrystals to enable mechano-bactericidal activity on recycled waste cotton films. *Green Chemistry, 24*(3), 1109-1113. https://doi.org/10.1039/d2gc00073c

Zhou, Q., Chen, J., Wang, C., Yang, G., Janaswamy, S., Xu, F., & Liu, Z. (2022). Preparation and characterization of lignin nanoparticles and chitin nanofibers reinforced PVA films with UV shielding properties. *Industrial Crops and Products, 188*, 115669. https://doi.org/10.

1016/j.indcrop.2022.115669

Zhou, X., Cheng, R., Wang, B., Zeng, J., Xu, J., Li, J., Kang, L., Cheng, Z., Gao, W., & Chen, K. (2021). Biodegradable sandwich-architectured films derived from pea starch and polylactic acid with enhanced shelf-life for fruit preservation. *Carbohydrate Polymers, 251*, 117117. https://doi.org/10.1016/j.carbpol.2020.117117

Connecting Text

Chapter 5 demonstrated the feasibility of the spray-coating method to fabricate compostable packaging films with antibacterial activity. However, the antibacterial capacity fully relied on the chemical modifications of CNCs. In chapter 6, we developed the mechano-bactericidal surfaces with cellulose materials without introducing any chemical antibacterial agents for enhanced sustainability and safety. The bactericidal materials were constructed by directly depositing CNCs on the surface of regenerated cellulose films, and the mechano-bactericidal effects of different CNC coatings and surface topography towards four types of bacteria were investigated.

Chapter 6. Mechano-Bactericidal Surface Developed from Cellulose Nanocrystals and Regenerated Cellulose Films as Sustainable Active Packaging

6.1. Abstract

Nature offers much inspiration in the quest for antibacterial surfaces. In this work, the bioinspired antibacterial materials were developed by depositing cellulose nanocrystals (CNCs) on the surface of regenerated cellulose (RC) films with the assistance of vacuum filtration. The shorter CNCs (HCNCs) from textile waste and the longer CNCs (t-CNCs) from tunicate cellulose were selected, and the effects of CNC dimensions and surface topography on the antibacterial activity were investigated via plate assay against four types of bacteria. The results demonstrated that all the RC/CNC films could eliminate over 80% of bacteria upon 3-minute contact. Compared to RC/HCNCs, RC/t-CNCs were relatively more effective in killing the bacteria due to their larger aspect ratio. Additionally, the compressed RC/CNC surface lost its antibacterial activity as the surface roughness decreased. However, the morphologies and biochemical structures of the bacterial cells didn't show any obvious changes before and after 3-minute treatment. Overall, this study provides guidance to the development of CNC-enabled mechano-bactericidal surfaces with potential applications in sustainable active packaging.

6.2. Introduction

Naturally occurring materials offer unique nanostructure that is antimicrobial, which inspired the quest for antibacterial surfaces. For instance, cicada, dragonfly, and damselfly are well-known winged insects possessing various nanotextured structures (e.g., nanopillars, nanospikes, and nanoneedles) on their wings with contact-killing ability (Chopra, Gulati, & Ivanovski, 2021). Dehghani et al. (Dehghani et al., 2021) demonstrated the mechano-killing properties of *Psalmocharias* cicada wings with 60% bactericidal activity against *Pseudomonas aeruginosa.*

Paikra & Mishra (Paikra & Mishra, 2021) revealed that dragonfly wings exhibited natural bactericidal efficiency against *Bacillus subtilis* and *Pseudomonas aeruginosa*. The antibacterial activity was found related to the height, width, and sharpness of the nanostructure, which would generate mechanical stress on the bacterial cells.

Nowadays, several methods have been explored to fabricate bioinspired nanostructures for achieving antibacterial efficacy, such as metal-assisted chemical etching, hydrothermal synthesis, nanoimprint lithography, and electrochemical anodization (Chopra et al., 2021). Currently, inorganic materials (e.g., metals, glass, and alloys) are the main substrates to fabricate nanopillars towards antibacterial functions (Maleki, Mirzaali, Guagliano, & Bagherifard, 2021; Zhao et al., 2021). For example, Michalska et al. (Michalska et al., 2021) used the regenerative secondary mask lithography method to enable customized glass nanopillars, which were capable of killing *S. aureus* with 81% efficiency. However, more efforts are required to develop a simple method for constructing bioinspired antibacterial surfaces with sustainable materials.

As the most abundant renewable biopolymer on Earth, cellulosic materials have triggered considerable research interest over the past few decades. Compared to metal and petroleum-based nanomaterials, nanocellulose is much less expensive (approximately US$20 per dry kilogram of nanocellulose), suggesting an economic advantage (Li et al., 2021). In addition to their wide availability and low cost, nanocellulose-based materials can be biodegraded in soil and ocean, which can address environmental concerns (Tu, Zhu, Duan, & Zhang, 2021). On account of these advantages, nanocellulosic materials have been employed in widespread

applications, such as packaging, bioplastics, and lightweight structural materials (Ferreira, Rezende, & Cranston, 2021; Huang & Wang, 2022; Lee et al., 2021). For example, nanocellulosic materials could be used to fabricate cellulose/graphene nanocomposites, cellulosic membranes, and chemically functionalized nanocellulose for the removal of pesticides from water (Rana, Mishra, Gupta, & Thakur, 2021).

The increased public awareness of food safety and environmental concerns have facilitated the development of sustainable materials with bactericidal behavior. Hence, we aimed to develop mechano-bactericidal materials with all-cellulose materials without introducing any chemical antibacterial agents for enhanced sustainability and safety. Our previous work has proved the potential of constructing the mechano-bactericidal structure by depositing cellulose nanocrystals (CNCs) on the surface of regenerated cellulose (RC) films with the assistance of vacuum filtration (Zhou, Girouard, O'Brien, Ronholm, & Wang, 2022). This work aimed to investigate the effects of CNC dimension and surface topography on antibacterial efficiency. Particularly, CNCs from waste textile and tunicate cellulose were selected as the short and long CNC models, respectively, and RC films were prepared from the same waste textile.

6.3. Materials and Methods

6.3.1. Materials

The waste textile was kindly provided by Renaissance (Montreal, QC, Canada). Sulfuric acid (H_2SO_4, 95.0-98.0%), sodium hydroxide (NaOH, ⩾98%), sodium chlorite ($NaClO_2$, 80%), glutaraldehyde solution (25% in H_2O), and poly-lysine solution (1.0 mg/mL) were purchased from Sigma-Aldrich (Oakville, ON, Canada). Luria–Bertani (LB) medium, tryptic soy broth

(TSB), and tryptic soy agar (TSA) were purchased from Becton, Dickinson and Company (Franklin Lakes, NJ, USA), and phosphate-buffered saline (10× PBS) was obtained from VWR International (Mississauga, ON, Canada).

6.3.2. Fabrication of antibacterial surfaces

The antibacterial surfaces were fabricated using all-cellulose materials. RC films were prepared according to our previous method (Zhou & Wang, 2021). The waste textile was pretreated in 20% (w/v) H_2SO_4 at 25 °C for 72 hours. After washing and drying, 1.00 g of pretreated fabrics was added into 50 mL 64% (w/v) H_2SO_4 solution that was pre-cooled to -20 °C and then stirred at 750 rpm for 8 minutes. The solutions were centrifuged to remove bubbles and poured onto a glass plate, followed by coagulation in 10% (w/v) NaOH for 15 minutes. The RC films were washed with running water before depositing CNCs on the surface. Extraction of t-CNCs from tunicate powder followed the method of Dunlop et al. with some modifications (Dunlop et al., 2020). Briefly, 2.50 g of tunicate powder were mixed with 50 mL 64 wt% H_2SO_4 and stirred at 45 °C for 2 hours. The hydrolysis was stopped by adding cool distilled water. Then 0.09 g $NaClO_2$ was added and stirred for 1 hour, and t-CNCs were obtained after washing with distilled water and dialysis for 3 days. HCNCs were extracted from the same textile waste by sulfuric acid hydrolysis as previously mentioned (Huang, Tao, Ismail, & Wang, 2020). These two types of CNCs (3% of RC film dry weight) were deposited on the RC films with the assistance of vacuum filtration, and the obtained films were coded as RC/t-CNCs and RC/HCNCs, corresponding to the type of CNCs used.

6.3.3. Characterizations

Transmission electron microscopy (TEM). The morphology of t-CNCs and HCNCs was observed on a transmission electron microscope (Talos™ F200X G2 TEM, Thermo Fisher Scientific Inc., Waltham, MA, USA) at ×28,500 magnification. A droplet of 0.1wt% CNC suspension was deposited on a polycarbon film supported on a copper grid, and the specimen was dried in air overnight. The TEM images were obtained at an accelerating voltage of 200 kV.

Fourier-transform infrared (FT-IR) spectroscopy. FT-IR spectra of t-CNCs and HCNCs were obtained by the Varian Excalibur 3100 FT-IR spectrometer (Varian, Melbourne, Vic, Australia) equipped with an attenuated total reflectance (ATR) accessory (Specac, Orpington, LDN, UK). The spectra were collected as the average of 64 scans with a resolution of 4 cm^{-1}, using the empty accessory as blank. The measurements were carried out at 650-4000 cm^{-1}.

X-ray diffraction (XRD). XRD patterns of t-CNCs and HCNCs were obtained using an Empyrean 3 (Malvern Panalytical Ltd., Malvern, Worcs, UK) X-ray diffractometer in a Bragg Brentano configuration, with Cu Kα radiation between 4° and 40°.

^{13}C solid-state nuclear magnetic resonance (NMR) spectroscopy. NMR spectra of t-CNCs and HCNCs were acquired using a VNMRS 400 (now Agilent, Santa Clara, CA, USA) wide bore spectrometer operating at 399.9 MHz for ^{1}H and 100.5 MHz for ^{13}C in a 7.5 mm Varian Chemagnetics double-resonance probe. The recycle delay was 3 seconds, and the samples were spun at 5 kHz. The cross-polarization contact time was 2 ms, and 4096 scans were acquired.

Atomic force microscopy (AFM). The surface topographies of RC/t-CNCs and RC/HCNCs were altered using a Carver laboratory press (Carver, Inc., Wabash, IN, USA) at room temperature under the forces of 1,000 lbs and 50,000 lbs for 15 minutes, and then measured using the MFP-3D AFM (Asylum Research, Santa Barbara, CA, USA). The images were obtained in tapping mode using silicon cantilevers (ACTA model, AppNano) with a nominal spring constant of 37 N/m and a nominal resonant frequency of 300 kHz.

Antibacterial activity analysis. Four types of bacteria were used for the antibacterial test, including two Gram-positive strains (*Staphylococcus aureus, S. aureus* and *Listeria monocytogenes, L. monocytogenes*) and two Gram-negative strains (*Escherichia coli, E. coli* and *Salmonella enterica, S. enterica*). Each strain was prepared from -80 °C 20% glycerol stock and streaked for isolation on LBA plates for *S. aureus* and *E. coli* and TSA plates for *L. monocytogenes* and *S. enterica*. The plates were incubated at 37 °C overnight, and the isolated colonies were picked for inoculation in 4 mL broth media at 37 °C with constant shaking at 175 rpm. After 16 hours, a concentration of ca. 10^8 CFU/mL was achieved, and the bacterial inoculums were prepared by diluting the culture with PBS to a certain concentration for further experiments.

The antibacterial activities of neat RC, RC/t-CNCs, and RC/HCNCs films were analyzed by a modified AATCC 100 test method (Xu et al., 2021). The films were cut into 1 cm × 1 cm, and 100 µL of bacterial suspension (~10^6 CFU/mL) were dropped on the surface. After 3 minutes of contact, PBS buffer was added and vortexed to rinse off bacteria. The rinsing solution was serially diluted and spread onto the surface of the agar plate, followed by incubation at 37 °C

for 24 hours. The colonies on the plate were enumerated to calculate the log reduction.

Scanning Electron Microscopy (SEM). The morphologies of RC/CNC films and bacteria before and after contacting with RC/CNC surfaces were observed using Quanta 450 environmental scanning electron microscope (FEI, Hillsboro, OR, USA). The RC/CNC films were mounted onto the stub and sputter coated with a 4 nm layer of gold-platinum (Leica EM ACE200, Leica Microsystems, Wetzlar, HE, Germany). The bacterial cells were collected by centrifugation and washed with PBS 3 times. Then the bacteria were fixed with 4% glutaraldehyde solution for 10 minutes, followed by washing with PBS 3 times and then sterile water twice. Thereafter, the samples were dehydrated in a sequential ethanol series (35%, 50%, 75%, 90%, 95%, 100%, and 100%) for 10 minutes each. After that, 100 µL of the samples were inoculated onto a poly-lysine coated coverslip and allowed to air dry at room temperature for 12 hours. The dried samples were mounted, sputter coated, and observed at an accelerating voltage of 5 kV.

Raman spectroscopy. A Renishaw inVia confocal Raman spectroscopic system (Renishaw, Wotton-under-Edge, Glos, UK) equipped with a 785-nm NIR diode laser and a Leica microscope was used. Bacterial samples before and after contacting with RC/CNC surfaces were collected and washed twice with sterile water. An aliquot of bacterial suspension was transferred onto a gold-coated microarray slide and dried at room temperature for 20 minutes. The Raman spectra were recorded in the range of 400 to 1,800 cm^{-1}.

6.3.4. Statistical analysis

The statistical analysis was carried out through a one-way analysis of variance (ANOVA) using IBM SPSS Statistics 26 software. Data were presented as the mean ± standard deviation, and

the differences between means were analyzed by LSD post-hoc analysis at the confidence level of 0.05.

6.4. Results and Discussion

6.4.1. Structure of CNCs and RC/CNC films

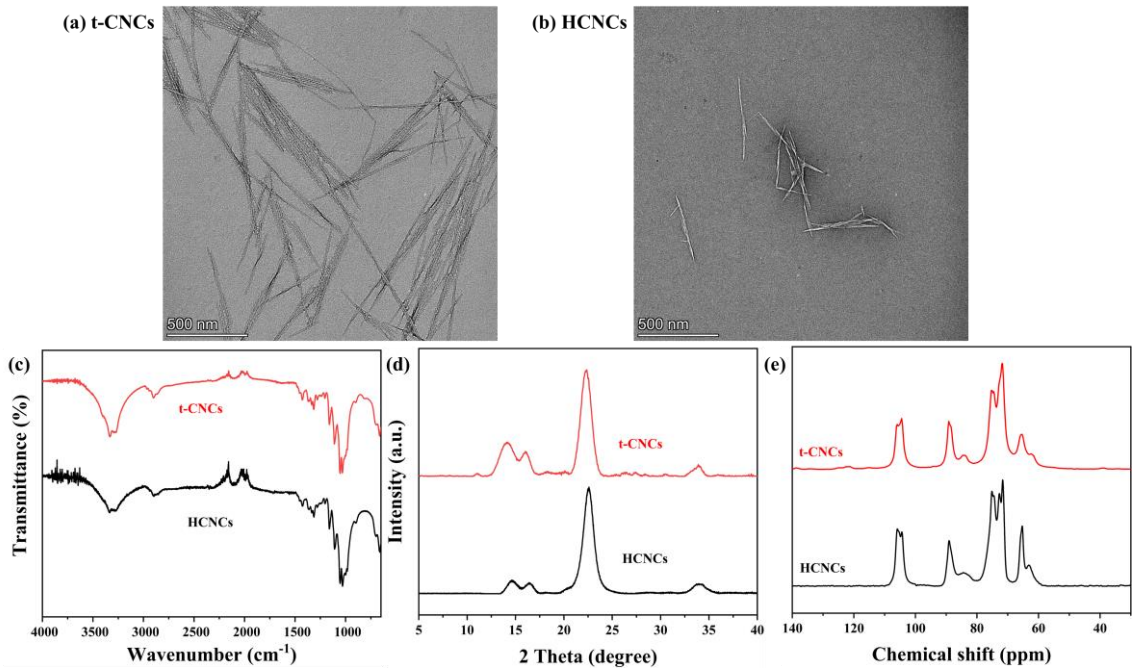

Figure 6.1. Representative TEM images (a, b), FTIR spectra (c), XRD patterns (d), and ^{13}C solid-state NMR spectra of t-CNCs and HCNCs.

The morphology of t-CNCs and HCNCs was observed by TEM. As shown in Figure 6.1 (a, b), HCNCs from waste textile had a typical rod-like shape, and the average length and diameter of HCNCs were 112 nm and 12 nm, respectively. Meanwhile, t-CNCs from tunicate presented a longer needle-like structure with an average length of 924 nm and a diameter of 17 nm. It indicated a significantly higher aspect ratio (55 ± 10) of t-CNCs and was in agreement with previously reported results (Dunlop et al., 2020; He, Bian, & Piao, 2020). Figure 6.1 (c) shows the FTIR spectra with analogous characteristic peaks of cellulose. For instance, the peaks at

3331, 2900, 1427, 1371, 1315, 1160, 1055, and 1031 cm^{-1} were attributed to the O-H stretching, C-H stretching vibration, C-H bending, CH_2 bending, OH bending, C-O-C asymmetric vibration, and C-O-C pyranose ring stretching vibration, respectively, and both CNC samples were assigned as β-linkage with a peak at 899 cm^{-1} (Verma, Chhajed, Gupta, Roy, & Maji, 2021). The XRD patterns of t-CNCs and HCNCs are shown in Figure 6.1 (d). The samples showed the same characteristic peaks at 14.6°, 16.4°, and 22.5°, which proved the cellulose I_β type crystalline structure (Ling et al., 2022). The crystallinity index of t-CNCs and HCNCs was calculated to be 85% and 89%, which were consistent with the previous reports (He et al., 2020; Kim et al., 2021). The solid-state NMR spectra of t-CNCs and HCNCs recorded the characteristic peaks of cellulose I_β crystalline structure in the range of 60-68 ppm for C-6, 68-80 ppm for C-2, C-3, and C-5, 84-89 ppm for C-4, and 100-110 ppm for C-1 (Pourmoazzen et al., 2020; Trilokesh & Uppuluri, 2019; Xia, Yuwen, & Lin, 2018).

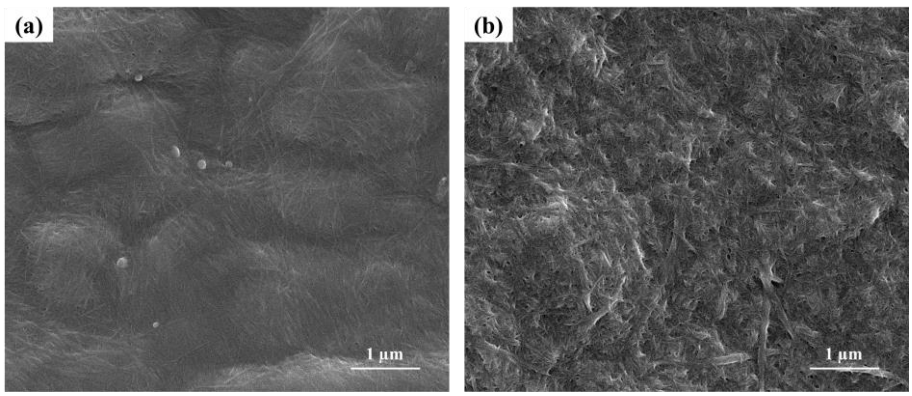

Figure 6.2. Representative SEM images of RC/t-CNCs (a) and RC/HCNCs (b).

The surface morphology of RC/t-CNCs and RC/HCNCs films was studied using SEM, and the images are shown in Figure 6.2. Although t-CNCs and HCNCs were not vertically fixed on the surface of RC films, the deposition of CNCs formed rough surfaces. Both CNCs were uniformly and randomly distributed on the surfaces without obvious pores or aggregates. It has

been reported that the coarse surface of solid film was important to the mechano-bactericidal property, while neither the RC films nor the free CNC suspensions with different concentrations showed any antibacterial effect (log reduction ranging from -0.100 to 0.136). It indicated the necessity of constructing a chevaux-de-frise-like nanostructure on the solid film surface (Zhou, Girouard, O'Brien, Ronholm, & Wang, 2022).

6.4.2. Antibacterial activity

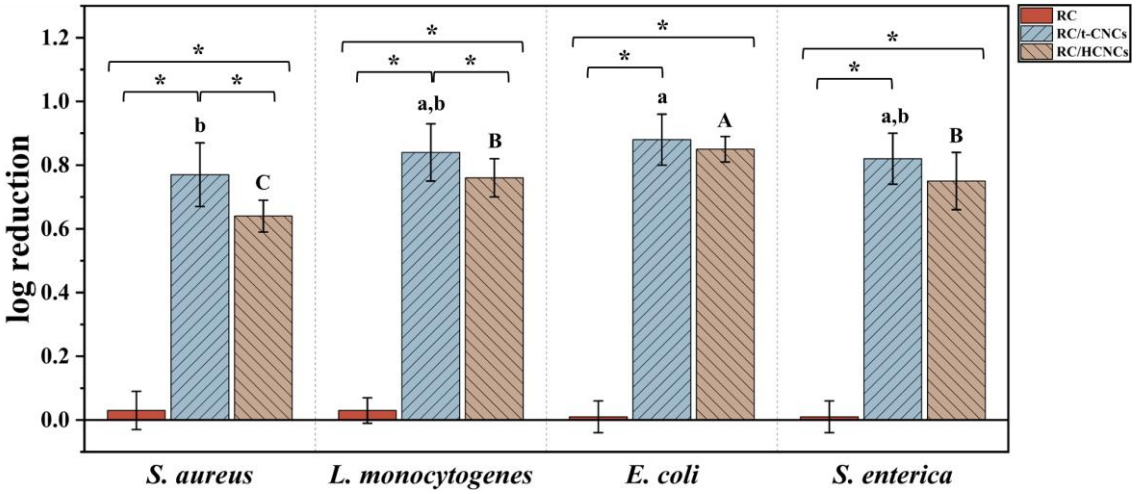

Figure 6.3. Antibacterial efficiency of RC, RC/t-CNCs, and RC/HCNCs against *S. aureus*, *L. monocytogenes*, *E. coli*, and *S. enterica.* Statistical significance ($p < 0.05$) among different bacterial strains is indicated by letters, and significant difference ($p < 0.05$) among the RC films is indicated by symbol*.

The antibacterial activities of RC and RC/CNC films were tested with four types of bacteria, namely *S. aureus* and *L. monocytogenes* (Gram-positive bacteria) and *S. enterica* and *E. coli* (Gram-negative bacteria). To quantify the number of viable bacteria on each surface, plate assay was performed. As shown in Figure 6.3, no obvious antibacterial effect was observed for the RC films (control group). On the contrary, significant log reduction ($p < 0.05$) of *S. aureus*,

S. enterica, *E. coli*, and *L. monocytogenes* was exhibited after 3-minute contact with both RC/CNC samples. For *S. aureus* and *L. monocytogenes*, there was statistical significance in the log reduction between the RC/t-CNCs and RC/HCNCs films ($p < 0.05$), while no significant difference existed towards *S. enterica* and *E. coli* ($p > 0.05$). Additionally, both the RC/t-CNCs and RC/HCNCs films showed the relatively higher antibacterial activity against *E. coli* and slightly lower activity for *S. aureus*. It suggested that the antibacterial efficiency of RC/CNC films was related to the characteristics of different bacteria. Among these four bacterium models, *S. enterica*, *E. coli*, and *L. monocytogenes* are rod-shaped bacteria with flagella-mediated motility, while *S. aureus* has a spherical shape and a non-motile organism without flagella (Huang, Lin, Huang, Yang, & Shih, 2022). Besides, gram-negative bacteria have thinner cell walls than Gram-positive bacteria (Ye et al., 2022). The death of bacteria cells on nano-patterned surfaces was associated with the physical stretching of the cell membrane and the balance between bacterial adhesion and stretching energy (Anselme et al., 2010; Zhou et al., 2021). Therefore, the relatively higher viability of *S. aureus* might be due to their less movement on the RC/CNC surface and thicker cell wall. Moreover, the RC/t-CNCs films were relatively more effective in killing the bacteria cells compared to RC/HCNCs. It might be the result of the higher aspect ratio of t-CNCs (Chopra et al., 2021; Patil, Overland, Stoller, & Chatterjee, 2021).

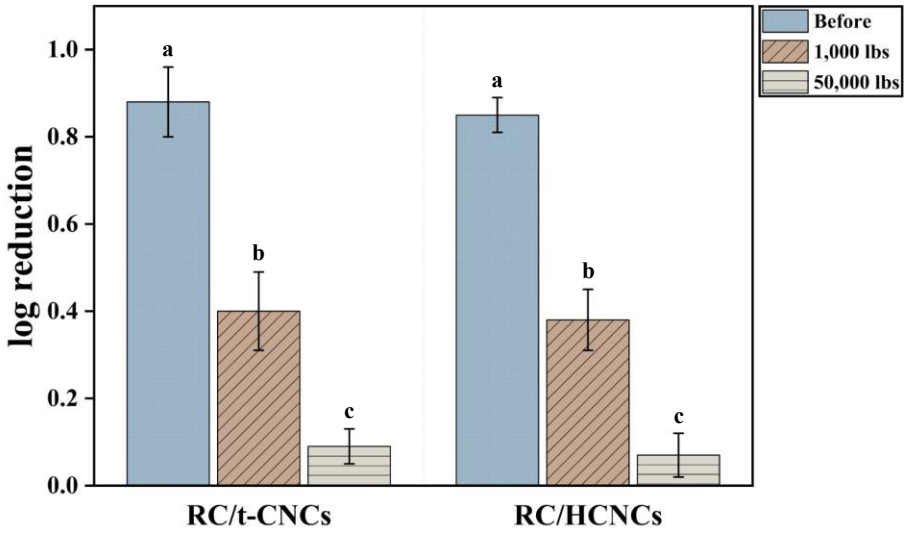

Figure 6.4. Antibacterial efficiency of RC/t-CNCs and RC/HCNCs against *E. coli* before and after pressing under the forces of 1,000 lbs and 50,000 lbs. Statistical significance ($p < 0.05$) between different pressing forces is indicated by letters.

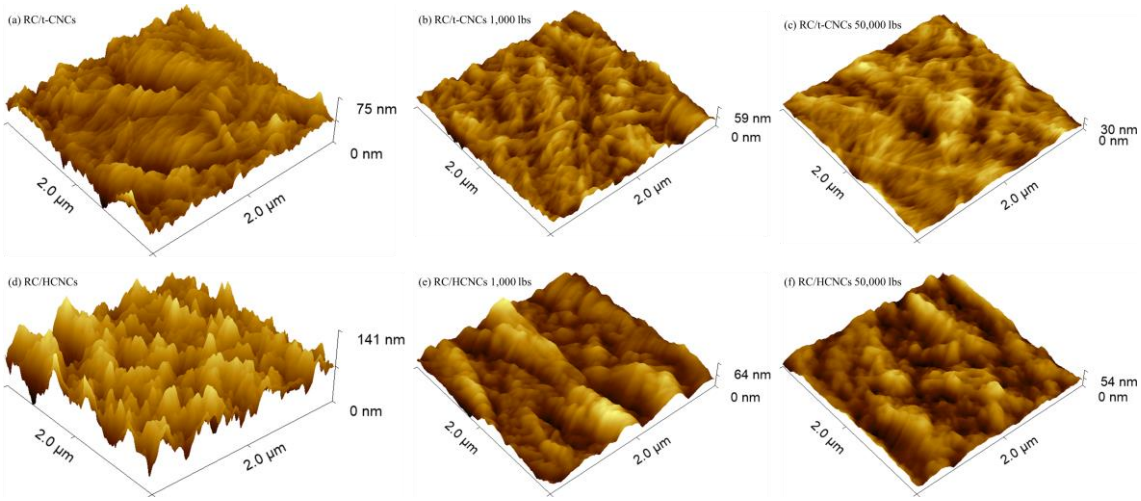

Figure 6.5. 3D AFM images of RC/t-CNCs (a-c) and RC/HCNCs (d-f) before and after pressing under the forces of 1,000 lbs and 50,000 lbs.

In order to investigate the relationship between the surface roughness and mechano-bactericidal activity, the RC/t-CNCs and RC/HCNCs films were pressed under the forces of 1,000 lbs and 50,000 lbs for 15 minutes, and their antibacterial efficiency was then tested with *E. coli*. As shown in Figure 6.4, an obvious decrease in log reduction was observed for both films after

pressing. Particularly, with the pressing force of 50,000 lbs, the antibacterial efficiency significantly decreased to around 0.07 log reduction ($p < 0.05$), indicating no bactericidal activity. The changes in the surface topography of the RC/CNC films were evaluated using AFM. As shown in Figure 6.5, pressing under the forces of 1,000 lbs and 50,000 lbs for 15 minutes obviously smoothed the surface of RC/CNC films. Wang et al. (Wang et al., 2021) reported a similar phenomenon where the fibrous membranes became denser with low surface roughness after pressing. It was confirmed that the nanostructures formed by the deposited t-CNCs and HCNCs were the key for killing the bacteria by contact.

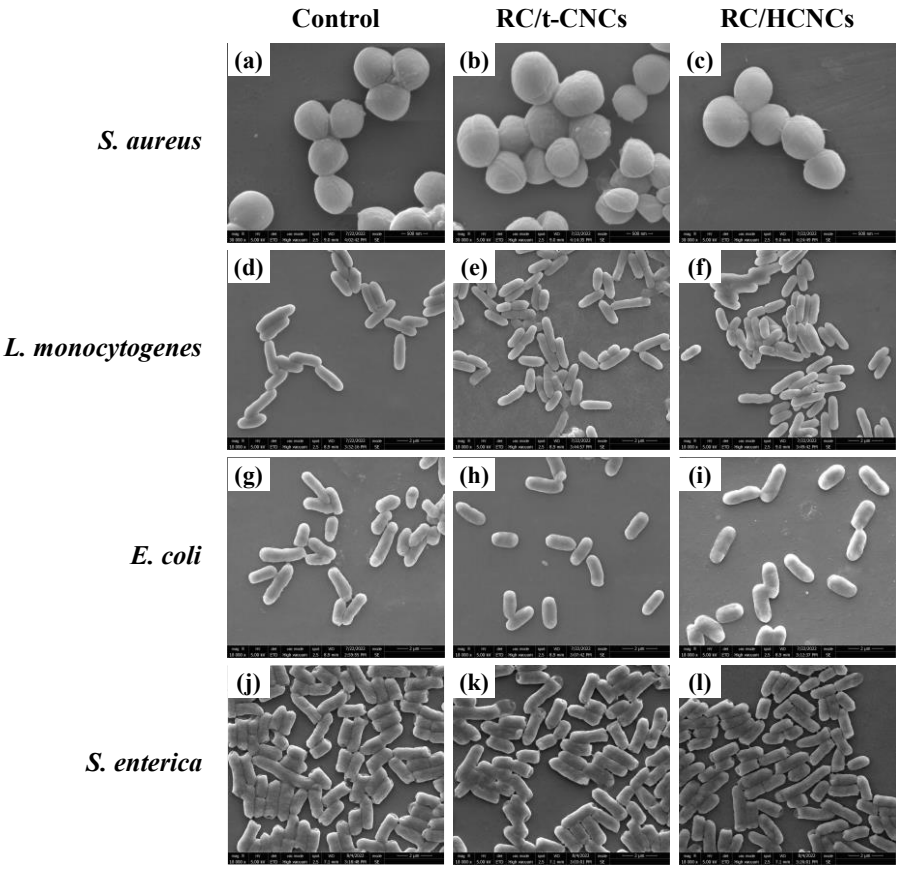

Figure 6.6. Representative SEM images of *S. aureus* (a-c), *L. monocytogenes* (d-e), *E. coli* (g-i), and *S. enterica* (j-l) without treatment (left), and after treatments on the surfaces of RC/t-CNCs (middle) and RC/HCNCs (right) for 3 minutes.

In an attempt to visualize the effects of the RC/CNC films on the four types of bacteria, SEM images of bacteria before and after contacting with the RC/t-CNCs and RC/HCNCs films for 3 minutes at room temperature are shown in Figure 6.6. The untreated bacterial cells of *S. enterica*, *E. coli*, and *L. monocytogenes* were smooth and rod-shaped with complete structure, and *S. aureus* cells appeared in a spherical shape. Cell death caused by nanopillars is usually accompanied by rupture of the cell membrane (Zhou et al., 2021). However, there was no significant change in the morphology of all the bacterial cells after contacting with the RC/CNC surfaces. It indicated that the bacteria cells were quickly killed in 3 minutes without causing any significant morphological changes.

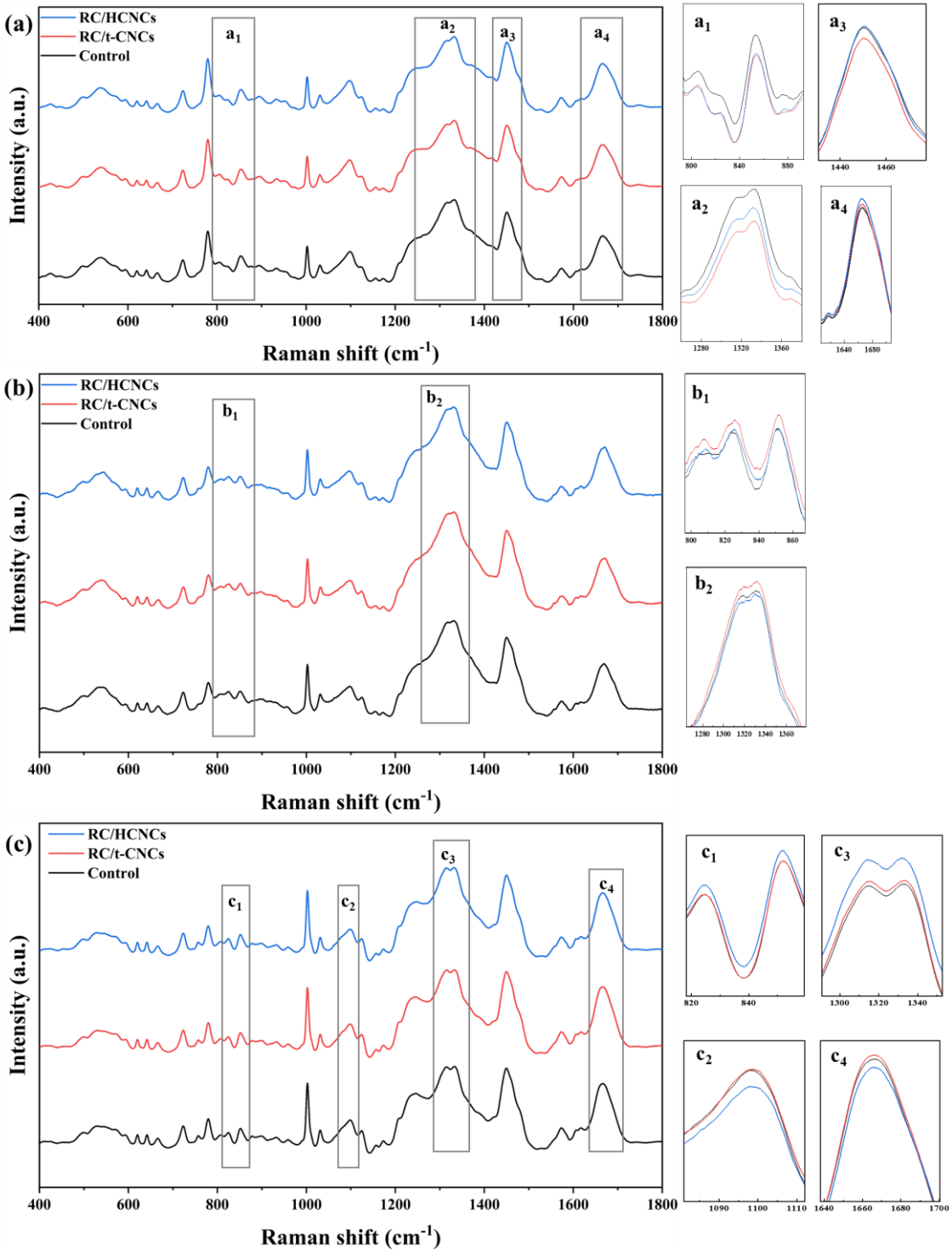

Figure 6.7. Average Raman spectra of *S. aureus* (a), *L. monocytogenes* (b), and *E. coli* (c) without and with treatments on the surfaces of RC/t-CNCs and RC/HCNCs for 3 minutes.

Raman spectra of bacteria without/with the contact of RC/CNC films were employed to investigate the biochemical composition changes and recorded with an excitation wavelength

of 785 nm. *S. aureus*, *L. monocytogenes*, and *E. coli* were selected as representative models of non-motile Gram-positive, motile Gram-positive, and Gram-negative bacteria, respectively. Raman spectral fingerprinting regions, from 400 to 1800 cm^{-1}, represent the biochemical compositions of the bacterial cells, such as proteins, lipids, and nucleic acids (Wang et al., 2020). For example, the peaks at 824 and 850 cm^{-1} correspond to polysaccharides and phospholipids on bacterial cell walls. The prominent peaks at 1002, 1331, and 1668 cm^{-1} are correlated with phenylalanine, nucleic acid, and amide I, respectively. The band at 1450 cm^{-1} is associated with the CH_2 deformation mode of protein and lipids (Barzan et al., 2020; Liu, Mukherjee, Wu, Huang, & Cai, 2021). As shown in Figure 6.7, the average spectra of the bacteria exhibit a high level of similarity between the spectra before and after 3-minute contact with RC/CNC films, and only slight peak intensity changes were observed. It suggested that the short contact period with mechano-bactericidal surfaces did not significantly change cell morphology or biochemical compositions.

6.5. Conclusions

This study demonstrated the effects of different CNC dimensions and surface topographies on the mechano-bactericidal activity against four types of bacteria. Both RC/t-CNCs and RC/HCNC films showed the significant antibacterial activities (>80% reduction) against *S. aureus*, *L. monocytogenes*, *E. coli*, and *S. enterica* within 3-minute of contact. Due to the different cell morphology and structures, the all-cellulose antibacterial surfaces showed relatively higher activity against *E. coli* and slightly lower activity for *S. aureus*. Compared to HCNCs, t-CNCs had a higher aspect ratio and contributed to a relatively more effective

bactericidal surface. The surface topography significantly affected the antibacterial performance. After compressing at 50,000 lbs, the RC/CNC films became smoother with no bactericidal activity. SEM and Raman spectra results indicated no obvious changes in the morphology and biochemical compositions of the bacterial cells after contacting with the RC/CNC surfaces for 3 minutes. Therefore, this work confirmed the feasibility to fabricate sustainable antibacterial surfaces from CNCs with potential applications in food packaging.

6.6. References

Anselme, K., Davidson, P., Popa, A. M., Giazzon, M., Liley, M., & Ploux, L. (2010). The interaction of cells and bacteria with surfaces structured at the nanometre scale. *Acta Biomaterialia*, *6*(10), 3824-3846.

Barzan, G., Sacco, A., Mandrile, L., Giovannozzi, A. M., Brown, J., Portesi, C., Alexander, M.R., Williams, P., Hardie, K.R., Rossi, A. M. (2020). New frontiers against antibiotic resistance: A Raman-based approach for rapid detection of bacterial susceptibility and biocide-induced antibiotic cross-tolerance. *Sensors and Actuators B: Chemical, 309*, 127774.

Chopra, D., Gulati, K., & Ivanovski, S. (2021). Bed of nails: Bioinspired nano-texturing towards antibacterial and bioactivity functions. *Materials Today Advances, 12*, 100176.

Dehghani, S., Mashreghi, M., Nezhad, A. H. N., Karimi, J., Hosseinpour, S., & Davoodi, A. (2021). Exploring mechano-bactericidal nature of *Psalmocharias cicadas* wings: an analytical nanotopology investigation based on atomic force microscopy characterization. *Surfaces and Interfaces, 26*, 101407.

Dunlop, M. J., Clemons, C., Reiner, R., Sabo, R., Agarwal, U. P., Bissessur, R., Sojoudiasli, H., Carreau, P.J., & Acharya, B. (2020). Towards the scalable isolation of cellulose nanocrystals from tunicates. *Scientific Reports, 10*(1), 19090.

Ferreira, E. S., Rezende, C. A., & Cranston, E. D. (2021). Fundamentals of cellulose lightweight materials: Bio-based assemblies with tailored properties. *Green Chemistry, 23*(10), 3542-3568.

He, J., Bian, K., & Piao, G. (2020). Self-assembly properties of carboxylated tunicate cellulose nanocrystals prepared by ammonium persulfate oxidation and subsequent ultrasonication. *Carbohydrate Polymers, 249*, 116835.

Huang, K., & Wang, Y. (2022). Recent applications of regenerated cellulose films and hydrogels in food packaging. *Current Opinion in Food Science, 43*, 7-17.

Huang, S., Tao, R., Ismail, A., & Wang, Y. (2020). Cellulose nanocrystals derived from textile waste through acid hydrolysis and oxidation as reinforcing agent of soy protein film. *Polymers, 12*(4), 958.

Huang, Y., Lin, T., Huang, S., Yang, T., & Shih, C. (2022). Copper-enhanced silver releasing from bimetal-containing bioactive glass (AgCu/80S) elicits antibacterial efficacy against drug-resistant *Staphylococcus aureus*. *Journal of Non-Crystalline Solids, 584*, 121509.

Kim, M., Pierce, K., Krecker, M., Bukharina, D., Adstedt, K., Nepal, D., Bunning, T., & Tsukruk, V. V. (2021). Monolithic chiral nematic organization of cellulose nanocrystals under capillary confinement. *ACS Nano, 15*(12), 19418-19429.

Lee, K., Jeon, Y., Kim, D., Kwon, G., Kim, U.-J., Hong, C., Choung, J., & You, J. (2021).

Double-crosslinked cellulose nanofiber based bioplastic films for practical applications. *Carbohydrate Polymers, 260*, 117817.

Li, T., Chen, C., Brozena, A. H., Zhu, J., Xu, L., Driemeier, C., Dai, J., Rojas, O.J., Isogai, A., Wågberg, L., & Wågberg, L. (2021). Developing fibrillated cellulose as a sustainable technological material. *Nature, 590*(7844), 47-56.

Ling, Z., Tang, W., Su, Y., Huang, C., Lai, C., Kirui, A., Wang, T., French, A.D., & Yong, Q. (2022). Stepwise allomorphic transformations by alkaline and ethylenediamine treatments on bamboo crystalline cellulose for enhanced enzymatic digestibility. *Industrial Crops and Products, 177*, 114450.

Liu, Z., Mukherjee, M., Wu, Y., Huang, Q., & Cai, P. (2021). Increased particle size of goethite enhances the antibacterial effect on human pathogen *Escherichia coli* O157:H7: A Raman spectroscopic study. *Journal of Hazardous Materials, 405*, 124174.

Maleki, E., Mirzaali, M. J., Guagliano, M., & Bagherifard, S. (2021). Analyzing the mechano-bactericidal effect of nano-patterned surfaces on different bacteria species. *Surface and Coatings Technology, 408*, 126782.

Michalska, M., Laney, S. K., Li, T., Portnoi, M., Mordan, N., Allan, E., Tiwari, M.K., Parkin, I.P., & Papakonstantinou, I. (2021). Bioinspired multifunctional glass surfaces through regenerative secondary mask lithography. *Advanced Materials, 33*(43), 2102175.

Paikra, S. K., & Mishra, M. (2021). Role of physicochemical organization of Rhyothemis variegata wing in monitoring bactericidal activity. *Surfaces and Interfaces, 27*, 101576.

Patil, D., Overland, M., Stoller, M., & Chatterjee, K. (2021). Bioinspired nanostructured

bactericidal surfaces. *Current Opinion in Chemical Engineering, 34*, 100741.

Pourmoazzen, Z., Sadeghifar, H., Chen, J., Yang, G., Zhang, K., & Lucia, L. (2020). The morphology, self-assembly, and host-guest properties of cellulose nanocrystals surface grafted with cholesterol. *Carbohydrate Polymers, 233*, 115840.

Rana, A. K., Mishra, Y. K., Gupta, V. K., & Thakur, V. K. (2021). Sustainable materials in the removal of pesticides from contaminated water: Perspective on macro to nanoscale cellulose. *Science of The Total Environment, 797*, 149129.

Trilokesh, C., & Uppuluri, K. B. (2019). Isolation and characterization of cellulose nanocrystals from jackfruit peel. *Scientific Reports, 9*(1), 16709.

Tu, H., Zhu, M., Duan, B., & Zhang, L. (2021). Recent progress in high-strength and robust regenerated cellulose materials. *Advanced Materials, 33*(28), 2000682.

Verma, C., Chhajed, M., Gupta, P., Roy, S., & Maji, P. K. (2021). Isolation of cellulose nanocrystals from different waste bio-mass collating their liquid crystal ordering with morphological exploration. *International Journal of Biological Macromolecules, 175*, 242-253.

Wang, C., Zhao, J., Liu, L., Zhang, P., Wang, X., Yu, J., & Ding, B. (2021). Transformation of fibrous membranes from opaque to transparent under mechanical pressing. *Engineering*.

Wang, K., Chen, L., Ma, X., Ma, L., Chou, K. C., Cao, Y., Khan, I.U., Gölz, G., & Lu, X. (2020). *Arcobacter* identification and species determination using Raman spectroscopy combined with neural networks. *Applied and Environmental Microbiology, 86*(20), e00924-00920.

Xia, T., Yuwen, H., & Lin, N. (2018). Self-bonding sandwiched membranes from PDMS and cellulose nanocrystals by engineering strategy of layer-by-layer curing. *Composites Science and Technology, 161*, 8-15.

Xu, D., Wang, S., Hu, J., Liu, Y., Jiang, Z., & Zhu, P. (2021). Enhancing antibacterial and flame-retardant performance of cotton fabric with an iminodiacetic acid-containing N-halamine. *Cellulose, 28*(5), 3265-3277.

Ye, J., Li, B., Zheng, Y., Wu, S., Chen, D., & Han, Y. (2022). Eco-friendly bacteria-killing by nanorods through mechano-puncture with top selectivity. *Bioactive Materials, 15*, 173-184.

Zhao, L., Liu, T., Li, X., Cui, Q., Wu, Q., Wang, X., Song, K., & Ge, D. (2021). Low-temperature hydrothermal synthesis of novel 3D hybrid nanostructures on titanium surface with mechano-bactericidal performance. *ACS Biomaterials Science & Engineering, 7*(6), 2268-2278.

Zhou, C., Girouard, F., O'Brien, B., Ronholm, J., & Wang, Y. (2022). Construction of chevaux-de-frise from cellulose nanocrystals to enable mechano-bactericidal activity on recycled waste cotton films. *Green Chemistry, 24*(3), 1109-1113.

Zhou, C., Koshani, R., O'Brien, B., Ronholm, J., Cao, X., & Wang, Y. (2021). Bio-inspired mechano-bactericidal nanostructures: A promising strategy for eliminating surface foodborne bacteria. *Current Opinion in Food Science, 39*, 110-119.

Zhou, C., & Wang, Y. (2021). Recycling of waste cotton fabrics into regenerated cellulose films through three solvent systems: A comparison study. *Journal of Applied Polymer Science*, *138*(48), 51255.

Chapter 7. Contribution to Knowledge and Recommendations for Future Research

7.1. Conclusions

The primary objective of this thesis was to explore the potential of CNCs derived from waste textile to construct antibacterial packaging materials. The literature review showed that in addition to traditional raw materials, waste biomass has become a trending feedstock of CNCs. Due to their unique properties, CNCs have great potential to fabricate active packaging materials (Chapter 2). Therefore, we investigated the extraction of CNCs from waste textile and the approaches to applying CNCs in antibacterial packaging materials (Chapters 3-6).

Chapter 3 demonstrated that textile waste materials offered a potential feedstock for extracting CNCs. Two kinds of CNCs with different functional groups were successfully extracted from textile waste using sulfuric acid hydrolysis and three-step oxidization. The results confirmed the rod-like morphology and cellulose I_β crystalline structure of CNCs with a high crystallinity index (ca. 89%). Besides, the addition of CNCs into soybean protein isolate films improved the mechanical strength and water vapor barrier property of the protein films.

Chapter 4 synthesized the N-halamine modified CNCs as functional nanofillers for the fabrication of nanocomposite packaging films with rechargeable antibacterial property. The modified CNCs had a high antibacterial efficiency (>99.999%) against both *S. aureus* and *E. coli*, and were incorporated into cellulose acetate and poly(vinyl chloride) films by solvent casting. With the addition of 3% modified CNCs, the nanocomposite films could inactivate *S. aureus* and *E. coli* at an initial concentration of 10^6 CFU/mL after 1-hour contact. Moreover, the antibacterial activity could be fully recharged without affecting the mechanical performance of the films.

In Chapter 5, the effects of different antibacterial modifications of CNCs on the performance of polylactic acid films were investigated. The modified CNCs were applied on the surface of polylactic acid films by a convenient method - spray coating. Among three modifications, the coating of N-halamine modified CNCs showed the highest antibacterial efficiency against *S. aureus* and *E. coli* even with low coating mass. The quaternary ammonium salt modified CNCs contributed significantly to the mechanical and gas barrier properties of polylactic acid films, and the films coated with zinc oxide modified CNCs exhibited a prominent compostable behavior. All the coated composite films could extend the shelf life of wrapped pork from 3 days to more than 10 days.

Finally, in Chapter 6, the mechano-bactericidal surfaces were developed by all-cellulose materials without introducing any chemical antibacterial agent. The bactericidal surfaces showed significant antibacterial activity of >80% reduction against *S. aureus*, *L. monocytogenes*, *E. coli*, and *S. enterica* within 3-minute contact. It was found that the bactericidal efficiency was related to the characteristics of bacteria, aspect ratio of CNCs, and surface topography of all-cellulose films. Interestingly, there was no obvious difference in the morphology and biochemical compositions of live and dead bacterial cells after contacting for 3 minutes.

Overall, waste textile was proved to be a potential feedstock to extract CNCs with comparable properties to CNCs derived from traditional raw materials. Different strategies were applied to construct antibacterial packaging materials with either pristine or modified CNCs, suggesting new perspectives on the development of sustainable antibacterial packaging materials.

7.2. Contribution to Original Knowledge

The important contributions of this research to knowledge are as follows:

1. This work provided the optimized conditions to extract CNCs from textile waste and the structure-property information of CNCs obtained from different extraction methods.

2. This work demonstrated the feasibility of using modified CNCs as antibacterial nanofillers in commercial plastic films and revealed their effects on the performance of packaging films.

3. This work provided the comparison of different antibacterial modifications of CNCs and will contribute to the development of sustainable functional nanofillers.

4. This work demonstrated that the modified CNCs can be simply sprayed on the surface of packaging materials to endow them with antibacterial property, and the CNC coating not only improved the mechanical and barrier properties of polylactic acid films but also facilitated their compostability.

5. This work revealed the factors that affect the mechano-bactericidal activity of novel all-cellulose surfaces and will promote the development of sustainable antibacterial materials without using any antibiotics.

7.3. Recommendations for Future Research

The following are the recommendations for future research based on the current study:

1. It is necessary to investigate if any organic residues, such as dye molecules, exist in the CNCs extracted from waste textile.

2. Further development is required to design modified CNCs that are compatible with different types of packaging materials.

3. It is still unknown how the bacteria were killed on the all-cellulose surface within 3 minutes. Further research on the mechanism of mechano-bactericidal activity is needed for better design of CNC-based antibacterial materials.

4. The toxicity of modified CNCs should be evaluated. Although the release of modified CNCs was not obvious in our tests, the long-time migration of modified CNCs from packaging materials to food products should be investigated to ensure safety.

General Reference List

Ahmed, S., Sameen, D. E., Lu, R., Li, R., Dai, J., Qin, W., & Liu, Y. (2022). Research progress on antimicrobial materials for food packaging. *Critical Reviews in Food Science and Nutrition*, *62*(11), 3088-3102.

Badawy, A., Ghanem, A., Yassin, M., Youssef, A., & Rehim, M. H. A. (2021). Utilization and characterization of cellulose nanocrystals decorated with silver and zinc oxide nanoparticles for removal of lead ion from wastewater. *Environmental Nanotechnology, Monitoring & Management, 16*, 100501.

do Nascimento, D. M., Nunes, Y. L., Feitosa, J. P., Dufresne, A., & Rosa, M. d. F. (2022). Cellulose nanocrystals-reinforced core-shell hydrogels for sustained release of fertilizer and water retention. *International Journal of Biological Macromolecules, 216*, 24-31.

Eghbalian, M., Shavisi, N., Shahbazi, Y., & Dabirian, F. (2021). Active packaging based on sodium caseinate-gelatin nanofiber mats encapsulated with *Mentha spicata* L. essential oil and MgO nanoparticles: Preparation, properties, and food application. *Food Packaging and Shelf Life, 29*, 100737.

Ezati, P., Riahi, Z., & Rhim, J. W. (2022). CMC-based functional film incorporated with copper-doped TiO_2 to prevent banana browning. *Food Hydrocolloids, 122*, 107104.

Ferreira, E. S., Rezende, C. A., & Cranston, E. D. (2021). Fundamentals of cellulose lightweight materials: Bio-based assemblies with tailored properties. *Green Chemistry, 23*(10), 3542-3568.

Kumar, R., & Chauhan, S. (2022). Cellulose nanocrystals based delivery vehicles for anticancer

agent curcumin. *International Journal of Biological Macromolecules, 221*, 842-864.

Li, H., Shi, H., He, Y., Fei, X., & Peng, L. (2020). Preparation and characterization of carboxymethyl cellulose-based composite films reinforced by cellulose nanocrystals derived from pea hull waste for food packaging applications. *International Journal of Biological Macromolecules, 164*, 4104-4112.

Li, T., Chen, C., Brozena, A. H., Zhu, J. Y., Xu, L., Driemeier, C., Dai, J., Rojas, O.J., Isogai, A., Wågberg, L., & Hu, L. (2021). Developing fibrillated cellulose as a sustainable technological material. *Nature*, *590*(7844), 47-56.

Moon, R. J., Martini, A., Nairn, J., Simonsen, J., & Youngblood, J. (2011). Cellulose nanomaterials review: structure, properties and nanocomposites. *Chemical Society Reviews, 40*(7), 3941-3994.

Niu, Z., Cheng, W., Cao, M., Wang, D., Wang, Q., Han, J., Long, Y., & Han, G. (2021). Recent advances in cellulose-based flexible triboelectric nanogenerators. *Nano Energy*, *87*, 106175.

Rojas-Lema, S., Nilsson, K., Trifol, J., Langton, M., Gomez-Caturla, J., Balart, R., Garcia-Garcia, D., & Moriana, R. (2021). Faba bean protein films reinforced with cellulose nanocrystals as edible food packaging material. *Food Hydrocolloids*, *121*, 107019.

Schiavi, D., Francesconi, S., Taddei, A. R., Fortunati, E., & Balestra, G. M. (2022). Exploring cellulose nanocrystals obtained from olive tree wastes as sustainable crop protection tool against bacterial diseases. *Scientific Reports, 12*(1), 6149.

Seabra, A., Bernardes, J., Fávaro, W., Paula, A., & Durán, N. (2018). Cellulose nanocrystals as

carriers in medicine and their toxicities: A review. *Carbohydrate Polymers, 181*, 514-527.

Sun, X., Zhang, H., Wang, J., Dong, M., Jia, P., Bu, T., Wang, Q., & Wang, L. (2021). Sodium alginate-based nanocomposite films with strong antioxidant and antibacterial properties enhanced by polyphenol-rich kiwi peel extracts bio-reduced silver nanoparticles. *Food Packaging and Shelf Life, 29*, 100741.

Wu, S., Ning, D., Xu, D., Cheng, Y., Mondal, A. K., Zou, Q., Zhu, H., & Huang, F. (2022). Preparation and characterization of super hydrophobic aerogels derived from tunicate cellulose nanocrystals. *Carbohydrate Research, 511*, 108488.

Zainal, S. H., Mohd, N. H., Suhaili, N., Anuar, F. H., Lazim, A. M., & Othaman, R. (2021). Preparation of cellulose-based hydrogel: A review. *Journal of Materials Research and Technology, 10*, 935-952.